

5-2019

Development of BAR-peptide nanoparticles and electrospun fibers for the prevention and treatment of oral biofilms.

Mohamed Yehia Mahmoud
University of Louisville

Follow this and additional works at: <https://ir.library.louisville.edu/etd>

 Part of the [Dentistry Commons](#), [Nanotechnology Commons](#), [Pharmacology Commons](#), and the [Toxicology Commons](#)

Recommended Citation

Mahmoud, Mohamed Yehia, "Development of BAR-peptide nanoparticles and electrospun fibers for the prevention and treatment of oral biofilms." (2019). *Electronic Theses and Dissertations*. Paper 3162.
Retrieved from <https://ir.library.louisville.edu/etd/3162>

This Doctoral Dissertation is brought to you for free and open access by ThinkIR: The University of Louisville's Institutional Repository. It has been accepted for inclusion in Electronic Theses and Dissertations by an authorized administrator of ThinkIR: The University of Louisville's Institutional Repository. This title appears here courtesy of the author, who has retained all other copyrights. For more information, please contact thinkir@louisville.edu.

DEVELOPMENT OF BAR-PEPTIDE NANOPARTICLES AND ELECTROSPUN
FIBERS FOR THE PREVENTION AND TREATMENT OF ORAL BIOFILMS

By

Mohamed Yehia Mahmoud

BVSc, Cairo University, 2011

MVSc, Cairo University, 2015

A Dissertation

Submitted to the Faculty of the
School of Medicine of the University of Louisville
in Partial Fulfillment of the Requirements
for the Degree of

Doctor of Philosophy

in Pharmacology and Toxicology

Department of Pharmacology and Toxicology

University of Louisville

Louisville, Kentucky

May 2019

Copyright 2019 by Mohamed Yehia Mahmoud

All rights reserved

DEVELOPMENT OF BAR-PEPTIDE NANOPARTICLES AND ELECTROSPUN
FIBERS FOR THE PREVENTION AND TREATMENT OF ORAL BIOFILMS

By

Mohamed Yehia Mahmoud
BVSc, Cairo University, 2011
MVSc, Cairo University, 2015

A Dissertation Approved on

April 18, 2019

by the following Dissertation Committee:

Dr. Jill M. Steinbach-Rankins

Dr. Donald R. Demuth

Dr. David W. Hein

Dr. Kenneth E. Palmer

Dr. Ayman El-Baz

DEDICATION

I dedicate this Ph.D. dissertation to my parents, brother, sister, wife and kids. I am eternally grateful for their love, and the sacrifices they made for me.

ACKNOWLEDGEMENTS

I would first and foremost like to thank my mentor, Dr. Steinbach-Rankins, for her guidance and support in the entire periods of research. I am really grateful to her for offering me this valuable opportunity to work in her lab. Dr. Steinbach-Rankins has spent countless hours guiding me and pushing me to pursue novel and challenging scientific questions. I am honored and feel very fortunate to work with such a dynamic, hardworking, intelligent person, and a great human being. I feel very blessed to have her as my mentor.

I would also thank my co-mentor, Dr. Donald Demuth, for his encouragement and guidance. I am grateful for the independence you were willing to give me. Dr. Donald Demuth provided invaluable timely help and continuous support on every step of my Ph.D. He has pushed me to be my best and think critically.

I also would like to thank my dissertation committee, Dr. David Hein, Dr. Kenneth Palmer and Dr. Ayman El-Baz for agreeing to offer their expertise, valuable time, feedback and assistance.

I am also to show my gratefully thank to all the present and former members in our lab, Kevin Tyo, Longyun Zhang, Sonali Sapare, Keegan Curry, Lee Sims, Farnaz Minooei and Melissa Henckel. I would also like to thank Jinlian Tan, Mohammad Roky and Maryta Sztukowska for their help, kindness and friendship.

I want to thank Dr. David Hein and Dr. Osama El-Tawil for their efforts to build the partnership between Department of Pharmacology & Toxicology, University of Louisville and Cairo University, providing me an opportunity to study here.

Lastly, I would like to acknowledge my wife, Alaa Bakr, who from the beginning supported me throughout this process and to press on when times were tough, she deserves more thanks than I could possibly express here. I am also extremely grateful of the love and encouragement I have received from my parents, brother and sister throughout my time here at the University of Louisville.

ABSTRACT

DEVELOPMENT OF BAR-PEPTIDE NANOPARTICLES AND ELECTROSPUN FIBERS FOR THE PREVENTION AND TREATMENT OF ORAL BIOFILMS

Mohamed Yehia Mahmoud

April 18, 2019

Background: Periodontal diseases are globally prevalent inflammatory disorders that affect ~47% of U.S adults. *Porphyromonas gingivalis* (*Pg*) has been identified as a “keystone” pathogen that disrupts host-microbe homeostasis and contributes to the initiation and progression of periodontitis. *Pg* associates with oral streptococci in supragingival plaque and this interaction represents a potential target for therapeutic intervention. Previously our group developed a peptide (designated BAR), that potently inhibits *Pg*/*Streptococcus gordonii* (*Sg*) adherence *in vitro* and *Pg* virulence in a murine model of periodontitis. While efficacious, BAR (SspB Adherence Region) provided transient inhibition and required higher concentrations of BAR to disrupt established biofilms.

Hypothesis and Aims: To address these challenges, we hypothesized that BAR-surface modified and BAR-encapsulated poly(lactic-co-glycolic acid) (PLGA) nanoparticles (NPs) may more potently inhibit and disrupt biofilms *in vitro* and *in vivo*, relative to free BAR.

In addition, a new rapid-release platform, composed of polymeric electrospun fibers (EFs) that encapsulate BAR peptide, was developed. Given this, our objectives were to evaluate BAR-surface modified NPs in a murine model of periodontitis; to fabricate and assess the ability of BAR-encapsulated NPs to inhibit and disrupt *in vitro* oral biofilm formation, and to evaluate a new dosage form, electrospun fibers, to inhibit and formation, and to evaluate a new dosage form, electrospun fibers, to inhibit and disrupt *in vitro* oral biofilm formation. In addition, the safety of all platforms was determined via viability, apoptosis, adenosine triphosphate (ATP), lactate dehydrogenase (LDH) and oxidative DNA assays using telomerase immortalized gingival keratinocytes (TIGKs).

Methods: BAR-encapsulated and BAR-surface modified PLGA NPs were synthesized using adapted double- and single-emulsion techniques, respectively. Electrospun fibers were formed using a uniaxial approach, with different hydrophobic polymers (PLGA, polycaprolactone, poly(L-lactic acid)); each blended with different polyethylene oxide ratios (PEO: 0, 10, 20, or 40% w/w) to achieve maximal release of BAR. Both BAR-encapsulated NPs and EFs were assessed for inhibition of two-species biofilm formation and for disruption of pre-existing biofilms, against an equimolar free BAR concentration. *In vivo* efficacy of BAR-surface modified NPs was assessed using a murine model of periodontitis by measuring alveolar bone resorption and gingival IL-17 expression as outcomes of *Pg*-induced inflammation.

Results: BAR-encapsulated NPs and EFs inhibited biofilm formation (IC₅₀s = 0.7 and 1.3 μM, respectively) in a dose-dependent manner, relative to free BAR (IC₅₀ = 1.3 μM). In addition, BAR-encapsulated NPs and EFs efficiently disrupted established dual-species biofilms (IC₅₀s = 1.3 and 2 μM, respectively). Treatment of *Pg/Sg* infected mice with BAR-surface modified NPs reduced alveolar bone loss and IL-17 expression almost to the levels of sham-infected mice and to a greater extent than treatment with an equimolar amount of free BAR. The *in vitro* cytotoxicity studies, which utilized the maximum concentration of BAR-encapsulated NPs, BAR-surface modified NPs, BAR EFs, and free BAR (1.3 and 3.4 μM) demonstrated > 90% viability for all samples and showed no significant lysis or apoptosis relative to untreated cells. In addition, all tested formulations exhibited a lack of hemolytic activity.

Conclusion: These data suggested that BAR NPs and EFs provide novel and potent platforms to inhibit and disrupt dual-species biofilms. All formulations exhibited minimal cellular toxicity or hemolytic activity, highlighting the potential of NPs and EFs as a biocompatible platform for translatable oral biofilm applications.

Chapters included in this dissertation represent papers that have been submitted, which may result in duplicate descriptions across chapters; however, these have been provided for the sake of completeness. Chapter 2 has been published in the Journal of Nanobiotechnology and Chapter 3 has been published in the Journal of Controlled Release. It is the intent to publish Chapters 4 and 5 in the near future.

TABLE OF CONTENTS

| | |
|--|-----|
| ACKNOWLEDGEMENTS..... | IV |
| ABSTRACT | VI |
| LIST OF TABLES | XI |
| LIST OF FIGURES | XII |
| CHAPTER 1 | 1 |
| BACKGROUND AND SIGNIFICANCE | 1 |
| CHAPTER 2 | 15 |
| BAR-ENCAPSULATED NANOPARTICLES FOR THE INHIBITION AND DISRUPTION OF <i>PORPHYROMONAS GINGIVALIS-STREPTOCOCCUS GORDONII</i> BIOFILMS | 15 |
| <i>Introduction</i> | 15 |
| <i>Materials and Methods</i> | 17 |
| <i>Results</i> | 24 |
| <i>Discussion</i> | 36 |
| CHAPTER 3 | 43 |
| FUNCTIONAL ASSESSMENT OF PEPTIDE-MODIFIED PLGA NANOPARTICLES AGAINST ORAL BIOFILMS IN A MURINE MODEL OF PERIODONTITIS | 43 |
| <i>Introduction</i> | 43 |
| <i>Materials and Methods</i> | 47 |
| <i>Results</i> | 57 |
| <i>Discussion</i> | 69 |
| CHAPTER 4 | 76 |

| | |
|--|-----|
| RAPID-RELEASE POLYMERIC FIBERS FOR INHIBITION OF <i>PORPHYROMONAS GINGIVALIS</i> AND <i>STREPTOCOCCUS GORDONII</i> BIOFILMS | 76 |
| <i>Introduction</i> | 76 |
| <i>Materials and Methods</i> | 78 |
| <i>Results</i> | 89 |
| <i>Discussion</i> | 105 |
| CHAPTER 5 | 113 |
| ASSESSMENT OF TARGETED BAR-ENCAPSULATED NPS AGAINST ORAL BIOFILMS..... | 113 |
| <i>Introduction</i> | 113 |
| <i>Materials and Methods</i> | 116 |
| <i>Results</i> | 124 |
| CHAPTER 6 | 130 |
| OVERALL DISCUSSION AND CONCLUSION | 130 |
| <i>Conclusion and Future Work</i> | 134 |
| REFERENCES | 136 |
| CURRICULUM VITAE | 148 |

LIST OF TABLES

| | |
|---|-----|
| Table 2.1 Physical characterization of NPs | 25 |
| Table 2.2 The amount of BAR (μg) loaded in PLGA and mPEG-PLGA NPs (mg). | 26 |
| Table 2.3 Percent disruption of established biofilms with different treatment groups. | 36 |
| Table 3.1 Physical characterization of NP diameter and surface charge. Data represent the mean \pm standard deviation of at least 3 independent samples..... | 58 |
| Table 3.2 TIGK cells apoptosis induced by 1.3 μM free BAR, 3.4 μM free BAR, 1.3 μM BAR-NPs, 3.4 μM BAR-NPs and 2 mM hydrogen peroxide relative to cells treated with medium alone, (*, $P \leq 0.05$, **, $P \leq 0.01$ and ***, $P \leq 0.001$). | 69 |
| Table 4.1 The amount of BAR loaded in non-blended and blended polymeric EF formulations ($\mu\text{g}/\text{mg}$) and percent of total BAR loaded in blended and blended EFs. Data represent the mean \pm standard deviation ($n=3$) of three independent samples. | 94 |
| Table 5.1 The amount of BAR (μg) loaded in unmodified and CafA-modified NPs (mg). | 127 |

LIST OF FIGURES

| | |
|---|----|
| Figure 1.1 Mechanism of <i>Pg</i> – <i>Sg</i> co-aggregation. Adapted from Trends in Molecular Medicine, 21(3), 172-183. | 10 |
| Figure 2.1 Schematic representation of BAR-encapsulated NPs synthesis. | 19 |
| Figure 2.2 Schematic representation of BAR surface-modified NPs synthesis. . | 20 |
| Figure 2.3 SEM images of BAR-encapsulated (A) PLGA NPs and (B) mPEG-PLGA NPs. Scale bars represent 1 μm | 25 |
| Figure 2.4 Cumulative release of BAR as a function of mass (μg BAR per mg NP, open symbols) and percent of total BAR loaded (closed symbols) over 48 hr.... | 27 |
| Figure 2.5 BAR-encapsulated PLGA NPs prevent <i>Pg</i> adherence to <i>Sg</i> . Biofilms were visualized with confocal microscopy and the ratio of green (<i>Pg</i>) to red (<i>Sg</i>) fluorescence in z-stack images was determined using Volocity image analysis software. Each grid represents 21 μm | 28 |
| Figure 2.6 BAR-encapsulated mPEG-PLGA NPs prevent <i>Pg</i> adherence to <i>Sg</i> . Biofilms were visualized with confocal microscopy and the ratio of green (<i>Pg</i>) to red (<i>Sg</i>) fluorescence in z-stack images was determined using Volocity image analysis software. Each grid = 21 μm | 29 |

Figure 2.7 BAR-encapsulated PLGA NPs disrupt pre-established *Pg-Sg* biofilms. Biofilms were visualized with confocal microscopy and the ratio of green (*Pg*) to red (*Sg*) fluorescence in z-stack images was determined using Volocity image analysis software. Each grid represents 21 μm 30

Figure 2.8 BAR-encapsulated mPEG-PLGA NPs disrupt pre-established *Pg-Sg* biofilms. Biofilms were visualized with confocal microscopy and the ratio of green (*Pg*) to red (*Sg*) fluorescence in z-stack images was determined using Volocity image analysis software. Each grid = 21 μm 31

Figure 2.9 Comparison of the concentration of BAR-encapsulated PLGA and mPEG-PLGA NPs needed to (A) inhibit or (B) disrupt *Pg/Sg* biofilms. 32

Figure 2.10 BAR-encapsulated PLGA NPs inhibit *Pg* adherence to *Sg* after different durations of release. Biofilms were visualized with confocal microscopy and the ratio of green (*Pg*) to red (*Sg*) fluorescence in z-stack images was determined using Volocity software. Each grid = 21 μm 33

Figure 2.11 Disruption of established *Pg/Sg* biofilms after different exposure times to BAR surface-modified NPs, BAR-encapsulated NPs and free BAR. Biofilms were visualized with confocal microscopy and the ratio of green (*Pg*) to red (*Sg*) fluorescence in z-stack images was determined using Volocity software. Each grid = 21 μm 35

Figure 3.1 SEM images of (A) BAR-modified PLGA NPs and (B) Unmodified PLGA NPs. Scale bar represents 1 μm . Images are representative of a minimum of 3 independent samples, with $n > 500$ NPs assessed in total. 58

Figure 3.2 Representative images from different *in vivo* treatment groups (n=8 per group), of the area between the cemento-enamel junction (CEJ) and alveolar bone crest (ABC), measured to determine bone loss. Images were taken using a dissecting microscope fitted with a video imaging marker measurement system (Sony model VIA-170K; Fryer) at a total magnification of 40x. 60

Figure 3.3 Alveolar bone loss in each group relative to uninfected, untreated control mice. Data represent the mean \pm standard deviation (n=8)... 61

Figure 3.4 Histological sections of murine periodontal tissues, with inflammatory cell infiltration denoted with black arrows. (H&E, 100x). 62

Figure 3.5 (A) Immunofluorescence staining of IL-17 on gingival tissue (B) Quantification of IL-17 levels. Data represent the mean \pm standard deviation (n=5) 64

Figure 3.6 (A) The hemolytic activity of free BAR or BAR-NPs (1.3, 3.4 μ M) was assessed after administration to sheep erythrocytes for 3 hr. (B) TIGK cell viability was assessed after free BAR or BAR-NPs administration for 2 days. (C) ATP levels from free BAR (3.4 μ M) and BAR-NP-treated (1.3, 3.4 μ M) cells showed decreases in ATP concentration, relative to control cells (treated with medium only). (D) No significant release of LDH was observed from TIGK cells treated with free BAR and BAR-NPs, relative to control cells. Data represent the mean \pm standard deviation (n=5)... 67

Figure 3.7 TIGK cells were treated with (A) medium alone, (B) 1.3 μ M free BAR, (C) 3.4 μ M free BAR, (D) 1.3 μ M BAR-NPs, (E) 3.4 μ M BAR-NPs and (F) 2 mM hydrogen peroxide. The FITC versus phycoerythrin (PE) fluorescence dot plots

show the live (bottom left quadrant) and apoptotic cell (bottom right quadrant) cell populations. Data represent the mean \pm standard deviation (n=3), 10,000 counts. 68

Figure 4.1 Schematic representation of electrospinning process..... 82

Figure 4.2 (A) SEM images of 1% w/w BAR PLGA, PLLA, and PCL non-blended fibers. (B) SEM images of 40:60, 20:80, and 10:90 1% w/w BAR blended PLGA:PEO, PLLA:PEO and PCL:PEO fibers. 90

Figure 4.3 Average diameters of electrospun fibers measured from SEM images, using ImageJ. (A) Non-blended and blended (B) 40:60, (C) 20:80, and (D) 10:90 PLGA:PEO, PLLA:PEO and PCL:PEO 1% w/w BAR fibers. Error bars represent the mean \pm the standard deviation (n=3) of three independent runs. 91

Figure 4.4 The cumulative release of F-BAR from 1% w/w F-BAR non-blended (100:0) PLGA, PLLA and PCL fibers. The cumulative release is reported as (A) μ g F-BAR per mg of fiber, and (B) percent of total loaded F-BAR. Error bars represent the mean \pm the standard deviation (n=3) of three independent runs. 95

Figure 4.5 The cumulative release of F-BAR from 1% w/w F-BAR blended PLGA:PEO, PLLA:PEO and PCL:PEO fibers (A) 40:60, (B) 20:80, and (C) 10:90. Error bars represent the mean \pm the standard deviation (n=3) of three independent runs. 96

Figure 4.6 The cumulative release of F-BAR from the non-blended and PEO-blended formulations as a function of hydrophobic polymer type (A) PLGA, (B) PLLA, or (C) PCL and PEO ratio in each blend. Data represent the mean \pm standard deviation (n=3) of three independent runs. 97

Figure 4.7 BAR-incorporated PLGA:PEO (10:90) EFs prevent *Pg* adherence to *Sg*. Biofilms were visualized with confocal microscopy and the ratio of green (*Pg*) to red (*Sg*) fluorescence in z-stack images was determined using Volocity image analysis software. Each grid represents 21 μm 99

Figure 4.8 BAR-incorporated PLGA:PEO (10:90) EFs disrupt pre-established *Pg*-*Sg* biofilms. Biofilms were visualized with confocal microscopy and the ratio of green (*Pg*) to red (*Sg*) fluorescence in z-stack images was determined using Volocity image analysis software. Each grid represents 21 μm 100

Figure 4.9 (A) Biofilm inhibition and (B) biofilm disruption, as a function of different concentrations of BAR-incorporated PLGA:PEO (10:90) EFs and free BAR (3 μM). Data represent the mean \pm standard deviation (n=6). 101

Figure 4.10 (A) The hemolytic activity of free BAR or 10:90 PLGA:PEO BAR-EFs (1.3, 3.4 μM) was assessed after administration to sheep erythrocytes for 3 hr. (B) Free BAR and BAR-EFs were non-toxic, relative to cells treated with DMSO (****, $P \leq 0.0001$). (C) BAR-EFs (3.4 μM) treated cells showed decreases in ATP levels relative to medium-only treated cells. (D) None of free BAR or BAR-EF (1.3, 3.4 μM) treated cells released a significant level of LDH relative to medium-only treated cells. Data represent the mean \pm standard deviation (n=5) of five independent experiments. 104

Figure 4.11 Amount of AP sites per 100000 bp of genomic DNA obtained from TIGK cells treated with free BAR or BAR-EFs (1.3, 3.4 μM). Data represent the mean \pm standard deviation (n=3) of three independent runs. 105

Figure 5.1 The total amount of CafA bound to the surface of PLGA NPs was determined using the microBCA assay..... 125

Figure 5.2 (A) CafA-modified C6 NPs initially ($t = 0$) bind to Sg with 2.25-fold greater concentration (5.7 ug/mL), relative to avidin-modified C6 NPs (2.5 $\mu\text{g/mL}$) and maintain a 2.5-fold increase in binding (3.7 $\mu\text{g/mL}$) after 8 hr, relative to avidin-modified C6 NPs (1.4 μg). (B) 65% of CafA-modified C6 NPs retain binding to Sg after 8 hr. 126

Figure 5.3 (A) Cumulative release of BAR as a function of mass (μg BAR per mg NP) and (B) percent of total BAR loaded over 24 hr..... 128

Figure 5.4 Percent of CafA retained on the PLGA NP surface after 24 hr..... 129

CHAPTER 1

BACKGROUND AND SIGNIFICANCE

Periodontal diseases are multifactorial common chronic diseases that destroy the tooth-supporting tissues and subsequently lead to alveolar bone loss and finally tooth loss. Periodontal diseases are also associated with increased risk for multiple systemic diseases including cardiovascular disease, diabetes, rheumatoid arthritis, pulmonary disease, and obesity^{1,2}. Periodontal diseases are globally prevalent diseases with the worldwide economic impact of direct treatment estimated at US \$298 billion yearly, corresponding to an average of 4.6% of global health expenditures³⁻⁶.

Gingivitis is a mild form of periodontal disease that is caused by bacterial colonization in the subgingival pocket leading to the formation of a biofilm (dental plaque). Gingivitis is usually diagnosed through the clinical signs of inflammation (erythema, edema, pain), bleeding and discomfort on gentle probing, and halitosis. Chronic gingivitis often results in mild bleeding from the gums during tooth brushing, which is generally only a minor inconvenience unless underlying blood dyscrasias or bleeding disorders exist⁷. Gingivitis is a reversible disease that can be resolved following treatment of gingival inflammation by proper oral health care to reduce gingival pocket depths to ≤ 3 mm.

An acute form of gingivitis (necrotizing ulcerative gingivitis) is characterized by gingival necrosis, bleeding, ulcerated papillae, severe gingival swelling and pain. Untreated ulcerative gingivitis may lead to rapid destruction of the periodontium resulting in necrotizing ulcerative periodontitis and can even spread as necrotizing stomatitis, into neighboring tissues in the cheeks, lips or the bones of the jaw⁸. Untreated gingivitis and poor oral health care can progress to periodontitis which exhibits a chronic inflammatory response that ultimately results in the destruction of connective tissue, resorption of alveolar bone and tooth loss⁷. Chronic periodontitis results in irreversible tissue damage that remains for life and requires diligent protective care to prevent disease recurrence⁹. Individuals with advanced periodontitis may also have recurrent periodontal abscesses and halitosis. The clinical diagnosis of chronic periodontal disease depends on visual and radiographic assessment of the periodontal tissues, and measurements of subgingival pocket depths (≥ 5 mm)⁷.

Aggressive periodontitis results in more rapid attachment loss and bone destruction and can occur earlier in life, often in children as young as 8 yr old. Secondary characteristics of aggressive periodontitis are described by the presence of relatively low levels of gingival bacteria although commonly, *Aggregatibacter actinomycetemcomitans* and *Pg* are the most abundant organisms associated with the disease¹⁰. In addition to rapid and severe periodontal tissue destruction, aggressive periodontitis is characterized by a hyper-responsive phenotype characterized by an increased inflammatory response upon stimulation of innate immune cells¹¹.

Periodontal diseases are also associated with a variety of systemic conditions. For example, periodontal diseases are associated with preterm births, which might be attributed to infection of decidual tissues by periodontal pathogens through bacteraemia or to an inflammatory cascade that results from systemic circulation of inflammatory mediators produced in the periodontal tissues¹². Previous studies demonstrated that intravenous injection of pregnant mice with periodontal bacteria leads to premature delivery and stillbirths¹³. However, it is important to note that currently there is no direct causal evidence that periodontal pathogens can cause preterm birth in humans and these organisms are not associated with chorioamnionitis, positive placental cultures, or markers of upper genital tract inflammation¹⁴.

Periodontal diseases may also have a potential role in the initiation or progression of coronary artery disease and stroke¹⁵. These effects may be attributed to increasing levels of C-reactive protein, fibrinogen, and cytokines, which have been linked to atherosclerosis-induced disease. In addition, a previous study showed that treatment of periodontal disease reduced serum inflammatory markers and C-reactive protein¹⁶ and other studies demonstrated that periodontal pathogens promote platelet aggregation and induce foam cell formation¹⁷. Finally, several additional studies suggested that a systemic antibody response to several periodontal pathogens was associated with coronary heart disease, stroke, and increased intima media thickening¹⁸⁻²⁰.

Periodontitis and rheumatoid arthritis are common chronic inflammatory diseases with very high morbidity worldwide. Previous studies showed that individuals with both periodontitis and rheumatoid arthritis may have more missing teeth and greater inflammation relative to periodontitis patients without rheumatoid arthritis²¹. *Pg* produces a proteolytic enzyme, *Pg* peptidyl-arginine deiminase (PPAD), which has the ability to convert arginine residues in proteins to citrulline. Citrullination of proteins can alter protein assembly and function and consequently deregulate immune evasion. Moreover, chronic exposure to citrullinated proteins that may exist in periodontitis patients may predispose susceptible individuals to the development of autoantibodies and the initiation of rheumatoid arthritis²²

Periodontal diseases are also a possible complication of diabetes. Treatment of periodontal disease has been shown to enhance diabetic control²³. Periodontal disease might also be an important predictor of deaths from ischaemic heart disease and diabetic nephropathy, but not from other causes²⁴.

Finally, periodontal diseases may be associated with various pulmonary infections²⁵. Pathogens causing pneumonia have been shown to colonize the oral cavity of high-risk individuals²⁶, and initial studies indicate that proper oral hygiene can reduce the rate of respiratory infections²⁷.

The gold standard for treatment of periodontal disease is instrumental debridement of dental plaque followed by antibiotic administration and surgery to reduce subgingival pocket depth if necessary^{28,29}. Although mechanical debridement has proven effective for treating periodontal diseases³⁰, this approach

has several limitations, For example, individual patients may not respond uniformly and favorably to treatment³¹, scaling instruments may be unable to fully penetrate deep subgingival pockets, mechanical debridement may be ineffective against certain pathogens, and the presence of other adverse conditions including tooth loss, dentin hypersensitivity, and gingival collapse may decrease the effectiveness of mechanical treatment strategies^{32,33}. As a result, antibiotic administration, in combination with mechanical debridement has been recommended to suppress periodontal pathogenic bacterial colonization and improve clinical outcomes^{30,34}.

Despite the advantages that adjunct localized or systemic antibiotics can provide, these treatment strategies often exhibit non-specific activity and affect beneficial organisms present in the oral cavity. Antibiotics may also fail to effectively penetrate the oral biofilms. Additional potential risks include the development of resistant species, emergence of fungal opportunistic infections, and potential allergic reactions³⁵⁻³⁷.

Many factors can influence the initiation and progression of periodontal disease including genetic predisposition, health status of the host, environmental factors, and risk factors such as diet and stress. In addition, the subgingival microbial community plays a vital role in periodontitis development. The role of bacteria in periodontitis can be illustrated by two main hypotheses. The non-specific plaque hypothesis suggests that no specific bacteria plays a role in periodontitis development. This hypothesis postulates that the host innate immune response keeps oral organisms and putative virulence factors under control and

disease only develops if the host immune response becomes compromised and bacterial virulence factors can no longer be neutralized. Since plaque of any composition can potentially cause disease, the best preventative approach would be mechanical removal of plaque³⁸.

In contrast, the specific plaque hypothesis purports that specific microbial species are associated with periodontitis progression³⁹. Early studies suggested that many organisms might be associated with periodontitis, including protozoa, spirochetes, *streptococci*; *actinomyces*, Gram-negative anaerobic organisms, and facultative anaerobic Gram-negative organisms of the genera *Capnocytophaga*, *Eikenella* and *Actinobacillus*⁴⁰. More recently, Socransky et al. identified the 'red complex' of organisms, composed of a group of three species including *Porphyromonas gingivalis*, *Treponema denticola* and *Tannerella forsythia*, and showed that these organisms predominate in the pathogenic dental plaque isolated from symptomatic subgingival sites of periodontitis patients⁴¹. However, a limitation of the specific plaque hypothesis is that it does not completely explain the absence of putative periodontal pathogens in some diseased individuals or the presence of these pathogenic organisms in healthy individuals⁴². In addition, a further limitation relates to the large number of uncultivable species⁴³ in the oral microbiome which creates bias toward easily cultivable species⁴⁴. This hypothesis proposed that the use of antibiotics against specific bacterial species could potentially cure and prevent disease.

More recently, a modified hypothesis has been proposed suggesting that changes in environmental factors may lead to a shift in the resident microflora resulting in microbial dysbiosis and that specific bacteria may contribute to the disruption of normal host-microbe homeostasis. Indeed, *Pg* is a gram negative anaerobic bacterium and has been found to be present in 88% of sub-gingival plaque samples isolated from chronic periodontitis patients⁴⁵. *Pg* has been identified as a “keystone pathogen” due to its ability to disrupt the host complement pathway, leading to a change in the microflora from a symbiotic microbiota to a dysbiotic community even though *Pg* may be present in low abundance^{46,47}. This recent study demonstrated that *Pg*-infected mice showed reduced innate immunity, increased oral microbial biomass, and significant changes in the composition of the periodontal microbiota leading to the induction of inflammatory bone loss. Consistent with the keystone pathogen hypothesis, *Pg* only induced inflammatory bone loss in wild type mice and was avirulent in germ free animals that lacked the indigenous oral microbiota⁴⁸.

Although the keystone pathogen hypothesis was initially established from studies conducted in a mouse model, it was consistent with observations in other animal models and in humans⁴². For example, it was shown that infection by *Pg* increased bacterial biomass of the dental biofilm in rabbit⁴⁹ and the use of a vaccine against *Pg* decreased total subgingival bacterial counts in non-human primates (*Macaca fascicularis*)⁵⁰. *Pg* has also been shown to alter the host immune response in other ways as well. A previous *in vitro* study showed that *Pg* inhibits the stimulation of gingival interleukin-8 like chemokines which may delay the

infiltration of neutrophils, consequently enabling its initial colonization and enhancing the growth of other organisms⁵¹. This study also revealed that the capability of *Pg* to persist in the periodontium relies on complement C5 convertase activity of its proteolytic enzymes and destructive crosstalk between the C5a receptor and toll-like receptor 2⁴⁸.

Pg initially adheres to primary colonizers of the oral cavity, i.e., commensal streptococci (e.g., *Streptococcus gordonii*) before becoming established in its ideal niche, the anaerobic environment of subgingival dental plaque⁵². In efforts to establish a more mechanistically-specific treatment or prophylactic modality, the recent identification of pathogenic mechanisms in polymicrobial communities and their relation to pathways of immune response have begun to elucidate targets relevant to inflammatory and disease states. As stated above, biofilm formation and bacterial colonization are initially prompted by association of *Pg* with oral streptococci in the supragingival niche, and this represents an ideal target for therapeutic intervention.

Previous studies suggested that *Pg* adherence to *Sg* is mediated by a protein-protein interaction that occurs between the minor fimbrial antigen (Mfa) of *Pg* and specific members of the antigen I/II family of proteins expressed by commensal streptococci, e.g., the SspB protein of *Sg* (Figure 1.1)⁵³. In addition, the region comprising amino acid residues 1167 to 1250 of the SspB polypeptide sequence was shown to be essential for adherence to *Pg*⁵⁴ and additional studies showed that within this region of SspB, amino acids 1167 to 1193 designated as

BAR (SspB Adherence Region) were required for adherence of *Pg*⁵³. These studies also demonstrated that a synthetic peptide encompassing the BAR motif potently inhibited biofilm formation by *Pg* and *Sg* *in vitro* and reduced virulence of *Pg* in a murine model of infection [refs]. While efficacious, the effectiveness of BAR as a potential therapeutic may be limited by the duration of exposure within the oral cavity and the increased complexity of the oral microbiome in humans. Indeed, higher concentrations of BAR were required to disrupt established *in vitro* biofilms^{15,17}. To address these delivery challenges, our goal was to develop a drug delivery system for BAR peptide that specifically targets *Pg* while providing higher localized concentrations, for longer duration in the oral cavity.

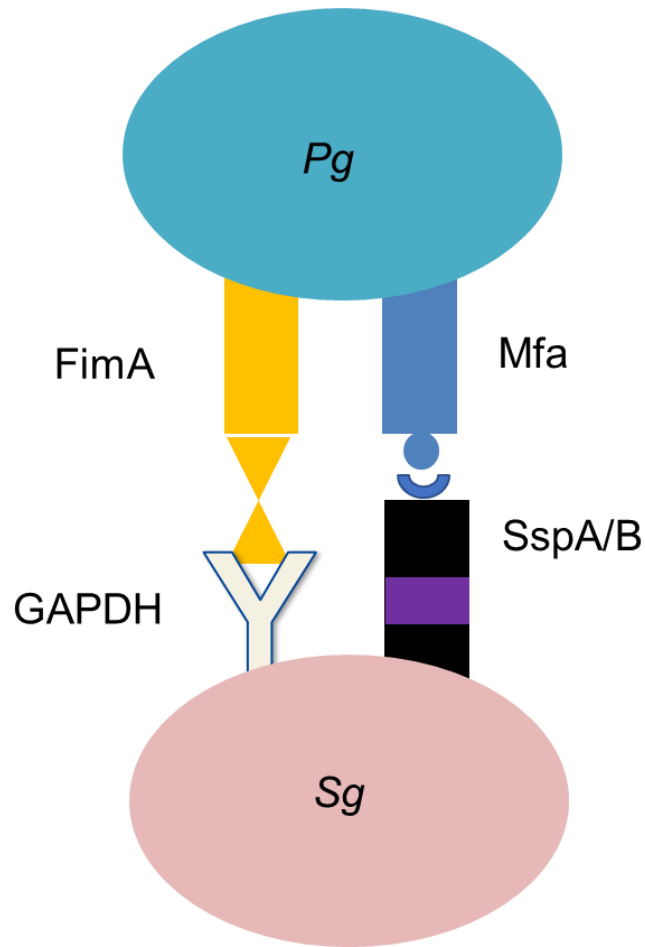


Figure 1.1 Mechanism of *Pg-Sg* co-aggregation. Adapted from Trends in Molecular Medicine, 21(3), 172-183.

Despite the attributes that delivery vehicles offer to biologic and drug delivery, there is currently a scarcity of drug delivery vehicles that enable specific and prolonged delivery of active agents to the oral cavity. One option to provide higher localized concentrations and prolonged delivery is to use polymeric nanoparticles (NPs)⁵⁵. The advantages of using NP delivery vehicles include the ability to: 1) highly encapsulate and deliver one or multiple active agents simultaneously; 2) protect the stability of active agents, especially molecules with

shorter half-lives (e.g. peptides); 3) provide tunable release and prolonged delivery of active agent; 4) facilitate penetration to target specific niches in cells and tissue; and 5) enable subsequent localization of active agent in target sites ⁵⁶.

A variety of nanoparticle platforms exist, fabricated from metals^{57,58}, semiconducting materials⁵⁹, ceramics⁶⁰⁻⁶³, lipids^{64,65}, and polymers^{66,67}. For dental applications specifically, metallic and metal oxide particles, made from silver⁶⁸⁻⁷¹, gold^{72,73}, copper⁷⁴⁻⁷⁶, zinc^{77,78} and titanium⁷⁸ have demonstrated antimicrobial properties in the oral microenvironment and have been utilized in the treatment of periodontal diseases. However, this inhibition is non-specific in nature, resulting from primarily electrostatic interactions with bacterial cells, subsequently decreasing bacterial replication or reduction of ATP production⁷⁹⁻⁸¹. Moreover, there have been several concerns regarding the toxicity associated with metallic NPs and their accumulation in various tissues and organs⁸²⁻⁸⁴.

Polymeric NPs have been widely utilized to deliver antibiotics to the oral cavity^{85,86}, and to avoid challenges of cytotoxicity and harmful accumulation of toxic metabolites observed after administration of metallic NPs. Moreover, polymeric NPs may offer biodegradability without toxic residues, and may be tailored to control the rate and duration of drug delivery. These attributes may be helpful to deliver high concentrations of active agents to target sites and to maintain functional activity of these agents for prolonged durations. Last, polymer NPs may be designed with mucoadhesive characteristics to adhere to oral tissue, thereby increasing the local concentration of active agents^{55,56,61,66}.

PLGA NPs have been FDA-approved and widely studied for drugs, protein, RNA and DNA delivery applications. PLGA NPs degrade into relatively inert metabolic by-products, poly(lactic acid) (PLA) and poly(glycolic acid) (PGA), enabling safe, biocompatible, and non-toxic delivery of associated cargo⁸⁶⁻⁹¹. As one example of antibiotic delivery, a previous study showed that minocycline-loaded PLGA NPs had potent antibacterial activity against *Aggregatibacter actinomycetemcomitans* infection with a minimum inhibitory concentration two times lower than free minocycline⁹².

Despite the utility of NPs to deliver antibiotics to treat periodontitis, high doses of antibiotics are needed to establish inhibitory concentrations in the subgingival pockets, which may result in antibiotic resistance and adverse side effects³⁷. Moreover, non-specific inhibition decreases the viability of commensal flora in the oral cavity, potentially causing fungal, viral and other bacterial infections. Due to these challenges, there is a need to develop targeted, sustained-release delivery vehicles that can specifically target *Pg*, a predominant pathogen in severe periodontitis, and provide higher localized concentrations of active agents for longer duration in the oral cavity^{93,94}.

Our preliminary studies have suggested that PLGA NPs that are surface-modified with BAR peptide increase the effectiveness of peptide-mediated inhibition of *Pg/Sg* adherence. Recently we demonstrated that this increased effectiveness is attributed to specific multivalent interactions between NPs and *Pg*. BAR-modified PLGA NPs enhanced BAR potency by promoting a multivalent

binding interface, thus increasing the avidity of BAR with *Pg*^{95,96}. Building upon this previous work, we next wanted to evaluate BAR-surface modified NPs in an *in vivo* murine model of infection and to increase the duration of exposure by developing sustained-release nanoparticles that control the release of BAR peptide to promote longer exposure time (12-24 hr) in the oral cavity. Our premise was that the incorporation of BAR peptide in PLGA NPs may provide sustained-release of BAR peptide, while BAR-surface modification offered a platform that provides higher localized concentration of BAR in the oral cavity.

Recently, polymeric electrospun fibers have been widely used in oral drug delivery^{97,98}. EFs may complement the delivery of, or offer advantages to NPs, including higher drug loading; more tunable modulation of drug release, dependent on the polymer properties; and less susceptibility to removal by salivary flow, resulting in longer retention in the oral cavity⁹⁹⁻¹⁰¹. A variety of natural, synthetic, semi-synthetic and biological polymers are used to provide biocompatibility and biodegradability. FDA-approved polymers including PLGA¹⁰², poly(L-lactic acid) (PLLA)¹⁰³, polycaprolactone (PCL)⁹⁷, and polyethylene oxide (PEO)¹⁰⁴ have been successfully used for drug delivery. In addition, fibers have the capacity to serve as a more durable delivery vehicle, providing enhanced retention in the oral cavity and ensuring active agent release within the oral cavity versus in the digestive tract. This durability may also offer a more convenient administration method, similar to films, but with the capability of providing prolonged release in desired applications. Given these attributes, we envisioned that designing EFs targeted to the oral cavity may provide a new dosage form in which to administer BAR, and

may provide a mechanism to improve therapeutic outcomes by increasing the localized concentration of BAR. We anticipated that completion of these aims would increase BAR effectiveness and longevity of exposure without influencing other commensal or beneficial bacteria that reside in the oral cavity. Moreover, the successful achievement of these objectives will provide new platforms for the delivery of BAR peptide in the oral cavity, with the potential to translate prevention and treatment to clinical practice. We envision that these research outcomes will have a significant impact on controlling a costly and widespread disease and may more broadly impact the serious systemic conditions that are associated with *Pg* infection.

CHAPTER 2

BAR-ENCAPSULATED NANOPARTICLES FOR THE INHIBITION AND DISRUPTION OF *PORPHYROMONAS GINGIVALIS*-*STREPTOCOCCUS* *GORDONII* BIOFILMS

Introduction

Periodontal disease is a group of chronic inflammatory diseases commonly caused by *Porphyromonas gingivalis*, *Tannerella forsythia*, and *Treponema denticola*. Together these pathogens are known as the “red complex”³⁶. The progression of periodontal disease can cause tissue destruction and tooth loss, and if left untreated can contribute to systemic conditions of increased cancer risk, cardiovascular disease, diabetes, rheumatoid arthritis, pulmonary disease, and obesity^{1,2}.

Current periodontal treatments aim to reduce bacterial plaque formation in the oral cavity using primarily physical and chemical (antibiotic) methods^{105,106}. However, current antibiotic treatment strategies exhibit non-specific activity, affecting beneficial organisms also present in the oral microbiome. Additional potential risks include the development of anti-bacterial resistant species, emergence of fungal opportunistic infections or *Pseudomonas* infection, and allergic reactions.

Last, most current antibiotics have difficulty penetrating periodontal biofilms, and must be frequently administered, due to their transient activity in the oral cavity^{35,37,107}.

Pg has been found to be associated with chronic periodontitis in 88% of sub-gingival plaque samples²³. Moreover, *Pg* and *Sg* association enhances the disruption of host–microbe homeostasis and induces population changes in the subgingival biofilm, driving inflammatory periodontal diseases^{47,48,108}. Previous work in our group has shown that *Pg* adherence to *streptococci* is driven by the interaction of the minor fimbrial antigen (Mfa) of *Pg* and the streptococcal antigen I/II (Agl/II)^{109,110}. From these studies, a peptide (designated BAR), was developed that potently inhibits *Pg/Sg* adherence *in vitro* and reduces *Pg* virulence in a mouse model of periodontitis¹¹¹⁻¹¹³. While efficacious, one of the challenges to free BAR administration is that it provides relatively transient inhibition of *Pg* in the oral cavity. Moreover, to treat established biofilms, relative to initial biofilm formation, higher concentrations of BAR are required.

Polymeric delivery vehicles provide one option to address these challenges, by offering prolonged and targeted delivery of active agents. In particular, for application to the oral cavity, polymeric nanoparticles are easy to fabricate and produce stable formulations. From a delivery perspective, polymeric NPs may offer rapid degradation in the acidic environment of the oral cavity, while providing mucoadhesive properties due to the electrostatic interactions between NPs and gingival epithelium¹¹⁴⁻¹¹⁶. Furthermore, for more labile molecules like biologics,

polymers have the potential to protect the functionality of the active agent and provide tunable release and prolonged delivery, while enabling localization of the active agent to target sites^{115,117}. In addition polymeric NPs may offer a safer and more biocompatible delivery method, relative to currently applied metallic NPs that exhibit broad antimicrobial effect^{118,119}.

Previous work in our groups has demonstrated that NPs surface-modified with BAR peptide more potently inhibit *Pg* adherence to *Sg*, relative to an equimolar administration of free BAR peptide *in vitro*⁹⁵. This increased potency was attributed to a higher localized dose of BAR, facilitating multivalent interactions with *Pg*. While surface-modified NPs provide targeting efficacy, a method of delivering high concentrations of BAR for prolonged duration has not been investigated. In this study, we sought to develop a formulation that encapsulates and prolongs the delivery of BAR, for durations relevant to oral delivery. BAR-encapsulated PLGA NPs were characterized and evaluated in two-species biofilm inhibition and disruption models. In addition, the kinetics of BAR-encapsulated, relative to BAR surface-modified NPs were assessed in a two-species model.

Materials and Methods

Peptide Synthesis

BAR peptide is comprised of residues 1167 to 1193 of the SspB (Antigen I/II) protein sequence of *Sg* (NH₂-LEAAPKKVQDLLKKANITVKGAFQLFS-COOH)¹¹². To enable peptide quantification and detection, the epsilon amine of the underlined lysine residue of BAR was covalently reacted with 6-

carboxyfluorescein to produce fluorescent BAR (F-BAR). Both unlabeled and labeled peptides were synthesized by BioSynthesis, Inc. (Lewisville, TX) and obtained with greater than 90% purity.

BAR-Encapsulated and BAR Surface-Modified Nanoparticle Synthesis

BAR and F-BAR encapsulated poly(lactic-co-glycolic acid) PLGA and methoxy-polyethylene glycol (mPEG-PLGA) NPs were synthesized using a double-emulsion technique^{89,120}. Briefly, BAR was encapsulated in PLGA carboxyl-terminated polymer (0.55–0.75 dL/g; LACTEL®; DURECT Corporation, Cupertino, CA, USA) or mPEG-PLGA (Mw ~5,000:55,000 Da; PolySciTech®; Akina, Inc., IN, USA) using laboratory facilities (**Figure 2.1**). One hundred milligrams of PLGA or mPEG-PLGA was dissolved in 2 mL methylene chloride (DCM) overnight. The next day, BAR was dissolved in 200 µL Tris EDTA (TE) buffer at a concentration of 43 µg BAR/mg PLGA. The resulting PLGA/DCM solution was vortexed while adding 200 µL of BAR peptide solution dropwise, and the mixture was ultrasonicated. Next, 2 mL of the PLGA/DCM/BAR solution was added dropwise to 2 mL of 5% (w/v) polyvinyl alcohol (PVA) while vortexing and was subsequently sonicated. The NP solution was added to 50 mL of 0.3% PVA for 3 hr to evaporate residual DCM. After evaporation, the NP solution was centrifuged at 13,000 rpm at 4°C and washed with distilled water twice. F-BAR encapsulated NPs were synthesized similarly, but were protected from light to avoid photo bleaching.

BAR surface-modified NPs were synthesized similarly as above using a previously described double-emulsion technique (**Figure 2.2**)^{88,121,122}. Briefly, the 5% (w/v) polyvinyl alcohol (PVA) solution was mixed with 2 mL of 5 mg/mL avidin-palmitate and the 2 mL PLGA/DCM solution was added dropwise to 4 mL PVA/avidin-palmitate while vortexing. After the first wash, the supernatant was discarded and the pelleted NPs were resuspended in 10 mL PBS for 30 min on a benchtop rotator, with biotinylated BAR peptide at a molar ratio of 3:1 BAR:avidin (18.5 nmol/mg) in PBS. After conjugation, the NPs were washed two times with distilled water by centrifugation at 13,000 rpm at 4°C. After washing, both BAR-encapsulated and BAR surface-modified NPs, were suspended in 5 mL of distilled water, frozen at -80°C, and lyophilized.

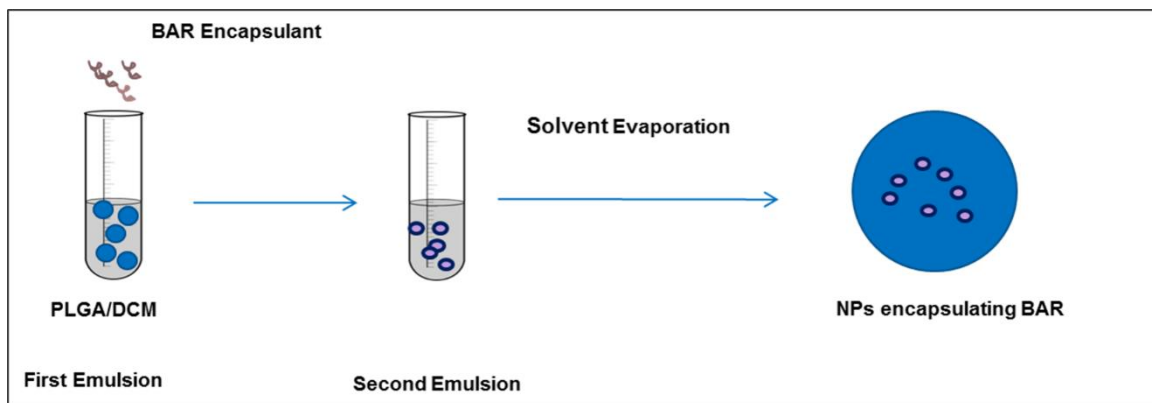


Figure 2.1 Schematic representation of BAR-encapsulated NP synthesis.

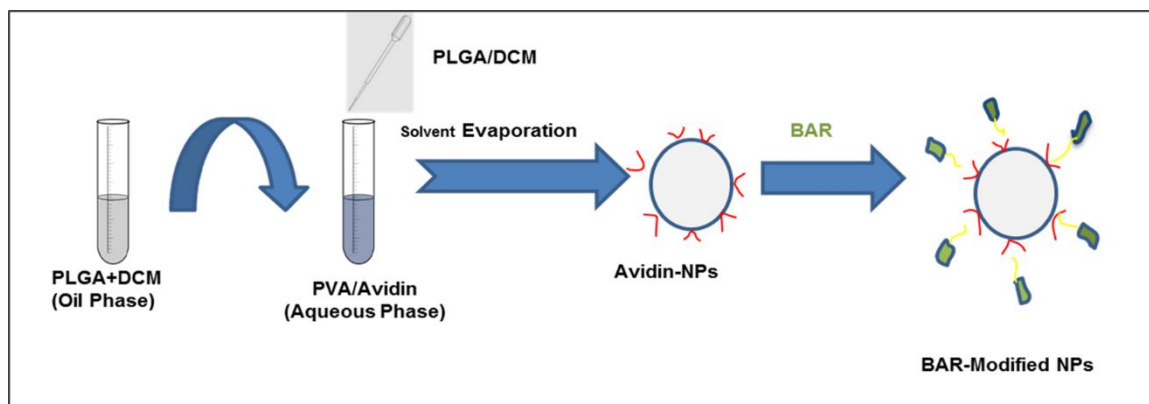


Figure 2.2 Schematic representation of BAR surface-modified NP synthesis.

NP Characterization: NP Morphology, Size, BAR Loading, Controlled Release

Unhydrated NP morphology, diameter, and size distribution were determined by analyzing scanning electron microscopy (SEM) images with NIH ImageJ software (version 1.5a, imagej.nih.gov). Dynamic light scattering and zeta potential analyses were performed on hydrated NPs to determine the hydrodynamic diameter and surface charge (Malvern, Malvern, UK). To determine BAR loading and encapsulation efficiency (EE), NPs were dissolved in dimethyl sulfoxide (DMSO). The quantity of extracted F-BAR was determined by measuring fluorescence (488/518 nm excitation/emission). For BAR-encapsulated NPs, *in vitro* release was measured by gentle agitation of NPs in phosphate buffered saline (PBS, pH 7.4) at 37°C. At fixed time points (1, 2, 4, 8, 24, 48 hr), samples were collected and the amount of BAR released from the NPs was quantified as described above.

Growth of Bacterial Strains

Pg ATCC33277 was grown in Trypticase soy broth (Difco Laboratories Inc., Livonia, MI, USA) supplemented with 0.5% (w/v) yeast extract, 1 µg/mL menadione, and 5 µg/mL hemin. The medium was reduced for 24 hr under anaerobic conditions (10% CO₂, 10% H₂, and 80% N₂) and *Pg* was subsequently inoculated and grown anaerobically for 48 hr at 37°C. *Sg* DL-1 was cultured aerobically without shaking in brain-heart infusion broth (Difco Laboratories Inc.) supplemented with 1% yeast extract for 16 hr at 37°C.

Biofilm Inhibition Assay

To assess the effectiveness of BAR-encapsulated NPs to prevent the interaction of *Pg* with *Sg*, *Sg* was harvested from culture and labeled with 20 µL of 5 mg/mL hexidium iodide for 15 min at room temperature. Following incubation, cells were centrifuged to remove unbound fluorescent dye. Subsequently, the bacterial concentration was measured by the O.D. at 600 nm from twenty-fold diluted cultures of *Sg*. The optical density of *Sg* cells was adjusted to 0.8 (1 × 10⁹ CFU/mL) to obtain uniformity between cell counts in each well. After adjusting the optical density, 1 mL of *Sg* cells was added to each well of 12-well culture plates containing a sterilized micro-coverslip. The cell culture plates were wrapped in aluminum foil to protect the labeled cells from light and placed on a rocker platform in the anaerobic chamber for 24 hr.

Pg cultures were optimized using a similar approach, utilizing a different fluorescent label (20 µL of 4 mg/mL carboxyfluorescein–succinylester). *Pg* was

incubated with the fluorescent dye for 30 min on a rocker platform and protected from light. The same procedures were followed as performed with *Sg* to determine cell concentration, with slight adaptations. The optical density of *Pg* was adjusted from 0.8 to 0.4 O.D. (5×10^7 CFU/mL) by diluting *Pg* cultures with an equal volume of BAR NPs or free BAR. The final concentration of BAR NPs or free BAR ranged from 0.3-3 μ M based on the previously determined IC₅₀ of free BAR (1.3 μ M). *Pg* was incubated with BAR NPs or free BAR at 25°C for 30 min before transferring to wells containing *Sg*.

Plates containing *Pg* and *Sg* were subsequently incubated for 24 hr at 37°C in anaerobic conditions⁹⁵. The following day, the supernatant was removed and cells were washed with PBS. Adherent cells were fixed with 4% (w/v) paraformaldehyde and the cover glass was mounted on a glass slide. Biofilms were visualized using a Leica SP8 confocal microscope (Leica Microsystems Inc., Buffalo Grove, IL) under 60x magnification. Background noise was minimized using software provided with the Leica SP8 and three-dimensional z-stack biofilm images were obtained from 30 randomly chosen frames using a z-step size of 0.7 μ m. Images were analyzed with Volocity image analysis software (version 6.3; Perkin Elmer, Waltham, MA, USA) to determine the ratio of green to red fluorescence (GR), representing *Pg* and *Sg*, respectively. Control samples were used to subtract background levels of auto-fluorescence. Briefly, triplicate samples of *Sg* alone were immobilized without *Pg* or BAR in 12-well culture plates and the same procedures for dual-species biofilm were followed. *Sg*-only coverslips were visualized and images were analyzed using the previously mentioned approach.

GR background was subtracted using the following formula: GR sample or control - GR *Sg*-only. Each treatment group (BAR NPs or free BAR) was analyzed in triplicate and three independent frames were measured for each well. The mean and variation (SD) between samples were determined using analysis of variance (ANOVA) and differences were considered to be statistically significant when $p < 0.05$. The percent inhibition of *Pg* adherence was calculated with the following formula: GR sample/GR control.

Biofilm Disruption Assay

The same procedures utilized in the inhibition assay were followed, except *Pg* was allowed to adhere to *streptococci* in the absence of BAR peptide or BAR NPs to demonstrate the ability of BAR-encapsulated NPs to disrupt or “treat” pre-established biofilms. The resulting *Pg/Sg* biofilms were then treated for 3 hr with free BAR or BAR-encapsulated NPs at various concentrations and processed and analyzed as described above.

Inhibitory Kinetics of BAR Released from BAR-Encapsulated NPs

Due to the similar release properties of BAR from PLGA and mPEG-PLGA NPs, PLGA NPs were selected to further assess the ability of NPs to release therapeutically relevant concentrations of BAR at different time points. PLGA BAR NPs (1.3 μM) were incubated with gentle agitation in PBS (pH 7.4) at 37°C. After 1, 2, 4 and 8 hr, the NP suspension was centrifuged, and the supernatant was collected for biofilm experiments. The NPs were re-suspended with new PBS. *Pg* was incubated with BAR NP eluate for 30 minutes, and subsequently transferred

to a well containing an *Sg* biofilm. The same biofilm inhibition assay procedure detailed above was used to visualize and analyze the samples.

Time-Dependent Comparison between Free BAR, BAR-Encapsulated, and BAR Surface-Modified NPs

In addition to delivering high concentrations of BAR during the time frame of interest, the temporal evaluation of BAR activity against established biofilms was evaluated and compared. Both BAR-encapsulated and BAR surface-modified NPs were assessed due to their previously demonstrated efficacy. *Pg* was allowed to adhere to *streptococci* in the absence of peptide, then BAR (3 μ M), BAR-encapsulated, and BAR surface-modified NPs (1.3 and 3 μ M) were applied to the biofilms. The biofilms were assessed 1, 2, and 3 hr post-administration and visualized as described above.

Results

Nanoparticle Characterization

The morphology, size, and zeta potential of BAR PLGA and mPEG-PLGA NPs were determined. The morphologies of BAR-encapsulated PLGA and mPEG-PLGA NPs are shown in **Figure 2.3**. Both PLGA and mPEG-PLGA NPs demonstrated spherical morphology with average unhydrated diameters of 227.5 ± 23.0 nm and 243.1 ± 31.2 nm respectively (**Table 2.1**). In comparison, the average hydrated diameters of PLGA and mPEG-PLGA NPs were 234.4 ± 19.2

nm and 278.9 ± 13.8 nm, respectively. PLGA and mPEG-PLGA NPs had zeta potentials of -13.1 ± 0.4 mV and -5.9 ± 0.1 mV.

Table 2.1 Physical characterization of NPs

| NP Type | Unhydrated Diameter (nm) | Hydrated Diameter (nm) | Zeta Potential (mV) |
|---------------|--------------------------|------------------------|---------------------|
| PLGA NPs | 227.5 ± 23.0 | 234.4 ± 19.2 | -13.1 ± 0.4 |
| mPEG-PLGA NPs | 243.1 ± 31.2 | 278.9 ± 13.8 | -5.9 ± 0.1 |

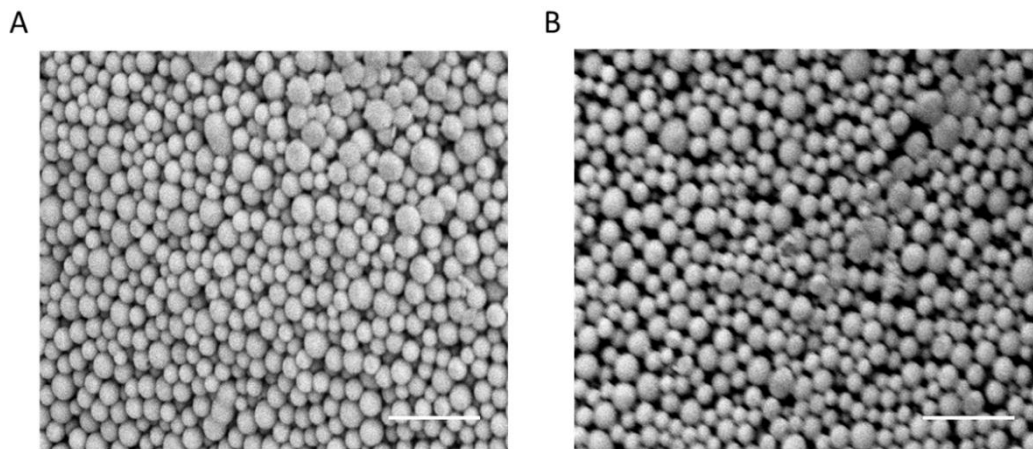


Figure 2.3 SEM images of BAR-encapsulated (A) PLGA NPs and (B) mPEG-PLGA NPs. Scale bars represent 1 μ m.

Quantification of BAR Loading and Release

The loading of BAR peptide in PLGA and mPEG-PLGA NPs was determined using fluorescence spectroscopy, and the fluorescence was compared to a known standard of F-BAR. Loading experiments demonstrated that both PLGA and mPEG-PLGA NPs highly encapsulated BAR with 19.0 ± 0.1 and 16.1 ± 0.2 μ g

of BAR per mg of NP, respectively, corresponding to encapsulation efficiencies of 44 and 37% (**Table 2.2**).

Table 2.2 The amount of BAR (μg) loaded in PLGA and mPEG-PLGA NPs (mg).

| NP Type | BAR input ($\mu\text{g}/\text{mg}$) | BAR output ($\mu\text{g}/\text{mg}$) | Encapsulation Efficiency (%) |
|---------------|---------------------------------------|--|------------------------------|
| PLGA NPs | 43 | 19.0 ± 0.1 | 44.2 |
| mPEG-PLGA NPs | 43 | 16.1 ± 0.2 | 37.3 |

To assess BAR release from the NPs, the fluorescence of supernatant from 1, 2, 4, 8, 24, 48 hr release time points was measured and compared to a known standard of F-BAR in PBS. Release experiments demonstrated that 47% of encapsulated BAR ($10.3 \mu\text{g}/\text{mg}$) was released from PLGA NPs, while 56% of BAR ($9.9 \mu\text{g}/\text{mg}$) was released from mPEG-PLGA NPs within 24 hr (**Figure 2.4**).

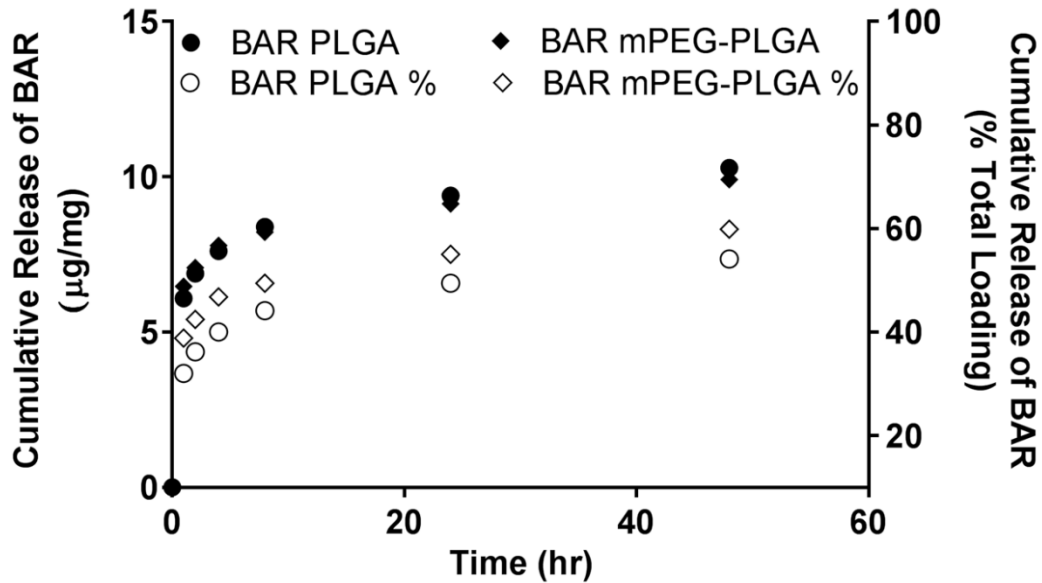


Figure 2.4 Cumulative release of BAR as a function of mass (μg BAR per mg NP, open symbols) and percent of total BAR loaded (closed symbols) over 48 hr.

Inhibition (or Prevention) of *Pg/Sg* Biofilm Formation

BAR-encapsulated PLGA and mPEG-PLGA NPs were functionally evaluated to determine their potential to inhibit *Pg* adherence to *Sg* after 24 hr, relative to free BAR. As shown in **Figure 2.5 and 2.6**, *Pg* adherence was significantly reduced in the presence of BAR-encapsulated PLGA and mPEG-PLGA NPs. Adherence was inhibited by 39% at the lowest administered concentration ($0.3 \mu\text{M}$), 59% at $0.7 \mu\text{M}$, and reached maximum inhibition (94%) at the highest concentration of PLGA NPs tested ($3 \mu\text{M}$). Similar inhibitory results were observed for mPEG-PLGA NPs, where *Pg/Sg* biofilm formation was inhibited by 37%, 55%, and 92% at concentrations of $0.3 \mu\text{M}$, $0.7 \mu\text{M}$ and $3 \mu\text{M}$ respectively. The ability of BAR-encapsulated NPs to inhibit biofilm formation was dose-dependent ($\text{IC}_{50} = 0.70 \pm 0.18 \mu\text{M}$) with no statistically significant differences

between PLGA and mPEG-PLGA BAR-encapsulated NPs ($p > 0.05$). Moreover these results indicate that a lower concentration of BAR is required if incorporated within NPs, relative to free BAR administration ($IC_{50} = 1.35 \pm 0.12 \mu M$) (**Figure 2.5**).

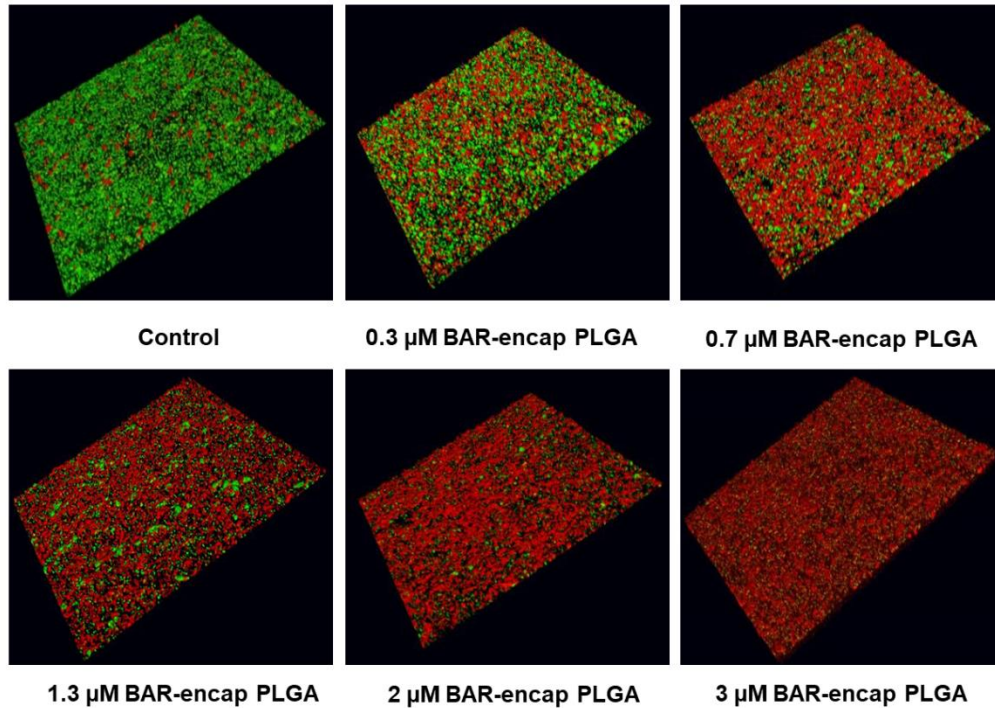


Figure 2.5 BAR-encapsulated PLGA NPs prevent *Pg* adherence to *Sg*. Biofilms were visualized with confocal microscopy and the ratio of green (*Pg*) to red (*Sg*) fluorescence in z-stack images was determined using Volocity image analysis software. Each grid represents 21 μm .

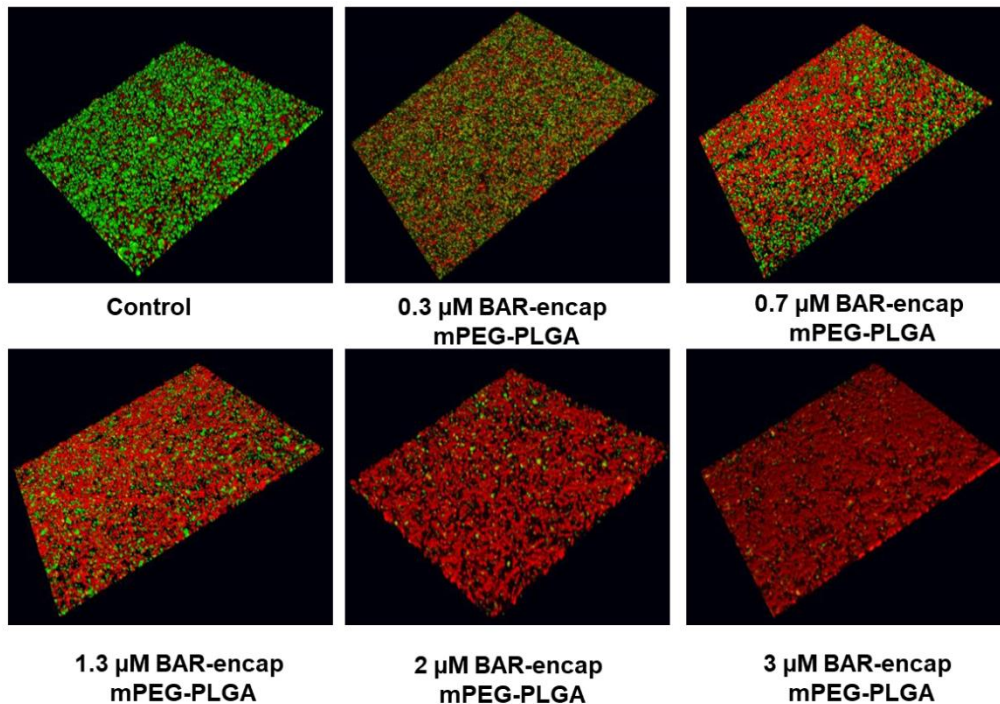


Figure 2.6 BAR-encapsulated mPEG-PLGA NPs prevent *Pg* adherence to *Sg*. Biofilms were visualized with confocal microscopy and the ratio of green (*Pg*) to red (*Sg*) fluorescence in z-stack images was determined using Volocity image analysis software. Each grid = 21 μm .

Disruption (or Treatment) of *Pg/Sg* Biofilms

To determine whether BAR peptide is capable of disrupting pre-existing *Pg/Sg* biofilms, dual-species biofilms were formed in PBS in the absence of BAR peptide for 24 hr, and were subsequently incubated for 3 hr with BAR-encapsulated PLGA or mPEG-PLGA NPs. Various molar concentrations of BAR NPs ranging from 0.3 to 3 μM were tested. The biofilms were visualized and the percent inhibition was calculated as described above. As shown in **Figure 2.7 and 2.8**, BAR-encapsulated PLGA and mPEG-PLGA NPs disrupted pre-existing dual-

species biofilms by ~25% with the lowest administered concentration (0.3 μM), 40% with 0.7 μM , and 85% with 3 μM of BAR-encapsulated PLGA NPs. Similar trends were observed for the disruption of pre-existing biofilms with 0.3, 0.7, and 3 μM mPEG-PLGA NPs (20%, 38%, and 80% disrupted). Overall the IC₅₀ values of PLGA and mPEG-PLGA ($1.35 \pm 0.12 \mu\text{M}$) NPs for biofilm disruption were not statistically significant ($p > 0.05$, **Figure 2.9**); demonstrating statistically significant improvements in efficacy relative to free BAR ($p < 0.05$).

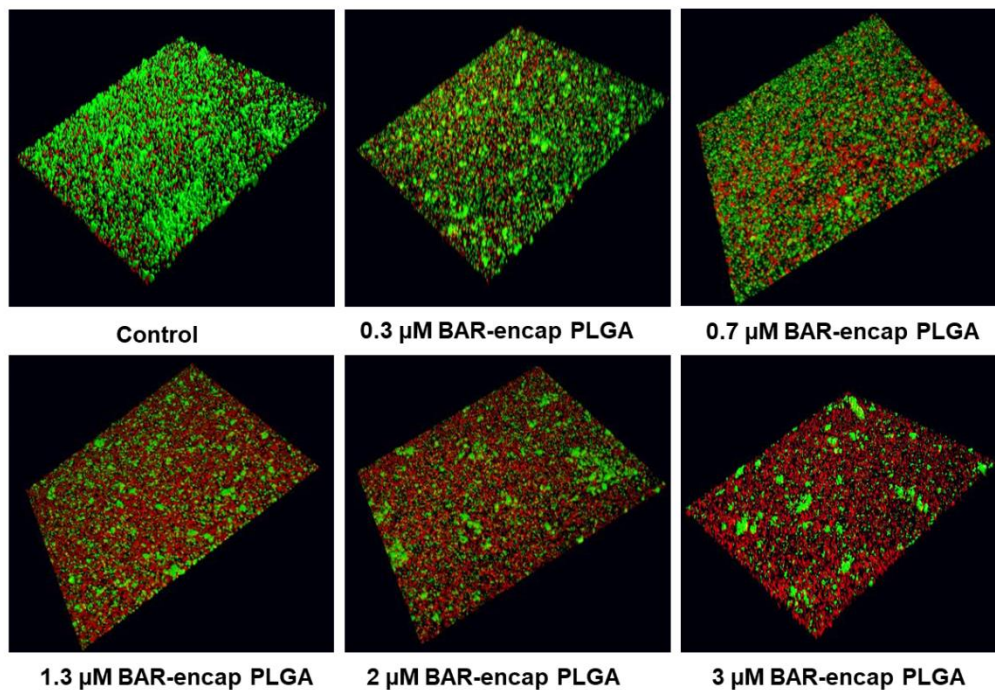


Figure 2.7 BAR-encapsulated PLGA NPs disrupt pre-established *Pg-Sg* biofilms. Biofilms were visualized with confocal microscopy and the ratio of green (*Pg*) to red (*Sg*) fluorescence in z-stack images was determined using Volocity image analysis software. Each grid represents 21 μm .

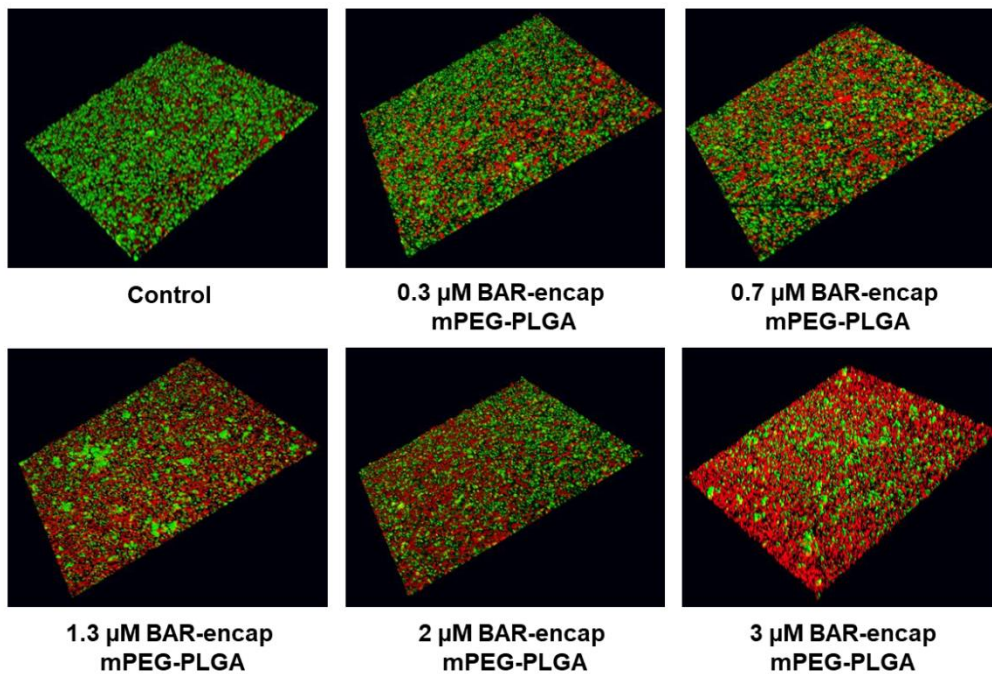


Figure 2.8 BAR-encapsulated mPEG-PLGA NPs disrupt pre-established *Pg-Sg* biofilms. Biofilms were visualized with confocal microscopy and the ratio of green (*Pg*) to red (*Sg*) fluorescence in z-stack images was determined using Volocity image analysis software. Each grid = 21 μm .

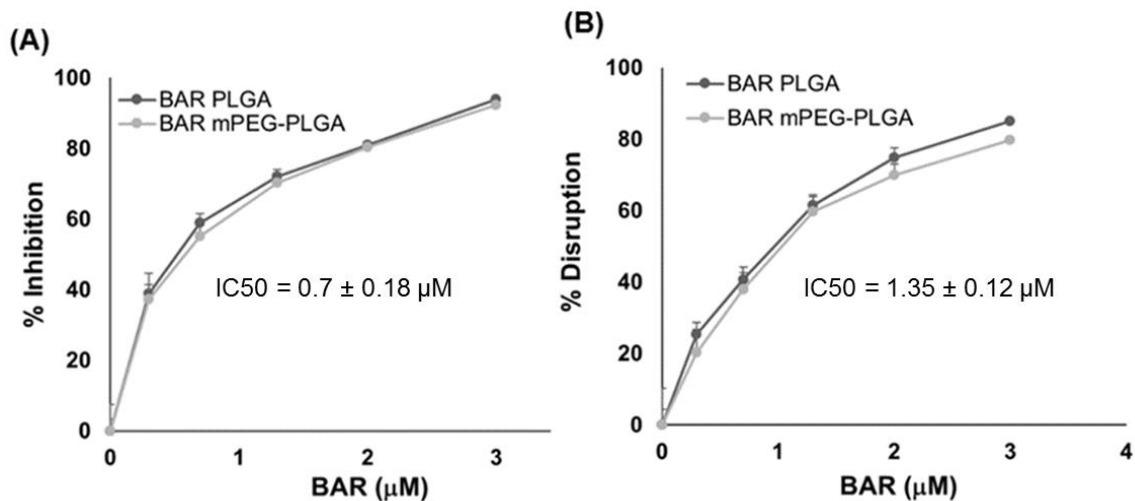


Figure 2.9 Comparison of the concentration of BAR-encapsulated PLGA and mPEG-PLGA NPs needed to (A) inhibit or (B) disrupt *Pg/Sg* biofilms.

Inhibitory Activity of BAR Released from BAR-Encapsulated NPs

To determine the inhibitory potential of BAR-encapsulated NPs, as a function of release duration, *streptococcal* cells were immobilized and *Pg* was incubated with eluate released from $1.3 \mu\text{M}$ BAR-encapsulated PLGA NPs at 1, 2, 4, and 8 hr. BAR-encapsulated PLGA NPs were selected due to their similar release and inhibitory properties, relative to mPEG-PLGA NPs. As shown in **Figure 2.10**, BAR released during the first two hours, inhibited biofilm formation (68% and 32%, respectively) when compared to the control untreated biofilm, whereas BAR released after 4 and 8 hr provided less inhibitory activity against biofilm formation (25% for both time points). These results indicate that BAR-encapsulated NPs release an inhibitory dose of peptide for at least 2 hr.

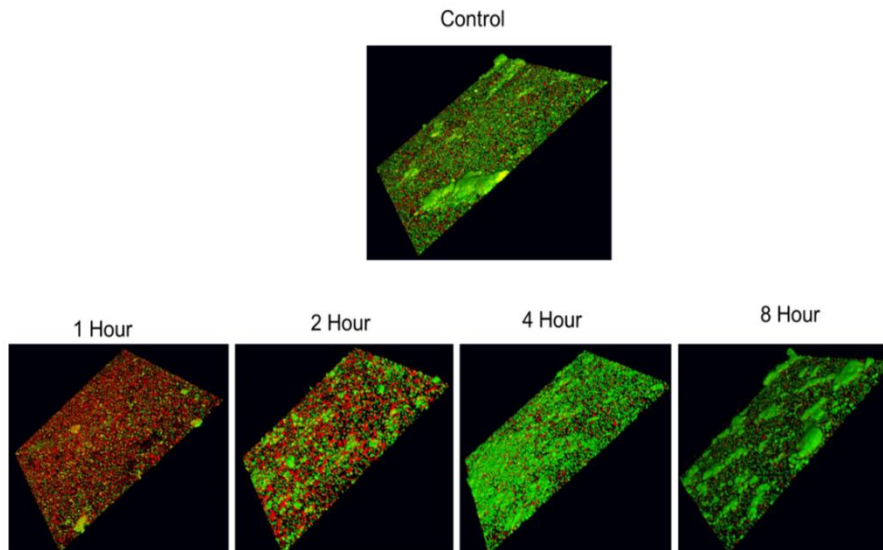


Figure 2.10 BAR-encapsulated PLGA NPs inhibit *Pg* adherence to *Sg* after different durations of release. Biofilms were visualized with confocal microscopy and the ratio of green (*Pg*) to red (*Sg*) fluorescence in z-stack images was determined using Volocity software. Each grid = 21 μm .

Time-Dependent Comparison of Free BAR, BAR-Encapsulated, and BAR Surface-Modified NP Biofilm Disruption

Previous studies demonstrated that BAR surface-modified PLGA NPs potentially disrupt pre-established *Pg/Sg* biofilms⁹⁵. To compare the temporal effect resulting from the administration of the newly formulated BAR-encapsulated NPs, relative to free BAR or previously tested BAR surface-modified NPs, two concentrations of BAR-encapsulated and BAR surface-modified PLGA NPs were compared with free BAR after 1, 2, and 3 hr administration to pre-established biofilms. As shown in **Table 2.3** and **Figure 2.11**, free BAR (3 μM) minimally disrupted pre-existing biofilms during the first hour of application (23%), and

demonstrated a slight increase in disruption after two hours (44%). After 3 hr, free BAR (3 μ M) disrupted 69% of the pre-existing biofilm. In comparison, administration of the same equimolar concentration of BAR-encapsulated NPs (1.3 and 3 μ M) disrupted the established biofilm during the first hour of exposure by 32% and 38%, respectively and demonstrated even more potent disruption (47% and 52%) after two hours. The maximum disruption for 1.3 and 3 μ M doses (66% and 77%, respectively) was achieved after 3 hr exposure to biofilms. Comparatively, both 1.3 and 3 μ M BAR surface-modified NPs disrupted pre-existing biofilms within one hour by 43% and 49%, respectively, and induced more potent biofilm disruption (59% and 69%) after 2 hr exposure, demonstrating statistically significant disruption, relative to disruption induced by free BAR peptide. The highest levels of disruption (71% and 83% respectively) were achieved after 3 hr BAR surface-modified NP administration. Overall, BAR surface-modified NPs were statistically more effective than free BAR ($p < 0.05$) in disrupting established biofilms after 1, 2, and 3 hr administration. However, no statistical differences were observed for BAR-encapsulated NPs ($p > 0.05$), relative to BAR surface-modified NPs or free BAR peptide after 1, 2, or 3 hr administrations.

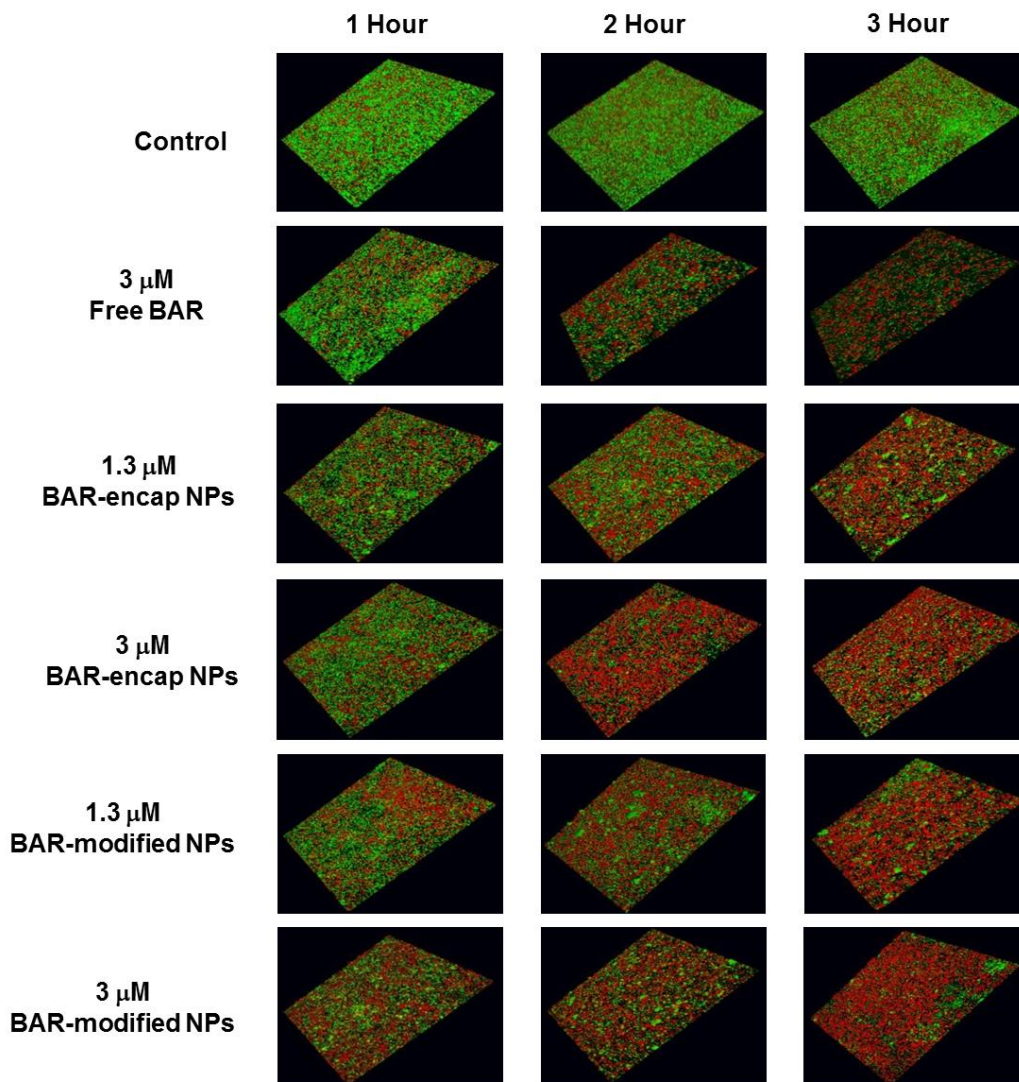


Figure 2.11 Disruption of established *Pg/Sg* biofilms after different exposure times to BAR surface-modified NPs, BAR-encapsulated NPs and free BAR. Biofilms were visualized with confocal microscopy and the ratio of green (*Pg*) to red (*Sg*) fluorescence in z-stack images was determined using Volocity software. Each grid = 21 μm .

Table 2.3 Percent disruption of established biofilms with different treatment groups.

| Time (Hr) | % Disruption of Pre-Formed Biofilms | | | | |
|--------------|-------------------------------------|------------------------------|----------------------------|--------------------------------|------------------------------|
| | Free BAR (3 μ M) | BAR-mod NPs (1.3 μ M) | BAR-mod NPs (3 μ M) | BAR-encap NPs (1.3 μ M) | BAR-encap NPs (3 μ M) |
| 1 | 22.6 \pm 0.2 | 43.4 \pm 0.2 | 48.9 \pm 0.1 | 32.3 \pm 0.1 | 37.7 \pm 0.1 |
| 2 | 44.4 \pm 0.2 | 59.2 \pm 0.1 | 68.7 \pm 0.1 | 46.6 \pm 0.2 | 52.4 \pm 0.2 |
| 3 | 69.0 \pm 0.0 | 71.2 \pm 0.1 | 83.4 \pm 0.0 | 66.1 \pm 0.1 | 77.0 \pm 0.0 |

Discussion

Porphyromonas gingivalis has been identified as a “keystone” pathogen involved in the initiation and progression of periodontal inflammatory disease, by disrupting host-microbe homeostasis and inducing population changes in the subgingival biofilm. This disruption and colonization is initially prompted by the association of *Pg* with oral *streptococci* in the supragingival niche, and is thus an ideal target for therapeutic intervention⁹. Previous studies have shown that BAR peptide inhibits biofilm formation by *Pg* and *Sg* *in vitro* and reduces the virulence of *Pg* in a murine model of infection^{15,17}. While efficacious, BAR effectiveness was limited by the duration of exposure within the oral cavity, and necessitated a higher concentration to disrupt previously established biofilms^{15, 17}. In previous work we sought to address these challenges by synthesizing BAR surface-modified NPs to multivalently inhibit biofilm formation⁹⁵. The goal of this study was to develop,

characterize, and compare BAR-encapsulated NPs that release BAR within a time frame relevant to delivery in the oral cavity.

Nanoparticle characterization revealed that PLGA and mPEG-PLGA BAR-encapsulated NPs exhibited spherical morphologies and average particle diameters of 234.4 ± 19.2 nm and 278.9 ± 13.8 nm, with respective zeta potentials of -13.1 ± 0.4 mV and -5.9 ± 0.1 mV. These values are in agreement with expected values for these polymeric NPs^{89,120}. Both PLGA and mPEG-PLGA NPs were synthesized with 43 μ g of BAR per mg NP, corresponding to loading concentrations deemed feasible for biofilm inhibition with free BAR¹¹¹⁻¹¹³. PLGA and mPEG-PLGA NPs demonstrated relatively high peptide loading with 19.0 ± 0.1 and 16.1 ± 0.2 μ g BAR per mg of NP respectively.

In addition to high loading, PLGA and mPEG-PLGA NPs released 40% and 48% of BAR within the first 4 hr, with no statistically significant differences between release profiles. The NP formulations were designed to achieve therapeutic concentrations of BAR in the oral cavity for a minimum of 2 hr. This initial window of 2 hr release was targeted as we envision formulating NPs in a mouth rinse or toothpaste product. Ideally, in future formulations, we seek to tailor the release of peptide for up to 12 hr since we envision these formulations may be applied once or twice daily, to exert immediate effect over a number of hours.

To assess the functionality of BAR-NPs, the inhibition and disruption concentrations of BAR-encapsulated PLGA and mPEG-PLGA NPs were determined against dual-species biofilms. As shown in **Figures 2.5 through 2.8**,

BAR NPs demonstrated potent inhibition and disruption with IC50s = 0.7 μ M and 1.3 μ M, respectively, with negligible differences observed between PLGA and mPEG-PLGA NPs. To explore the temporal effect of BAR released from PLGA NPs on biofilm inhibition (prevention) in greater depth, the efficacy of BAR-encapsulated NPs was assessed in a dual-species biofilm after 1, 2, 4 and 8 hr post-application. Sufficient BAR release was achieved, relating to inhibitory concentrations of 1.3 μ M during the first 4 hr of administration (**Figure 2.10**). Moreover, the temporal dependence of free BAR, BAR-encapsulated, and BAR surface-modified NPs to disrupt pre-established biofilms (treatment) was measured after 1, 2, and 3 hr application. As shown in **Figure 2.11 and Table 2.3**, BAR-encapsulated and BAR surface-modified NPs achieved moderate biofilm inhibition within 1 hr in a dose-dependent manner; however, similar concentrations of free BAR required prolonged exposure of up to 3 hr to achieve more potent effect. These results demonstrate that BAR-encapsulated NPs provide a feasible alternative to free BAR and BAR surface-modified NPs to target dual-species oral biofilms and provide rapid onset of action. Together, these studies indicate that BAR-encapsulated NPs may serve as a short-term delivery formulation to enhance BAR delivery and potency in the oral cavity. Moreover, by encapsulating versus surface-modifying NPs with BAR, these NPs may offer the potential to specifically target NPs with modifications that can complement BAR activity to engage with these or other bacterial species in future work.

To date, a variety of polymeric nanoparticle formulations have been developed for oral delivery; however, these vehicles have primarily focused on the

delivery of non-specific active agents such as antibiotics^{86,90,91,94,123-128}. Antibiotics such as chlorhexidine^{123,124}, minocycline^{86,94}, clarithromycin¹²⁶, vancomycin¹²⁵, doxycycline¹²⁷, and tetracycline^{90,91,128} are among the antibiotics that have been incorporated into a variety of polymeric vehicles^{86,90,94,124-127} to provide sustained-delivery, prolong activity, exert antibacterial activity, and decrease antibiotic cytotoxicity^{86,90,94,124-127}. Yet, despite antibiotic choice, primary concerns of antibacterial resistance and cytotoxicity remain^{90,123,124}. While chitosan and PLGA NPs that encapsulated chlorhexidine dihydrochloride (CHX) demonstrated strong adherence to tooth surfaces and sustained-release for 48 hr in neutral pH conditions, moderate cytotoxicity due to CHX was observed in human gingival fibroblasts¹²⁴. Similar studies seeking to ameliorate periodontal infection caused by *A. actinomycetemcomitans* and *P. nigrescens* with PLGA lovastatin-chitosan-tetracycline NPs demonstrated potent inhibition up to one week after administration. However, significantly elevated alkaline phosphatase was observed in cells treated with 0.1% or 0.3% tetracycline-loaded nanoparticles on days 7 and 9⁹⁰. Overall, these studies have shown that delivery vehicles have the potential to increase antibiotic effectiveness by decreasing the concentration required. However, bacterial resistance, non-specific targeting, and cytotoxicity concerns with chronic use suggest that the development of more specifically acting active agents will offer safer alternatives for biofilm inhibition.

More recently, specifically targeted biological agents have been investigated to treat periodontal diseases. Delivery of *thyA* gene¹²⁹, Punica granatum extract¹³⁰, *H. madagascariensis* leaf extract¹³¹, miR-146a¹³², and the

anti-inflammatory agent 15d-PGJ2¹³³ have been investigated to vaccinate against and target periodontal diseases. Recent work assessed the delivery of an oral vaccine comprised of an auxotrophic complementation of the *thyA* gene to produce an immune response against *Sg*. Although this study demonstrated promise utilizing *Sg* as a live oral vaccine, to date there are few formulations available to localize or sustain biologic administration to the oral cavity¹²⁹. In other work, PLGA NPs encapsulating a novel anti-inflammatory agent (15d-PGJ2), demonstrated promise in reducing inflammatory response and bone resorption in mouse model of periodontitis after daily administration¹³³, demonstrating the feasibility of combined biologic and delivery vehicle against oral pathogens. Despite this recent progress in the delivery of biological agents for oral applications, currently few biological agents in combination with delivery vehicles have been developed to inhibit keystone-specific interactions during the initial stages of periodontal disease⁹⁵.

In addition to progress in the development of vehicles to encapsulate antibiotic and biological agents in polymeric delivery vehicles, polymeric platforms have also been surface-modified with a variety of molecules including RGD⁹⁴, chitosan^{124,126}, tertiary amines bearing two t-cinnamaldehyde substituents¹³⁴, dimethyl-octyl ammonium¹³⁴, and BAR peptide⁹⁵ to increase the mucoadhesivity (and in the latter case, specificity) of oral delivery formulations.

A variety of polymers have been modified with biological ligands to impart enhanced therapeutic effect^{94,95}. As one example, the delivery of antibiotic

minocycline-loaded poly(ethylene glycol)–poly(lactic acid) (PEG–PLA) nanoparticles have targeted oral epithelial cells by surface-modification with RGD peptides. Surface-modification of PEG-PLA NPs increased epithelial cell attachment and maintained effective drug concentrations in gingival fluid for more than two weeks *in vivo*, relative to unmodified minocycline NPs. Similarly, chitosan-modified polyvinyl caprolactam-polyvinyl acetate-polyethylene glycol graft copolymer (Soluplus) and poly-(DL-lactide-co-glycolide) nanoparticles loaded with clarithromycin, increased antibacterial efficacy and provided sustained-release against oral biofilms¹²⁶. Although this study demonstrated effective treatment of periodontitis, the limitations of antibiotic delivery still pose challenges⁹⁴. Surface modification of nanoparticles has imparted new attributes to target active agents to oral-specific niches. We expect that combining our current work, with surface functionalization demonstrated in our previous study⁹⁵, may confer additional advantages in targeting keystone species by providing prevention and treatment via adhesion and a localized release-mediated platform.

Taken together, our results demonstrate that BAR-encapsulated NPs achieve more potent inhibition and disruption than equimolar free BAR administration. We believe that incorporation of BAR peptide in NPs provides gradual release of BAR peptide, while BAR-modification offers a platform to provide a higher localized concentration of BAR in the oral cavity via multivalent interactions. BAR-encapsulated NPs offer a platform to improve efficacy, and potentially longevity in the oral cavity compared to the transient activity of free BAR. These experimental results will be helpful in developing NPs in therapeutic

formulations such as toothpaste, mouth rinse or chewing gum. Future studies may focus on developing blended polymeric NPs to more gradually release inhibitory concentrations for 8-12 hr. Moreover, combining this platform with surface functionality to provide mucoadhesive or specific interactions with gingival tissue may be pursued to enhance the targeting potential. Ongoing and future work in our groups seeks to assess the efficacy of both BAR-modified and BAR-encapsulated NPs in a murine model of periodontitis.

CHAPTER 3

FUNCTIONAL ASSESSMENT OF PEPTIDE-MODIFIED PLGA NANOPARTICLES AGAINST ORAL BIOFILMS IN A MURINE MODEL OF PERIODONTITIS

Introduction

The most common and currently employed periodontal treatments consist of physical methods such as scaling and root planing to remove the oral biofilm, followed by antibiotic therapy. However, variation in patient response and the immediate reformation of the oral biofilm post-removal can promote disease recurrence. In addition to the challenges associated with mechanical debridement, the administration of local and systemic antibiotics can enhance opportunistic fungal infections, potential allergic reactions, or the emergence of antibacterial resistant species. Moreover, current antibiotics may non-specifically disrupt microbial homeostasis by killing commensal organisms, and often high, frequently administered doses are required to penetrate periodontal biofilms^{35,37,107}. Given these challenges, the development of more specific agents targeting periodontal pathogens has the potential to offer safer and more effective alternatives against oral biofilms.

While several studies have investigated natural and synthetic biologics against oral inflammation and biofilms, including Punica granatum extract¹³⁰, *H. madagascariensis* leaf extract¹³¹, miR-146a¹³², and the anti-inflammatory agent 15d-PGJ2¹³³, our approach has been to target the specific interaction between *Pg* and oral streptococci that contributes to the initial colonization of the oral cavity leading to the development of periodontal disease¹¹¹.

Previous work in our group has shown that *Pg* adherence to streptococci is driven by the interaction of the minor fimbrial antigen (Mfa) of *Pg* with streptococcal antigen (e.g., SspB) I/II (Agl/II)^{109,110}. SspB polypeptide is a multifunctional surface protein of *Sgi* and is a member of antigen I/II complex that is expressed by nearly all streptococci that inhabit the oral cavity. SspB is 1,500 residues in length and includes seven structural domains that are effectively maintained in all antigen I/II polypeptides. Previous studies in our group have shown that the region encompassing residues 1167 to 1250 of SspB (designated BAR) was required for the *in vitro* adherence of *Pg* to *Sg* cells. From these studies, a peptide (designated BAR), was developed that potently inhibited *Pg* adherence to streptococci *in vitro* and reduced *Pg* virulence in a mouse model of periodontitis. However, while BAR inhibited the initial formation of *Pg*/streptococcal biofilms, much higher concentrations of peptide were required to disrupt an established biofilm. In addition, disruption of more complex three-species biofilms containing a bridging organism such as *Fusobacterium nucleatum* also required higher concentration and prolonged exposure to BAR.

Currently, a variety of localized delivery approaches, including gels, implants, fibers, and films are used to deliver antibiotics. These formulations are often administered following the scaling process to retain antibiotics for prolonged duration in periodontal pockets. However, non-degradable implants such as nylon fibers¹³⁵, and acrylic and ethyl cellulose strips^{136,137} require surgical removal, while burst release of active agents is often observed after the administration of films and gels^{94,138}. Recently, polymeric nanoparticles have been investigated as a potential alternative to deliver active agents, due to their proven safety and biocompatibility. Moreover, in contrast to the ubiquitous activity of metallic NPs with inherent antimicrobial efficiency^{139,140}, FDA-approved polymers such as poly(lactic-co-glycolic) acid (PLGA), have demonstrated biocompatibility and flexible tuning of physical properties, enabling tailored drug release and favorable dosing profiles¹¹⁵. In addition, polymer NPs have the ability to impart mucoadhesive properties due to the electrostatic interactions between NPs and gingival epithelium¹¹⁴⁻¹¹⁶. While a variety of polymer types can promote mucoadhesion, NPs synthesized from commonly used polymers, such as PLGA, may achieve mucoadhesion via hydrogen bonding, polymer entanglement with mucins, hydrophobic interactions, or a combination of these mechanisms^{141,142}. Furthermore, NP transport and internalization through the epithelium is dependent on particle size, surface charge, polymer hydrophobicity, mucoadhesivity, and the presence or absence of surface ligands like chitosan or PEG^{116,132,141}. From a fabrication perspective, PLGA NPs are easily synthesized and provide long lasting

formulations that can protect active agents, especially more labile biological agents, thereby maintaining their functional activity.

Given the attributes of PLGA NPs, we sought to address some of the delivery challenges confronting free BAR, including the relatively transient inhibition of *Pg* in the oral cavity and higher localized doses of BAR required to disrupt established biofilm^{111-113,143}. Multivalency is one option to improve the binding of BAR by enhancing the avidity and decreasing the detachment rate from *Pg*^{95,144,145}. Previous studies have demonstrated that multivalently targeted NPs can improve binding, increase localized concentration and decrease the effective therapeutic doses and frequencies^{94,95,121,134,146}. Previous work from our groups demonstrated that BAR-modified NPs (BAR-NPs) delivered a high localized concentration of BAR peptide and improved the *in vitro* effectiveness of BAR through multivalent interactions with *Pg*, relative to free BAR⁹⁵. Thus, we hypothesized that conjugating BAR to the NP surface may similarly decrease the therapeutic dose of BAR required to inhibit biofilm formation *in vivo* through multivalent binding to *Pg*, more effectively inhibiting oral biofilm formation^{95,134}. For oral administration, we administered free BAR and BAR-modified NP with 2% carboxymethylcellulose to test BAR-NPs against the “best” case adhesive formulations to improve retention in the oral cavity and to target *Pg*. In future work, we propose to incorporate BAR-NPs in a mouthwash or gel formulation to be applied twice daily. Here our goal was to advance our previous *in vitro* work to assess the *in vivo* efficacy and safety of BAR-modified NPs in a murine model of periodontitis and in gingival and erythrocytic cell lines.

Materials and Methods

Peptide Synthesis

BAR peptide is comprised of residues 1167 to 1193 of the SspB (Antigen I/II) protein of *Sg* with the sequence NH₂-LEAAPKKVQDLLKKANITVKGAFQLFS-COOH¹¹². To facilitate conjugation of BAR to the NP surface, the peptide was synthesized with an N-terminal biotin. Biotinylated BAR was subsequently attached to NPs that had been modified with palmitylated avidin. To enable peptide quantification and detection, some preparations of BAR were modified such that the epsilon amine of the underlined lysine residue of BAR was covalently reacted with 6-carboxyfluorescein to produce fluorescent BAR (F-BAR). All preparations of peptides were synthesized by BioSynthesis, Inc. (Lewisville, TX) and were guaranteed to have greater than 90% purity via RP-HPLC analysis.

BAR Surface-Modified Nanoparticle Synthesis

BAR surface-modified NPs were synthesized using a previously described single-emulsion technique^{88,121}. PLGA with a 50:50 monomer ratio and 0.55–0.75 dL/g inherent viscosity, was purchased from LACTEL®. Briefly, 100 mg PLGA was dissolved in 2 mL dichloromethane (DCM) overnight. The following day, 2 mL of a 5% (w/v) polyvinyl alcohol (PVA) solution was mixed with 2 mL of 5 mg/mL avidin-palmitate. The 2 mL PLGA/DCM solution was added dropwise to 4 mL PVA/avidin-palmitate solution while vortexing. The NP solution was added to 50 mL of 0.3% PVA for 3 hr to evaporate residual DCM. After evaporation, the NP solution was centrifuged at 13,000 rpm (20,442 x g) at 4°C. Supernatant was

discarded, and the pelleted NPs were resuspended in 10 mL phosphate buffered saline (PBS) for 30 min on a benchtop rotator, with biotinylated BAR peptide at a molar ratio of 6:1 BAR:avidin (18 nmol/mg) in PBS. After conjugation, the NPs were washed two times with deionized water (diH₂O) by centrifugation at 13,000 rpm (20,442 x g) at 4°C to obtain NPs with sizes less than ~200 nm. After washing, BAR surface-modified NPs were suspended in 5 mL of diH₂O, frozen at -80°C, and lyophilized. F-BAR-modified NPs were synthesized similarly, but were protected from light during synthesis.

NP Characterization: NP Morphology, Size, BAR Conjugation

Unhydrated NP morphology, diameter, and size distribution were determined using scanning electron microscopy (SEM) (XL-30 ESEM-FEG SEM, FEI Company, USA). Lyophilized NPs were mounted on carbon tape and sputter coated with a thin layer of gold/palladium. Average diameters of 500 particles were determined from SEM images (n=3) using image analysis software (ImageJ, National Institutes of Health, version 1.5a, ImageJ.nih.gov). Dynamic light scattering and zeta potential analyses were performed to determine the hydrodynamic diameter and surface charge of hydrated NPs. The unhydrated and hydrated diameters of NPs are typically assessed to establish the size characteristics within different conditions of dry storage and more physiologically relevant aqueous environments. Briefly, a 1 mg/mL sample of BAR-modified PLGA NPs in diH₂O was prepared. After vortexing and sonication, samples were diluted at a 1:50 ratio in diH₂O. One mL was aliquoted to the cuvette for analysis [Malvern,

Malvern, UK (Zetasizer Nano ZS90), courtesy of Dr. Martin O'Toole, Univ. of Louisville] to measure dynamic light scattering and zeta potential with Zetasizer Nano software. Samples were run in triplicate, using a refractive index of 1.57 for PLGA, absorption coefficient of 1, and water refractive index of 1.33. The equations used by the Zetasizer to calculate nanoparticle size are shown in Supplementary Data.

To measure the amount of BAR peptide that was conjugated to the NP surface, a fluorescence binding assay was conducted with F-BAR NPs. After conjugation, NPs were centrifuged and washed twice with diH₂O to remove unbound BAR from the formulated NPs. NPs were then suspended in 1X PBS to create a 1 mg/mL NP solution and the resulting samples were transferred to a microtiter plate in triplicate. Total NP-associated fluorescence was determined using Victor3 Multilabel spectrophotometer (488/518 nm excitation/emission), and peptide quantity was determined from a standard curve of known F-BAR concentrations⁹⁵. The stability of the avidin palmitate interaction with the NP surface has been previously tested by assessing the release of avidin and biotinylated ligand from the NP surface with respect to time^{146,147}. In addition, the functional stability of BAR-NPs was tested through *in vitro* inhibition assays against biofilms prior to these *in vivo* experiments⁹⁵.

Growth of Bacterial Strains

Pg (ATCC 33277) was grown in Trypticase soy broth (Difco Laboratories Inc., Livonia, MI, USA) supplemented with 0.5% (w/v) yeast extract, 1 µg/mL

menadione, and 5 µg/mL hemin. The medium was reduced for 24 hr under anaerobic conditions (10% CO₂, 10% H₂, and 80% N₂) and *Pg* was subsequently inoculated and grown anaerobically for 48 hr at 37°C. *Sg* DL-1 was cultured aerobically without shaking in brain-heart infusion broth (Difco Laboratories Inc.) supplemented with 1% yeast extract for 16 hr at 37°C¹¹¹⁻¹¹³.

***In Vivo* Model of Periodontitis**

The protocols used for the study were approved by the Institutional Animal Care and Use Committee (IACUC) at the University of Louisville, as described in the federal guidelines for the care and use of laboratory animals. Ten weeks-old specific-pathogen-free BALB/cByJ mice were obtained from the Jackson Laboratory (Bar Harbor, ME) and housed in the University of Louisville Research Resource Center animal facility. The mice were fed with Lab Diet 5001 meal (Purina Mills, LLC, Gray Summit, MO) during the entire experiment.

The oral infection of mice was performed as previously described¹¹³. A total of 8 mice per group were used per experiment. Animals were initially treated with sulfamethoxazole (MP Biomedical, Solon, OH) at a final concentration of (800 µg/mL) and trimethoprim (Sigma, St. Louis, MO) at a final concentration of (400 µg/mL) ad libitum for 10 days, every two days. Four days after the last antibiotic treatment, all groups of mice with the exception of the sham-infected control group were orally infected with 10⁹ CFU of *Sg* cells suspended in 1 mL of 2% carboxymethylcellulose (CMC; MP Biomedical, Solon, OH) in sterile PBS using a 2.25 mm feeding needle (Popper and Sons, Inc., New Hyde Park, NY). *Sg* was

administered five times in total, every two days. Sham-infected animals received CMC without bacteria. Following confirmation of *Sg* colonization by PCR, two groups of animals were infected five times with 10^7 CFU of *Pg* in CMC containing BAR (0.7 and 3.4 μM) at two day intervals and another group was infected five times with 10^7 CFU of *Pg* in CMC containing BAR-NPs (BAR concentration = 0.7 μM) at two day intervals. Two additional groups of animals were infected either with *Pg* alone or *Sg* alone. After the infection process, all animals were subsequently rested for 47 days with daily observation to record death or sickness and then euthanized via CO_2 asphyxiation.

Infection Confirmation

Sg and *Pg* colonization were confirmed by collecting oral samples from the gingiva of the upper molars using a 15 cm sterile polyester-tipped applicator (Puritan Medical Products Co., Guilford, ME), 14 days after the last oral infection. Samples were then added to 10 mL of brain-heart infusion broth (Difco Laboratories Inc.) for streptococcal species enrichment and trypticase soy broth (Difco Laboratories Inc., Livonia, MI, USA) supplemented with 0.5% (w/v) yeast extract, 1 $\mu\text{g}/\text{mL}$ menadione, and 5 $\mu\text{g}/\text{mL}$ hemin to select for *Pg*. Samples were incubated at 37°C for 24 hr under anaerobic conditions. The resulting cells were identified by PCR using *Sg*- and *Pg*-specific primers¹¹³.

Determination of Maxillary Alveolar Bone Loss

Mouse skulls were autoclaved for 15 min to remove skin and muscles, and were subsequently soaked in 3% hydrogen peroxide overnight at room temperature to remove remaining muscle. Skulls were washed with diH₂O and cleaned with a 1% bleach solution for 30 s, sonicated at 14 V for 1 min, and washed again with diH₂O. To confirm skull cleaning, toothpaste was applied and brushed away, followed by immersion in a 1% bleach solution for 30 s and sonication (14 V). To stain the skulls, skulls were immersed in 1% methylene blue for 15 s and rinsed with DI water to remove excess dye. The stained skulls were air-dried prior to alveolar bone loss measurements. Bone loss was assessed by measuring the distance between the alveolar bone crest (ABC) and the cemento-enamel junction (CEJ) at 7 sites on the buccal side of the right and left maxillary molars for a total of 14 measurements. This was accomplished using a dissecting microscope fitted with a video imaging marker measurement system (model VIA-170K; Fryer) at a total magnification of 40x¹¹³. Measurements were taken in millimeters. The average of the total bone loss for each mouse group was assessed and subtracted from the baseline bone loss observed in sham-infected mice. Statistical differences in bone loss were analyzed by ANOVA after passing Bartlett's and Brown-Forsythe tests for homogeneity of variances using GraphPad InStat (La Jolla, CA). A pairwise, parametric analysis of variance using a Bonferroni multiple comparison post-test was used to determine the statistical difference among the individual mouse groups. A *P* value of ≤ 0.05 was considered to be statistically significant.

Histological Analysis

Samples of maxillary molar regions were dissected from each mouse, and then fixed in 4% paraformaldehyde overnight. Periodontal tissues were dehydrated by passing through ascending concentrations of ethanol then cleared in xylene and embedded in paraffin. Serial sections (5-6 μm) were cut and mounted on glass slides (Sigma, St. Louis, MO). Microscopic examination for slides was carried out after hematoxylin and eosin staining¹⁴⁸.

Immunofluorescence Assay

An immunofluorescence assay was used to assess IL-17 expression in gingival sections. Tissue sections, 5-6 μm in thickness, were mounted on glass slides. Tissue sections were deparaffinized by immersion in xylol two times for 15 min each, and rehydrated in absolute, 95% and 70% ethanol. Excess ethanol was removed then slides were placed in water. Antigen IL-17 was recovered by microwave heating in water and non-specific binding was blocked with 5% bovine serum albumin for 1 hr. Then, slides were incubated for 24 hr at 4°C with IL-17A monoclonal antibody AlexaFluor 488 (eBioscience™), examined via confocal microscopy, and IL-17 immunofluorescence was quantified using Volocity software¹⁴⁹.

Tissue Culture

Telomerase immortalized gingival keratinocytes (TIGKs) were grown on 24-well collagen-coated plates (Becton Dickinson, Bedford, MA) and cultured using

DermaLife K Calcium Free Medium (LifeFactors®) supplemented with penicillin/streptomycin (100 U/mL final concentration; St. Louis, MO), recombinant human (rh) insulin (5 µg/mL), L-glutamine (6 mM), epinephrine (1 µM), apo-transferrin (5 µg/mL), rh TGF-α (0.5 ng/ mL), extract P™, hydrocortisone hemisuccinate (100 ng/mL), and calcium chloride (0.06 mM). The epithelial cells were incubated at 37°C in the presence of 5% CO₂ for 6 days until they reached 95% confluence. The cells were washed and administered media without antibiotics during toxicity testing.

Determination of BAR and BAR-NP *In Vitro* Cytotoxicity

Hemolytic Assay: A total of 250 µL of 1% sheep erythrocytes (Rockland Inc, Pennsylvania, USA) was suspended in sterile PBS containing 5% fetal bovine serum (FBS buffer). BAR-NPs or free BAR peptide were suspended in FBS at concentrations of 1.3 and 3.4 µM (the maximum concentrations used in *in vitro* and *in vivo* studies) and were added to the erythrocyte suspension. The mixtures were incubated at 37°C for 3 hr. After centrifugation (3,500 x g), hemoglobin released due to cell lysis was analyzed by spectrophotometry at 541 nm. A positive control group was run in which PBS was replaced with diH₂O.

MTT Assay: TIGK cells were seeded in 12-well plates at a density of 6 x 10⁴ cells in 1 mL media per well, and incubated for 24 hr to allow for 60–70% confluency and sufficient adhesion. Cells were treated with 1.3 or 3.4 µM of free BAR or BAR-NPs. After 24 hr, 100 µL of MTT solution (10% of total volume) was added to the media of all samples. The solution was incubated at 37°C for 4 hr. After this period,

550 μL of lysis buffer (50% of total volume) was added to the media of each well and plates were incubated for overnight. The absorbance of each well was read at 570 nm, and the sample absorbance was normalized to the absorbance of untreated cells (media only). Treatment with 10% DMSO media (100 μL DMSO in 900 μL media) was used as a positive control for cell death.

ATP Assay: Total ATP levels in cell culture were assessed by using the CellTiter-Glo reagent (Promega, Madison WI), as described by the manufacturer. TIGK cells were seeded at a density of 6×10^4 cells in 1 mL media per well and incubated at 37°C, 5% CO_2 for 24 hr in a 12-well flat bottom plate. Cells were then incubated with free BAR or BAR-NPs (1.3 or 3.4 μM) for 24 hr at 37°C in 5% CO_2 . Cells were then lysed with 500 μL of 0.1% Triton X-100 for 30 min at 37°C. The lysates were collected and centrifuged at 1,000 x g for 10 min at 4°C, and 50 μL of supernatant was mixed with 50 μL of CellTiter-Glo reagent. Samples were incubated at ambient temperature for 10 min in a black 96-well plate in the dark. Total luminescence was measured with a Victor 3 luminometer (Perkin-Elmer, Inc). Cells incubated with 1 ng of staurosporine or with medium only served as positive and negative controls for cell death, respectively.

LDH Assay: Cell membrane leakage was measured by the release of lactate dehydrogenase (LDH). Extracellular LDH was quantified using a CytoTox96® non-radioactive cytotoxicity assay (Promega, Madison WI) as described by the manufacturer. TIGK cells were plated at density of 6×10^4 cells in 1 mL media per well in a 12-well flat bottom plate, and incubated at 37°C, 5% CO_2 for 24 hr. Free

BAR or BAR-NPs (1.3 or 3.4 μM) were added to cells in triplicate for 24 hr at 37°C in 5% CO_2 . Fifty microliters of supernatant from free BAR and BAR-NP-treated (1.3 and 3.4 μM) cells were added to the LDH substrate and incubated at room temperature for 30 min. The reactions were subsequently terminated by adding 50 μL of stop solution. LDH activity was determined by measuring the optical density of the solution at 490 nm. Cells treated with staurosporine or with medium only served as positive and negative controls for cell death, respectively.

Apoptosis: The degree to which free BAR or BAR-NPs (1.3 or 3.4 μM) induced apoptosis in TIGK cells was determined using the PE Annexin V/Dead Cell Apoptosis Kit with SYTOX® Green for Flow cytometry (Invitrogen). TIGK cells were cultured in 12-well microtiter plates with an initial density 2×10^5 cells in 1.5 ml media. After 24 hr at 37°C, the medium was decanted, replaced with fresh medium containing the desired concentration of BAR or BAR-NPs and incubated for an additional 18 hr. The cells were washed with PBS, trypsinized and centrifuged at 250 x g. The cell pellet was suspended in 100 μL of binding buffer supplemented with 1 μL Sytox and 5 μL Annexin fluorescent dye and incubated for 15 min at 37°C. Samples were then diluted by addition of 400 μL binding buffer and analyzed by flow cytometry using a FACScalibur flow cytometer (Becton Dickinson), measuring the fluorescence emission at 530 nm and 575 nm. Cells treated with 2 mM hydrogen peroxide or medium only for 4 hr at 37°C and 5% CO_2 , served as positive and negative controls for apoptosis.

Statistical analysis

Data from each of the toxicity tests and IL-17 ELISA were analyzed using ANOVA after passing Bartlett's and Brown-Forsythe tests for homogeneity of variances using GraphPad InStat (La Jolla, CA). A pair-wise, parametric analysis of variance using a Bonferroni multiple comparison post-test was used to determine the statistical difference among the individual groups. A *P*-value of ≤ 0.05 was considered to be statistically significant.

Results

Nanoparticle Characterization

The morphology of BAR-NPs, relative to unmodified NPs, is shown in **Figure 3.1**. BAR-NPs demonstrated a spherical morphology without any observed changes resulting from conjugation with BAR peptide. The average unhydrated diameters of BAR-NPs and unmodified NPs measured from SEM images were 87.9 ± 29.4 nm and 155.8 ± 37.6 nm, respectively. In comparison, the average hydrated diameters of BAR-NPs and unmodified NPs, as measured with dynamic light scattering (Malvern Zetasizer) were 333.8 ± 17.8 nm and 312.6 ± 11.2 , respectively. This is in agreement with previous data demonstrating that BAR-NP hydrated diameters were higher than unhydrated diameters⁹⁵. The addition of positively charge avidin and subsequent conjugation with BAR increased the overall charge of BAR-NPs to -10.3 ± 0.9 mV, relative to unmodified PLGA NPs (-22.6 ± 1.2 mV), demonstrating BAR conjugation to the PLGA NP surface (**Table 3.1**).

Table 3.1 Physical characterization of NP diameter and surface charge. Data represent the mean \pm standard deviation of at least 3 independent samples.

| NP Type | Unhydrated Diameter (nm) | Hydrated Diameter (nm) | Zeta Potential (mV) |
|------------------------------|--------------------------|------------------------|---------------------|
| BAR-Modified PLGA NPs | 87.9 \pm 29.4 | 333.8 \pm 17.8 | -10.3 \pm 0.9 |
| Unmodified PLGA NPs | 155.87 \pm 37.6 | 312.6 \pm 11.2 | -22.6 \pm 1.2 |

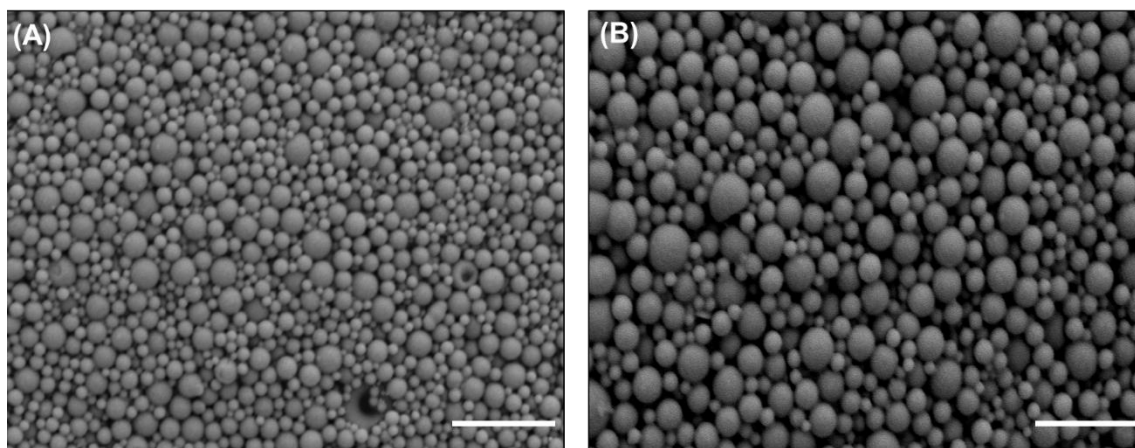


Figure 3.1 SEM images of (A) BAR-modified PLGA NPs and (B) Unmodified PLGA NPs. Scale bar represents 1 μ m. Images are representative of a minimum of 3 independent samples, with $n > 500$ NPs assessed in total.

Quantification of BAR Conjugation

The amount of BAR peptide conjugated to PLGA NPs was determined using fluorescence spectroscopy, and the fluorescence was compared to a known standard of F-BAR. Previous work in our groups has shown that 3 nmol avidin conjugated per mg of PLGA NPs and avidin has four binding sites, with the potential to bind 12 nmol of BAR, if all avidin sites were available^{95,146,150}. Loading

experiments demonstrated that 7.1 nmol of BAR were bound per mg of PLGA NPs (corresponding to 9024 BAR ligands/mg of NP), with a conjugation efficiency 40%.

Alveolar Bone Loss

The effectiveness of free BAR and BAR-NPs to inhibit *Pg* virulence was evaluated by measuring *Pg*-induced alveolar bone loss. Microscopic images of the maxilla of sham-infected, *Pg/Sg* infected, free BAR and BAR-NP-treated mice are shown in **Figure 3.2**. Quantification of alveolar bone loss showed that mice that were infected with both *Sg* and *Pg* exhibited significantly ($P \leq 0.0001$) increased bone loss (-1.37 ± 0.31 mm), relative to uninfected mice or animals infected with *Sg*-only (-0.33 ± 0.07 mm) or *Pg*-only (-0.44 ± 0.025 mm). Mice that were infected with both *Sg* and *Pg* and treated with 0.7 or 3.4 μM free BAR exhibited a significant reduction in bone loss (-0.69 ± 0.1 mm and -0.56 ± 0.09 mm, respectively), relative to infected untreated animals ($P \leq 0.0001$). Mice that were treated with 0.7 μM BAR-NP exhibited levels of bone loss (-0.24 ± 0.05 mm) that approached uninfected animals. Moreover, 0.7 μM BAR-NP-treated mice showed bone loss levels that were significantly lower than bone loss observed in 0.7 or 3.4 μM free BAR-treated mice ($P \leq 0.0001$ and $P \leq 0.01$, respectively) (**Figures 3.3**).

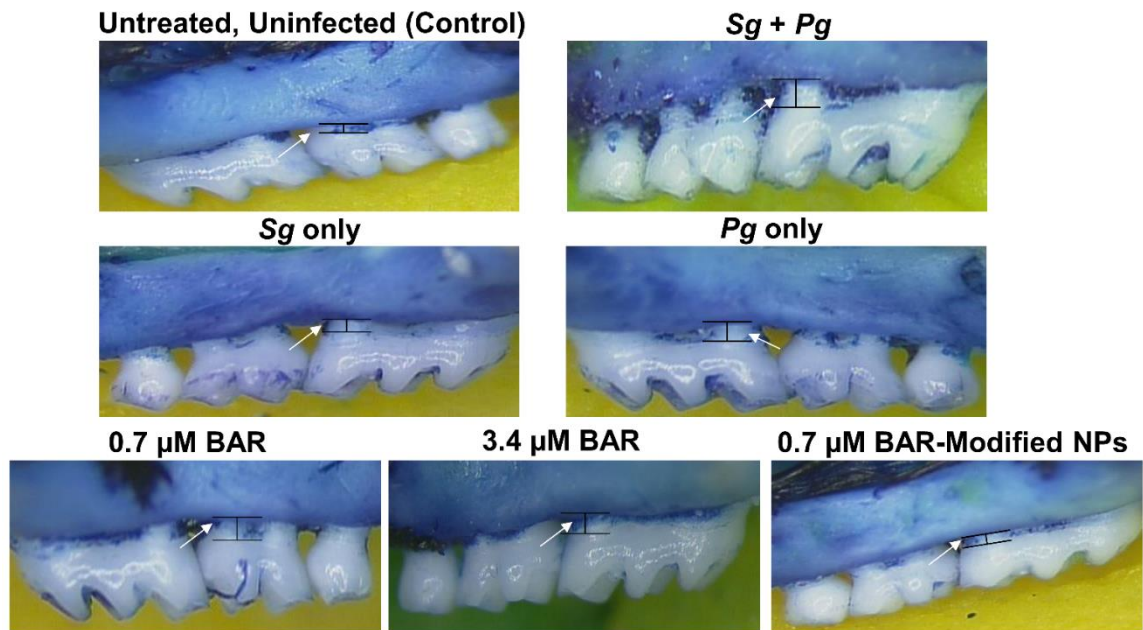


Figure 3.2 Representative images from different *in vivo* treatment groups (n=8 per group), of the area between the cemento-enamel junction (CEJ) and alveolar bone crest (ABC), measured to determine bone loss. Images were taken using a dissecting microscope fitted with a video imaging marker measurement system (Sony model VIA-170K; Fryer) at a total magnification of 40x.

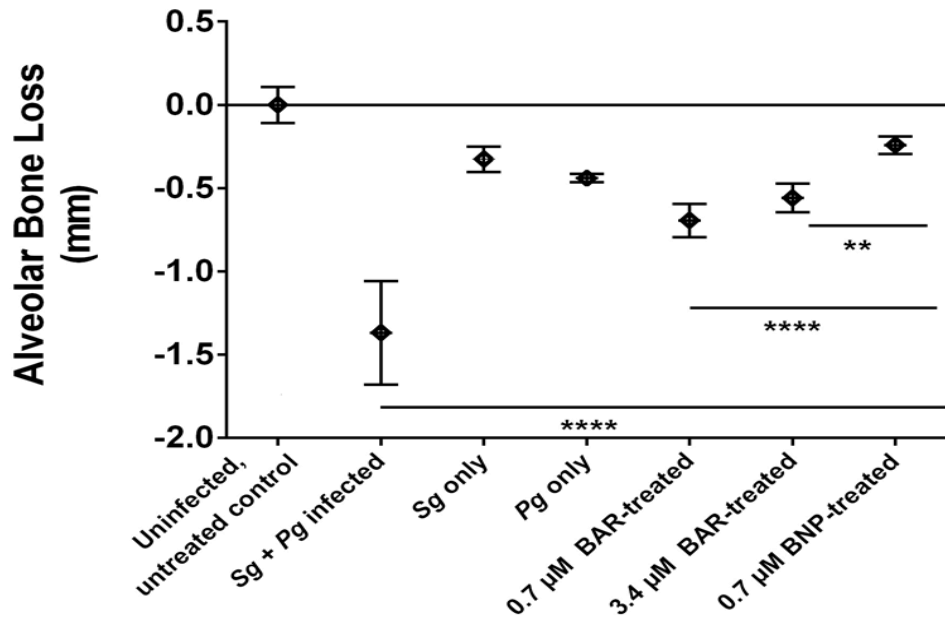


Figure 3.3 Alveolar bone loss in each group relative to uninfected, untreated control mice. BAR-NP-treated mice showed significant reduction of bone loss relative to high and low concentrations of free BAR-treated mice. Data represent the mean \pm standard deviation (n=8). Statistical differences between groups are denoted by **, $P \leq 0.01$; ****, $P \leq 0.0001$).

Histological analysis

Representative histopathological images of gingival tissues of all mice are shown in **Figure 3.4**. Untreated uninfected gingival tissue shows normal structure without inflammatory cell infiltration. However, heavy infiltration of inflammatory cells and engorgement of blood vessel are observed in gingival tissue of *Pg/Sg* infected mice as a sign of chronic inflammation, as depicted with black arrows (**Figure 3.4B**). While, gingival tissues of free BAR and BAR-NP-treated mice exhibit normal structure with minimal infiltration of inflammatory cells (**Figure 3.4C-**

E), suggesting that free BAR and BAR-NPs inhibit biofilm formation and consequently periodontitis. Mice treated with 0.7 μM BAR demonstrated higher levels of inflammatory cell infiltration relative to control mice; however, still lower than that observed in *Pg/Sg* infected mice.

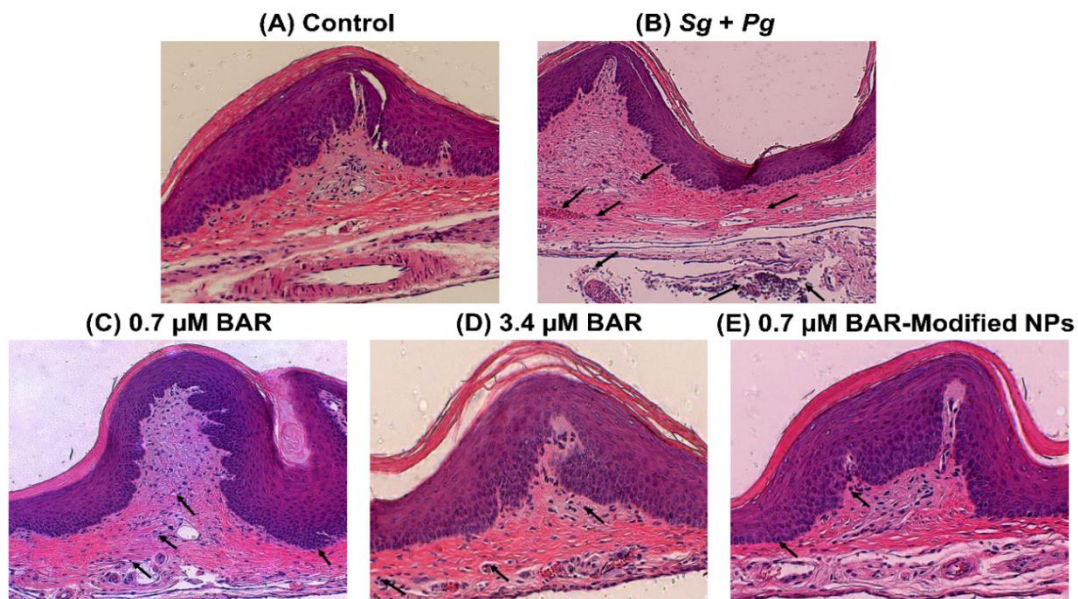


Figure 3.4 Histological sections of murine periodontal tissues, with inflammatory cell infiltration denoted with black arrows. (A) Periodontal tissue of uninfected, untreated (control) mice shows normal histological structure without inflammatory cell infiltration. (B) Periodontal tissue of *Pg/Sg* infected mice demonstrates prominent chronic inflammation through proliferation of connective tissue and heavy infiltration of inflammatory cells. (C) Periodontal tissue of mice treated with 0.7 μM BAR exhibits medium infiltration of inflammatory cells. (D) & (E) Periodontal tissues treated with a higher concentration of free BAR (3.4 μM) or BAR-NPs show normal histological structure with minimal infiltration of inflammatory cells. (H&E, 100x).

IL-17 in Periodontal Tissues

To determine whether free BAR and BAR-NPs reduced gingival inflammation, IL-17 levels in gingival tissues were evaluated across all treatment groups (see **Figures 3.5A and 3.5B**). The gingival tissue of *Pg/Sg* infected mice and mice treated with 0.7 μ M free BAR demonstrated a statistically significant increase in IL-17 gingival tissue fluorescence (~2-fold, $P \leq 0.0001$ and ~1.5-fold, $P \leq 0.01$) relative to uninfected mice. In contrast, animals treated with 3.4 μ M free BAR or with BAR-NPs exhibited only a slight increase in IL-17 fluorescence (~1.13-fold), whereas mice treated with 0.7 μ M free BAR showed a ~1.5-fold increase in IL-17 fluorescence significantly higher than BAR-NP treated mice ($P \leq 0.05$). These results are consistent with the histological analysis of gingival tissues.

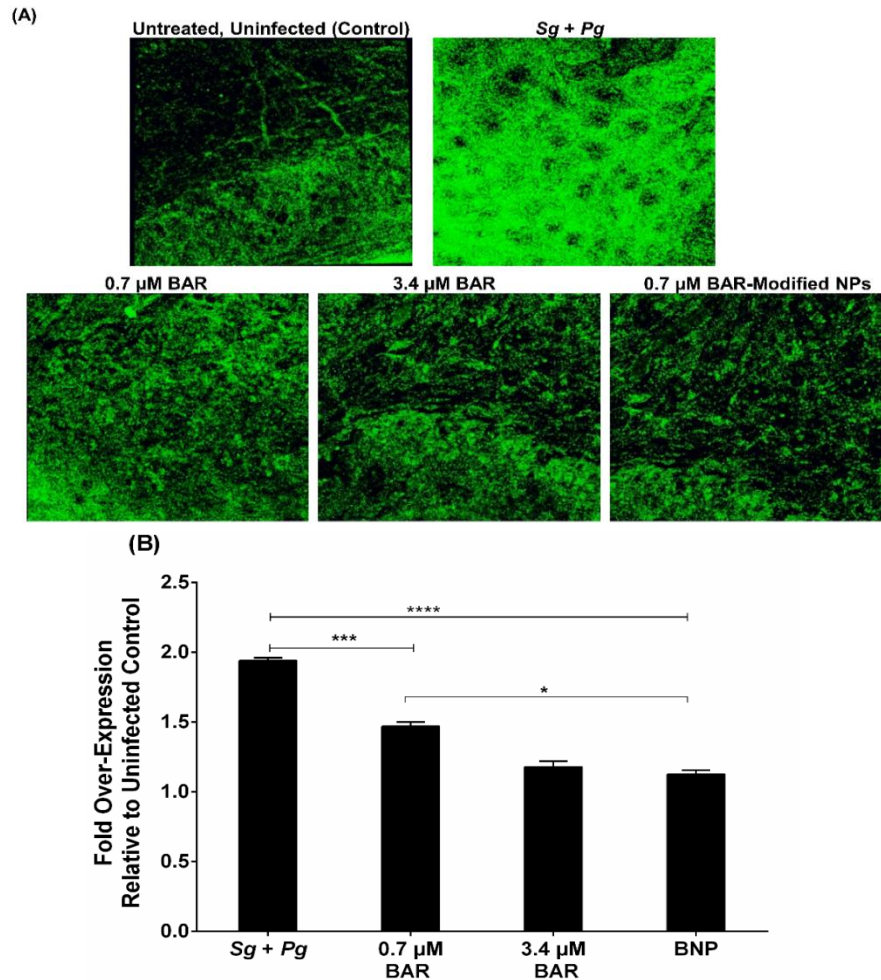


Figure 3.5 (A) Immunofluorescence staining of IL-17 on gingival tissue demonstrated strong staining of the *Pg* and *Sg* infected group compared to the uninfected, untreated; 0.7 μM BAR; 3.4 μM BAR; and BAR-NP-treated groups. (B) Quantification of IL-17 levels show that free BAR and BAR-NP-treated groups had similar IL-17 expression relative to the untreated, uninfected mice; however, mice treated with a lower concentration (0.7 μM) of free BAR showed slightly higher, statistically significant IL-17 levels relative to untreated, uninfected and BAR-NP-treated mice. Data represent the mean \pm standard deviation ($n=5$); (*, $P \leq 0.05$, ***, $P \leq 0.001$ ****, $P \leq 0.0001$).

Determination of BAR and BAR-NP *In Vitro* Cytotoxicity

Hemolytic Assay: The cytotoxicity of free BAR and BAR-NPs was initially evaluated by measuring the hemolytic activity against 1% sheep red blood cells (RBCs). As shown in **Figure 3.6A**, RBCs that were incubated with free BAR or BAR-NPs (1.3 or 3.4 μM), or with PBS (control) showed no hemolysis, suggesting that free BAR or BAR-NPs have negligible hemolytic activity in erythrocytes.

MTT Assay: To assess the effect of free BAR or BAR-NPs on the viability of TIGK cells, cultures were incubated with 1.3 or 3.4 μM free BAR for 2 d and viability was measured using MTT. As shown in **Figure 3.6B**, treated cells exhibited little loss in viability, suggesting that free BAR and BAR-NPs are biocompatible with TIGK cells when applied for up to 2 d.

ATP Assay: Cytotoxicity was also determined by assessing the metabolic activity of TIGK cells by measuring ATP levels. As shown in **Figure 3.6C**, staurosporine-treated cells demonstrated significantly lower levels of ATP ($P \leq 0.0001$) than were observed for uninfected, untreated; free BAR; and BAR-NP-treated cells. Although the levels of ATP in free BAR and BAR-NP-treated cells were statistically different from control cells, their levels were still elevated relative to staurosporine-treated cells.

LDH Assay: Since some peptides are known to damage the cell membrane, we next measured LDH activity as a marker for cell membrane integrity after treatment with free BAR or BAR-NPs. **Figure 3.6D** shows that LDH levels released from cells treated with free BAR or BAR-NPs (1.3 or 3.4 μM) was negligible when

compared to control (medium treated) cells. In contrast, LDH activity released from cells treated with staurosporine was significantly ($P \leq 0.0001$) higher than control or treated cells, suggesting that free BAR and BAR-NPs do not compromise cell membrane integrity. Finally, we examined the ability of free BAR or BAR-NPs to induce apoptosis in TIGK cells. Flow cytometry results showed the presence of minimal apoptotic populations (lower right quadrant) when cells were incubated with 1.3 and 3.4 μM free BAR (3.5 and 14.9%, respectively) or BAR-NPs (12.2 and 14.2%). In contrast, 89% of cells were apoptotic after treatment with 2 mM hydrogen peroxide (**Figure 3.7, Table 3.2**). These results indicate that free BAR and BAR-NPs do not induce prominent apoptosis of TIGK cells.

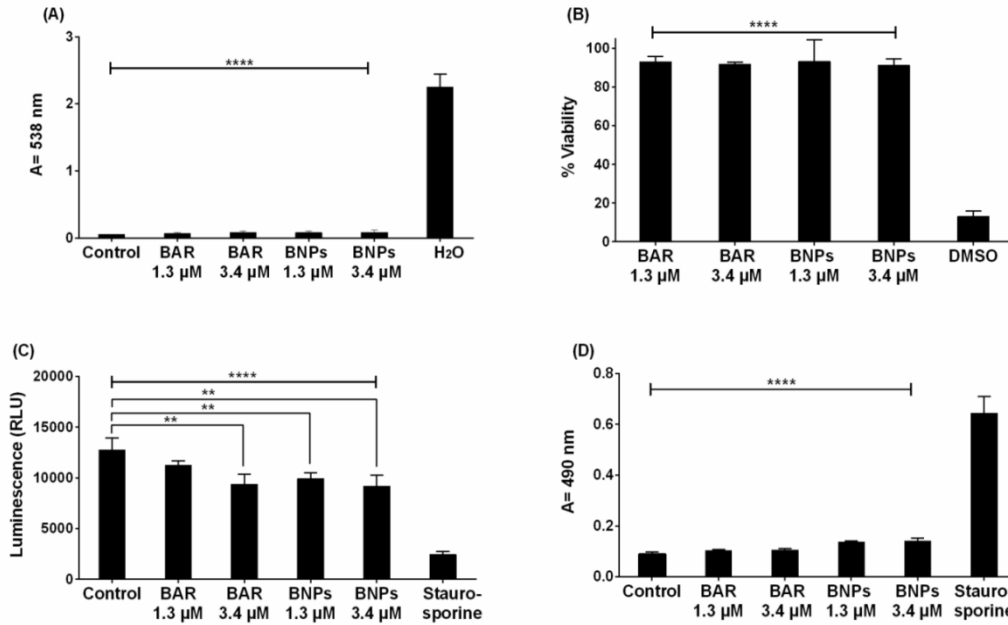


Figure 3.6 (A) The hemolytic activity of free BAR or BAR-NPs (1.3, 3.4 μM) was assessed after administration to sheep erythrocytes for 3 hr. Hemoglobin release from free BAR and BAR-NP-treated cells was negligible relative to release from H₂O-treated cells (****, $P \leq 0.0001$). (B) TIGK cell viability was assessed after free BAR or BAR-NPs administration for 2 days. Free BAR and BAR-NPs were non-toxic, relative to cells treated with DMSO (****, $P \leq 0.0001$). (C) ATP levels from free BAR (3.4 μM) and BAR-NP-treated (1.3, 3.4 μM) cells showed decreases in ATP concentration, relative to control cells (treated with medium only), while ATP levels in the staurosporine-treated cells were significantly lower than the control (treated with medium only), free BAR, and BAR-NP-treated cells (****, $P \leq 0.0001$). (D) No significant release of LDH was observed from TIGK cells treated with free BAR and BAR-NPs, relative to control cells. Staurosporine-treated cells demonstrated significantly elevated LDH levels (****, $P \leq 0.0001$). Data represent the mean \pm standard deviation (n=5).

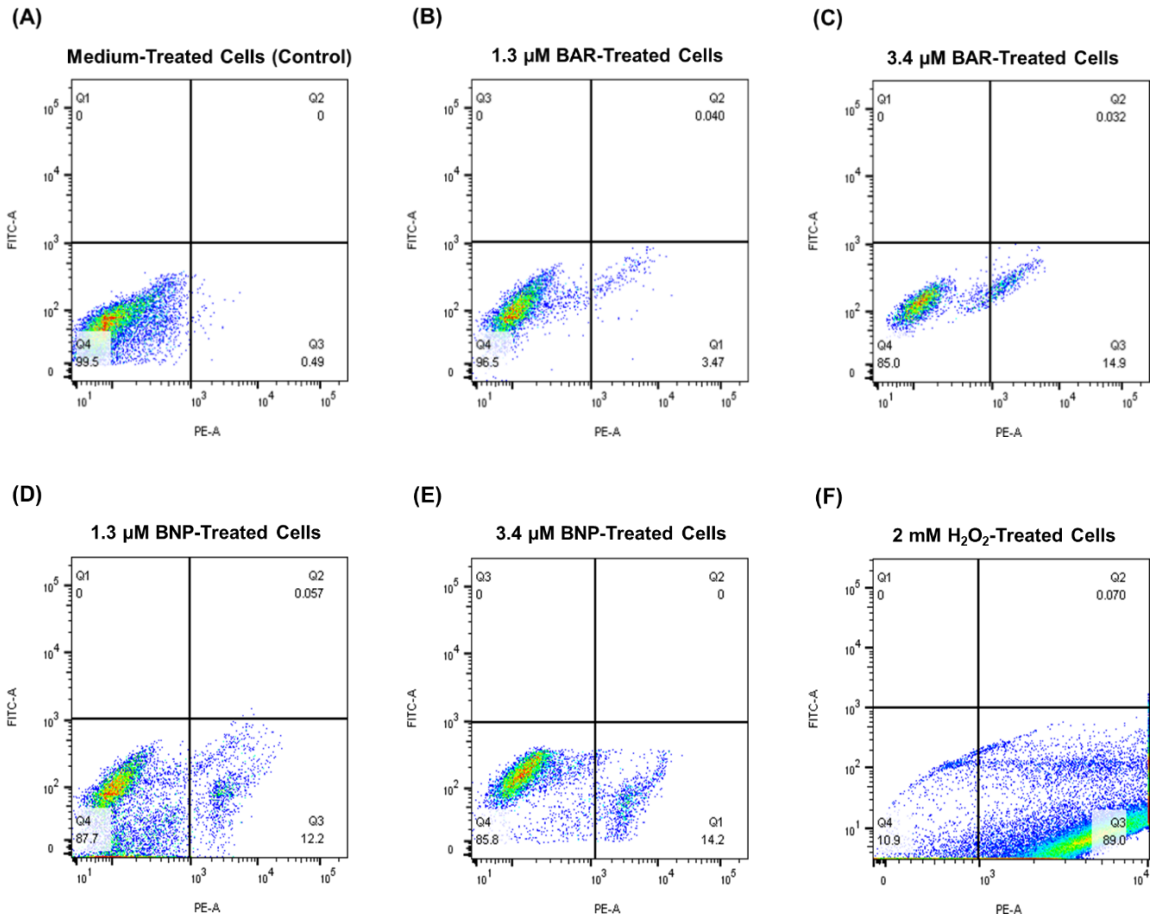


Figure 3.7 TIGK cells were treated with (A) medium alone, (B) 1.3 μM free BAR, (C) 3.4 μM free BAR, (D) 1.3 μM BAR-NPs, (E) 3.4 μM BAR-NPs and (F) 2 mM hydrogen peroxide. The FITC versus phycoerythrin (PE) fluorescence dot plots show the live (bottom left quadrant) and apoptotic cell (bottom right quadrant) cell populations. Data represent the mean \pm standard deviation ($n=3$), 10,000 counts.

Table 3. 2 TIGK cells apoptosis induced by 1.3 μM free BAR, 3.4 μM free BAR, 1.3 μM BAR-NPs, 3.4 μM BAR-NPs and 2 mM hydrogen peroxide relative to cells treated with medium alone, (*, $P \leq 0.05$, **, $P \leq 0.01$ and ***, $P \leq 0.001$).

| Treatment | % Live Cell | % Early Apoptosis | % Late Apoptosis |
|------------------------------------|---------------------|--------------------|------------------|
| Medium | 99.00 \pm 1.22 | 0.80 \pm 0.56 | 0.097 \pm 0.06 |
| BAR 1.3 μM | 95.60 \pm 1.01 | 3.39 \pm 0.17 | 0.18 \pm 0.09 |
| BAR 3.4 μM | 84.07 \pm 0.81* | 15.33 \pm 0.51* | 0.41 \pm 0.24 |
| BAR-NPs 1.3 μM | 86.57 \pm 2.23* | 12.53 \pm 1.92* | 0.22 \pm 0.12 |
| BAR-NPs 3.4 μM | 83.90 \pm 2.55* | 14.77 \pm 1.53* | 0.60 \pm 0.44 |
| 2 mM H ₂ O ₂ | 12.73 \pm 1.59*** | 87.03 \pm 1.70** | 0.23 \pm 0.17 |

Discussion

Porphyromonas gingivalis adherence to oral streptococci is a key event in the initiation and pathogenesis of periodontal diseases, representing a specific target for therapeutic intervention¹⁰⁵. Previous work in our groups has demonstrated that BAR peptide inhibits biofilm formation by preventing *Pg* adherence to streptococci *in vitro* and in a murine model of infection^{109,110}. However, the administration of free BAR was significantly less effective in disrupting existing *Pg*/streptococcal biofilms¹¹¹⁻¹¹³. A recent study by our groups demonstrated the ability of BAR-NPs to deliver a high concentration of peptide to potently and multivalently inhibit *in vitro* biofilm formation⁹⁵. Given this, the aim of this work was to translate our previous *in vitro* BAR-NP results to a murine model

of periodontitis, highlighting the potential of novel specifically-targeted NPs in a prophylactic oral biofilm application.

Morphological characterization of BAR-modified PLGA NPs showed spherical NPs with an average diameter of 87.9 ± 29.4 nm and zeta potential of -10.3 ± 0.9 mV, while, the diameter and negative surface charge of unmodified NPs increased to 155.87 ± 37.6 nm and -22.6 ± 1.2 mV, respectively. The decrease in BAR-NP size may be attributed to the increased surface charge imparted by avidin conjugation, which typically reduces aggregation, consequently decreasing NP size^{122,151}. The similar, but large increase in size of hydrated NPs, relative to unhydrated NPs, may be attributed to PLGA swelling in an aqueous solution^{115,122}. These results are in agreement with typically observed NP values^{95,122}. BAR-NPs were fabricated using 18 nmol BAR per mg PLGA NP to provide maximum conjugation of BAR peptide (7.1 nmol/mg NPs) to the NP surface and the functional stability of BAR-NPs relative to free BAR, was tested through *in vitro* biofilm inhibition assays prior to these *in vivo* experiments.

To expand upon our *in vitro* studies, we assessed the efficacy of BAR-NPs, relative to free BAR, to prevent alveolar bone loss in a mouse model of periodontitis. Mice infected with *Pg* and *Sg* showed significantly increased bone loss relative to that observed in untreated, uninfected mice, or animals infected with *Sg* or *Pg* alone. Treatment with either free BAR or BAR-NPs significantly reduced bone loss in *Pg/Sg* infected mice. Treatment with 0.7 μ M or 3.4 μ M free BAR reduced bone loss in a dose-dependent manner, but interestingly, treatment

with 0.7 μ M BAR-NPs reduced bone loss to a significantly greater extent than either dose of free BAR. This is consistent with our previous *in vitro* observations that BAR-NPs promote multivalent interactions with *Pg*⁹⁵. The reduction of bone loss arose from reduced *Pg*-induced gingival inflammation that most likely occurred through BAR-NP-mediated inhibition of *Pg* colonization of the oral cavity.

In corroboration with efficacy data, histopathological examination of gingival tissues showed minor levels of inflammatory cell infiltration in the gingiva of uninfected animals but significantly increased inflammatory cell infiltration in the gingiva of *Pg/Sg* infected mice. Consistent with the bone loss data, treatment with free BAR or BAR-NPs significantly reduced inflammation. In addition, gingival tissue levels of the pro-inflammatory cytokine, IL-17, were significantly increased upon infection and significantly reduced upon treatment. Finally, free BAR and BAR-NPs exhibited minimal toxicity against TIGK cells using various approaches to assess cell lysis, induction of apoptosis, or effects of cell viability or metabolism. Together, these results indicate the utility of BAR-NPs to provide and enhance protection in a murine model of periodontitis, relative to treatment with free BAR.

To date, a variety of groups have developed polymeric delivery vehicles to improve traditional treatment and prevention approaches to periodontal diseases⁸⁶. However, polymeric delivery vehicles have been primarily developed to deliver antibiotics^{85,86,90,152,153} for prolonged durations, and to decrease antibiotic dose, administration frequency, and associated adverse effects. However, antibacterial resistance and non-specificity still remain challenges to effectively

eradicate initial and recurrent biofilms, pathogen resistance, and associated diseases^{35,37,107}. While recent studies have demonstrated some success using various polymeric NPs in dental pathogen murine models^{85,86}, these studies have focused on targeting antibiotic NP formulations to epithelial cells with gingival targeting RGD peptides. Results from these studies indicated that NP surface-modification improved NP attachment to epithelial cells, maintaining antibacterial (i.e., minocycline) concentrations in gingival fluid for prolonged durations and improved therapeutic activity relative to unmodified NPs⁹⁴. Other studies have similarly sought to use RGD⁹⁴, or more general bioadhesive molecules such as chitosan^{124,126} or dimethyl-octyl ammonium¹³⁴, to obtain improved localization and adhesion to the dental surface. Strong mucoadhesive properties and adhesion to the tooth surface were demonstrated for antibacterial NPs modified with these agents¹²⁴.

Although non-specific mucoadhesive molecules and broad targeting molecules such as RGD have demonstrated promise in establishing adhesion, the challenges surrounding antibiotic active agents have spurred the discovery and investigation of specifically-targeted molecules against oral biofilms. Antimicrobial peptide (HHC-36) loaded titanium oxide nanotubes, titanium binding peptide (TiBP-1), histatin 5, and lactoferricin peptides have been developed to enhance pre-implant protection against bacterial infection and prevent biofilm formation¹⁵⁴⁻¹⁵⁶. In addition, a terminal product of the cyclooxygenase (COX)-2 pathway (15d-PGJ2) has been administered to inhibit bone resorption *in vivo*¹³³. PLGA NPs, encapsulating 15d-PGJ2, localized in gingival tissue, showed potent anti-

inflammatory response by decreasing proinflammatory cytokines, demonstrated immunomodulatory effects, and decreased bone resorption in a mouse model of periodontitis after daily s.c. injection¹³³.

In contrast with the non-specific bioadhesive and targeting developments described above, the goal of this work was to incorporate a pathogen-specific biological active agent within a surface modification, to exploit the specific and adhesive interactions between two bacteria known to initiate the process of periodontal infections. Previous *in vitro* studies conducted by our group have demonstrated that BAR-modified NPs exhibit potent biofilm inhibition with a 7-fold lower IC₅₀, relative to free BAR⁹⁵, highlighting the benefits of a multivalent delivery system to enhance binding to target sites. Seminal work in the area of multivalency demonstrated that multivalent ligands can enhance the strength or binding avidity to target sites, relative to that observed with monovalent ligands, by increasing the affinity to target entities while decreasing detachment rates^{121,145,157}. Our prior *in vitro* results with BAR-NPs are consistent with the enhanced binding anticipated via these mechanisms, demonstrating improved effectiveness, with lower BAR concentration. Importantly, results from our current *in vivo* studies corroborate the *in vitro* multivalent effects, by demonstrating that 0.7 μ M BAR, conjugated to a NP surface, safely and significantly reduces bone loss and inflammation, relative to a higher concentration of monovalent free BAR (3.4 μ M), in a murine model of infection. Moreover, BAR-NPs, within the range of concentrations examined in this study, provide a safe method, as assessed with four different studies, to induce biofilm inhibition. The use of biodegradable FDA-approved polymers, such as

PLGA, as a core platform, offers the potential for the incorporation of other complementary active agents, and more seamless integration in pre-clinical and clinical studies. Ongoing studies in our group will utilize these particles in dual capacity to both multivalently target specific species of bacteria and to release active agents simultaneously.

In future studies, we intend to examine different temporal administration regimens to optimize prevention and treatment approaches with this platform. In addition, we plan to extend our studies to assess the kinetics of BAR-NPs in the oral cavity after gingival application, and correlate this with BAR-NP effectiveness in preventing (or treating) biofilm formation. Moreover, we will evaluate the stability and longevity of BAR-NP binding with *Pg* in the oral cavity. Long-term, clinical studies will focus on formulating BAR-NPs to more conveniently apply BAR-NPs to the oral cavity, for example, in a mouthwash or gel, with the goal of retaining BAR-NPs in oral niches for durations spanning 12-24 hr. While existing products designed for localized periodontal prevention and treatment contain antibiotics, analgesic, or anesthetic cargos, we envision that this technology may offer a new way to deliver specifically- acting biologics to the oral cavity.

Conclusions

Building upon our previous *in vitro* work, the goal of these studies was to assess the *in vivo* efficacy and safety of BAR-NPs in a murine model of periodontitis. We hypothesized that BAR-NPs may more potently and safely inhibit *Pg* virulence *in vivo* by delivering a high localized concentration of BAR, and

improving BAR effectiveness through multivalent interactions with *Pg*. The *in vivo* efficacy of BAR-NPs was evaluated in a periodontitis murine model by measuring bone loss, histologic changes, and gingival IL-17 expression as outcomes of *Pg*-induced inflammation. The safety of BAR-NPs was evaluated by measuring cell viability, apoptosis, ATP and LDH levels in TIGK cells and hemolytic activity in sheep erythrocytes. BAR-NPs significantly reduced bone loss and IL-17 expression in *Pg/Sg* infected mice to levels of sham-infected mice, and to a greater extent than an equimolar amount of free BAR. Moreover, BAR-NPs and free BAR showed non-hemolytic activity and demonstrated greater than 90% viability, with apoptosis, ATP and LDH levels similar to untreated cells. Our results suggest that BAR-NPs provide a potent platform to inhibit *Pg* virulence, relative to free BAR, while eliciting a safe, non-toxic effect within the evaluated concentration range of 1.3 - 3.4 μ M on gingival and erythrocytic cells, suggesting this novel therapeutic approach for delivery to the oral cavity.

CHAPTER 4

RAPID-RELEASE POLYMERIC FIBERS FOR INHIBITION OF *PORPHYROMONAS GINGIVALIS* AND *STREPTOCOCCUS GORDONII* BIOFILMS

Introduction

Various mechanical prophylactic therapies including scaling and root planning are only temporarily effective in removing the subgingival biofilm to halt the inflammatory cascade²⁹, since the biofilm begins to re-form shortly after prophylaxis is completed. Furthermore, while current medicinal therapies, consisting of systemic and local administration of antibiotics are initially effective, they can result in side effects due to an inadequate concentration of drug reaching the periodontal pockets resulting in transient activity^{35,37,107}, and lead to the development of antimicrobial resistance. Moreover, the non-specific nature of current antibiotic agents can adversely impact the commensal microbial community. Given these challenges, new prophylactic and therapeutic approaches that provide more specific targeting of periodontal pathogen interactions are urgently needed to address these shortcomings and to improve oral therapeutic outcomes.

Delivery vehicles that localize the delivery and maintain the stability of specifically-targeted biologics, such as BAR peptide, may offer improved functional activity, thereby enhancing the therapeutic efficacy²⁸. Delivery platforms such as electrospun fibers (EFs) have been used in a variety of applications like wound dressing¹⁵⁸, tissue regeneration^{159,160} and antimicrobial delivery^{98,97} to incorporate water-soluble bioactive agents such as proteins, peptides, nucleic acids and hydrophilic/hydrophobic drugs. Polymeric fibers can protect encapsulated cargo from systemic absorption and associated side effects. Moreover, electrospinning offers a cost-effective, reproducible, and highly tunable method to provide efficient encapsulation and release based on the needs of rapid-onset or prolonged delivery applications. Many studies have shown that fibers composed of polymer blends have the potential to tune drug miscibility and that the resulting drug-polymer interactions may lead to different release profiles⁹⁹. A number of natural, synthetic and semi-synthetic polymers have been used. Since biocompatible, biodegradable, and Food and Drug Administration (FDA) approved polymers including poly(lactic-co-glycolic) acid (PLGA)¹⁰², poly(L-lactic acid) (PLLA)¹⁰³, polycaprolactone (PCL)⁹⁷, and polyethylene oxide (PEO)¹⁰⁴ have been successfully electrospun into fibers, using this approach, we hypothesized that EFs may offer advantages to the administration of BAR peptide in the oral cavity.

We previously showed that BAR-modified and BAR-encapsulated nanoparticles (NPs) inhibit *Pg* biofilm formation^{95,96,143}. These NPs were envisioned to serve in formulations such as an oral gel, varnish or mouthwash that require two to three daily applications. Here we sought to develop and characterize

EFs that may be administered in future applications, as rapid-release dental strips in the oral cavity. We hypothesized that BAR release may be modulated by changing the hydrophobic:hydrophilic polymer ratios of the blended fibers. We synthesized blended EF formulations and showed that changing the hydrophobic:hydrophilic polymer ratios altered the release kinetics of BAR peptide and functionally characterized their effectiveness in preventing the formation of *Pg/Sg* biofilms *in vitro*. These results suggest that BAR-incorporated EFs can be formulated to release peptide over a time window of hours and may represent a new dosage form that can release targeting molecules in the oral cavity. Long-term, we envision that BAR-EFs may provide a promising rapid-release platform to deliver BAR peptide to the oral cavity in the form of strips or gum that can be applied twice daily to inhibit biofilm formation.

Materials and Methods

Materials

Hydrophobic polymers including poly(lactic-co-glycolic acid) (PLGA, 50:50 lactic:glycolic acid, MW 30,000-60,000), poly(L-lactic acid) (PLLA, MW 50,000), and polycaprolactone (PCL, MW 80,000), and the hydrophilic polymer, polyethylene oxide (PEO, MW 100,000) were purchased from Sigma-Aldrich (St. Louis, MO, USA). Tris-EDTA (TE) buffer (pH 8.0), phosphate buffered saline (PBS) and the organic solvents chloroform, dimethyl sulfoxide (DMSO), and hexafluoroisopropanol (HFIP) were also purchased from Sigma-Aldrich (St. Louis, MO, USA). All chemicals were used directly without further purification. One

milliliter plastic syringes, petri dishes, and 20 mL scintillation vials were obtained from VWR. One milliliter glass syringes were purchased from Fisher Scientific. The electrospinner was provided courtesy of Dr. Stuart Williams at the Cardiovascular Innovative Institute, University of Louisville.

Peptide Synthesis

The peptide used in this study (NH₂-LEAAPKKVQDLLKKANITVKGAFQLFS-COOH)¹¹² was synthesized by BioSynthesis, Inc. (Lewisville, TX). It was obtained with purity greater than 90% and comprised residues 1167 to 1193 of the SspB (Antigen I/II) protein sequence of *Sg*. A fluorescent BAR peptide (F-BAR), synthesized by covalently attaching 6-carboxyfluorescein (F-BAR) to the epsilon amine of the lysine residue underlined in the sequence above, was used to more easily characterize BAR loading and release from the fibers via fluorescence detection.

Preparation of Polymer Solutions

To prepare the hydrophobic-only polymer fiber batches, PLGA and PLLA were dissolved in HFIP at a concentration of 15% (w/w), while PCL was dissolved in HFIP at a concentration of 12% w/w due to increased viscosity. The polymer solutions were aspirated into a 7 mL glass scintillation vials, and sealed using parafilm to prevent evaporation of the organic solvent. The vials were placed in a shaker at 150 rpm and incubated at 37°C overnight to solubilize the polymer. The final volume of each polymer solution was 1 mL. The following day, F-BAR peptide

was dissolved in 200 μ L TE buffer. The F-BAR solutions were mixed with the polymer solvents at a concentration of 1% w/w (e.g., 2.4 mg BAR/240 mg polymer).

To prepare blended polymers, the hydrophobic polymers PLGA, PLLA, and PCL were mixed with PEO at different ratios (40:60, 20:80, 10:90 w/w) to form PLGA:PEO, PLLA:PEO, and PCL:PEO blends in chloroform at a concentration of 15% (w/v). The blended solutions were aspirated into 20 mL glass scintillation vials, and sealed using parafilm to prevent evaporation of the organic solvent. The vials were placed in a shaker at 150 rpm and incubated at 37°C overnight to solubilize the polymer. The final volume of each polymer solution was 1 mL. The following day, F-BAR peptide was dissolved in 60 μ L DMSO. The F-BAR solutions were mixed with the polymer solvent at a concentration of 1% w/w (BAR/polymer content).

Electrospinning

For the non-blended polymer solutions, 1 mL of the mixed polymer suspension was aspirated into a 1 mL plastic syringe with an 18-gauge blunt needle tip. The internal diameter of the BD plastic syringe (4.78 mm), was set in the syringe pump program. The collector was adjusted such that there was at least 10 cm distance maintained from the needle tip. The syringe pump motor controls were adjusted by setting the “slide” control to 4.5 and the “rotor” to 8. The voltage supply was set at 20 kV, and the syringe pump flow rate was set to 0.8 mL per hour. The polymer solution was electrospun at room temperature, under atmospheric conditions, for 1 hr 15 min, and the resulting fine mist was collected

on the mandrel and allowed to dry for 15 min (**Figure 4.1**). The mandrel was removed from the collector and the fiber was cut and gently peeled off the mandrel. The fiber was placed in a labeled petri dish and kept in a desiccator for 24 hr before characterization. The desiccated fibers were stored in 4°C until use.

For the blended polymer solutions, 1 mL of the mixed dual-polymer suspension was aspirated into a 1 mL glass syringe with a 22-gauge blunt needle tip. The internal diameter of the Hamilton gastight syringe (4.61 mm), was set in the syringe pump program. A distance of 15 cm was kept between the needle tip and the collector. The “slide” control was set to 4.5 and the “rotor” control was set to 8. A voltage of 20-25 kV was applied, at a flow rate of 0.3 mL per hr. The electrospinning processes were employed under ambient conditions for 3 hr 20 min. The stretched and solidified polymeric fibers were collected on a 4 mm diameter stainless steel mandrel and allowed to dry for 15 min. Similar desiccation and storage conditions were followed, as noted for the non-blended fibers.

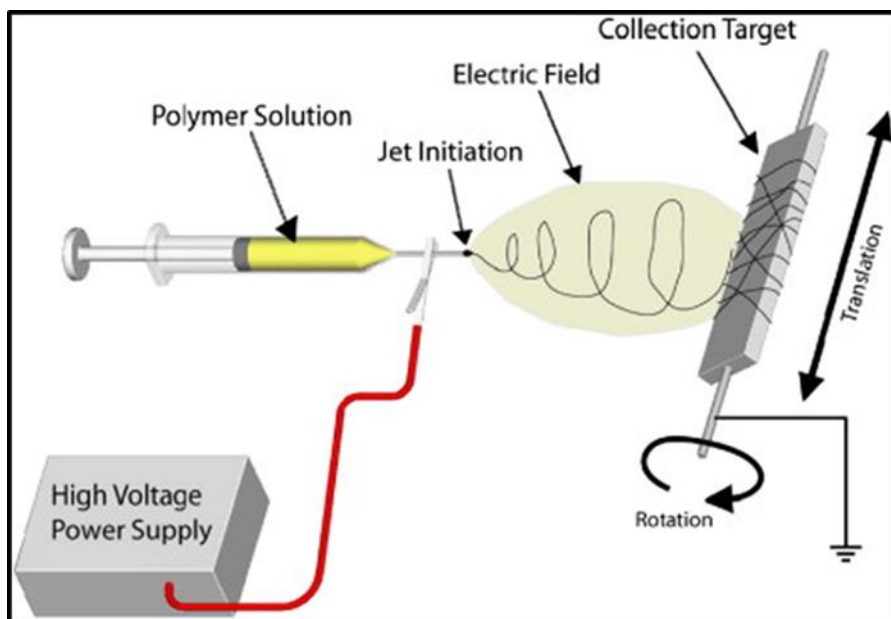


Figure 4.1 Schematic representation of electrospinning process. Adapted from <http://www.people.vcu.edu/~glbowlin/research.html>.

EF Characterization: EF Morphology, Diameter, BAR Loading, and Release

Fiber morphology and size were evaluated using scanning electron microscopy (SEM) (JSM-820, JEOL, Tokyo, Japan), and fiber diameters were obtained by analyzing SEM images with NIH ImageJ. The loading and encapsulation efficiency (EE) of F-BAR peptide in the non-blended and blended fibers were determined by dissolving F-BAR fibers in DMSO. The fiber solution was subsequently vortexed, sonicated for 5 min, and dissolved for 1 hr in a dark room. The quantity of extracted F-BAR was determined by measuring the fluorescence using a spectrophotometer (488/518 nm excitation/emission), relative to an F-BAR standard. A standard curve of F-BAR was obtained by adding 0.1 mg F-BAR to 1 mL of 1:9 DMSO:TE, and serially diluting in 1:9 DMSO:TE. The

diluted solutions (100 μ L/well) were transferred to a 96-well clear bottom microtiter plate in triplicate. For the dissolved fiber samples, after the incubation period, the fiber sample solutions were vortexed and sonicated again. The solutions were diluted 1:2, 1:5, 1:10 and 1:100 in 1:9 DMSO:TE solution, and transferred to a microtiter plate.

The *in vitro* release of F-BAR from fibers was measured by gentle agitation of EFs in phosphate buffered saline (PBS, pH 7.4) at 37°C. At fixed time points (1, 2, 4, 8, 12, and 24 hr), samples were collected and the amount of F-BAR released from the EFs was quantified via fluorescence spectroscopy, against an F-BAR standard in PBS.

Growth of Bacterial Strains

Pg (ATCC 33277) was grown in Trypticase soy broth (Difco Laboratories Inc., Livonia, MI, USA) supplemented with 0.5% (w/v) yeast extract, 1 μ g/mL menadione, and 5 μ g/mL hemin. The medium was reduced for 24 hr under anaerobic conditions (10% CO₂, 10% H₂, and 80% N₂) and *Pg* was subsequently inoculated and grown anaerobically for 48 hr at 37°C. *Sg* DL-1 was cultured aerobically without shaking in brain-heart infusion broth (Difco Laboratories Inc.) supplemented with 1% yeast extract for 16 hr at 37°C.

Biofilm Inhibition Assay

To assess the effectiveness of BAR-incorporated EFs to prevent the interaction of *Pg* with *Sg*, *Sg* was harvested from culture and labeled with 20 μ L of

5 mg/mL hexidium iodide for 15 min at room temperature. Following incubation, cells were centrifuged to remove unbound fluorescent dye. The bacterial concentration was subsequently measured by the O.D. (600 nm) from twenty-fold diluted cultures of *Sg*. The optical density of *Sg* cells was adjusted to 0.8 O.D. (1×10^9 CFU/mL) to obtain uniformity between cell counts in each well. After adjusting the optical density, 1 mL of *Sg* cells was added to each well of 12-well culture plates containing a sterilized micro-coverslip. The cell culture plates were wrapped in aluminum foil to protect the labeled cells from light and placed on a rocker platform in the anaerobic chamber for 24 hr. *Pg* cultures were optimized using a similar approach, utilizing a different fluorescent label (20 μ L of 4 mg/mL carboxyfluorescein–succinylester). *Pg* was incubated with the fluorescent dye for 30 min on a rocker platform and protected from light. The same procedures were followed as performed with *Sg* to determine cell concentration, with slight adaptations. The optical density of *Pg* was adjusted from 0.8 to 0.4 O.D. (5×10^7 CFU/mL) by diluting *Pg* cultures with an equal volume of 1X PBS containing BAR-EFs, free BAR, or blank EFs as a control, to a final volume 1 mL. The final concentration of BAR- EFs or free BAR ranged from 0.3-3 μ M based on the previously determined IC₅₀ of free BAR (1.3 μ M). *Pg* was incubated with BAR-EFs, free BAR, or blank EFs at 25°C for 30 min before transferring to wells containing *Sg*.

Plates containing *Pg* and *Sg* were subsequently incubated for 24 hr at 37°C in anaerobic conditions. The following day, the supernatant was removed and cells were washed with PBS. Adherent cells were fixed with 4% (w/v) paraformaldehyde

and the cover glass was mounted on a glass slide. Biofilms were visualized using a Leica SP8 confocal microscope (Leica Microsystems Inc., Buffalo Grove, IL) under 60x magnification. Background noise was minimized using software provided with the Leica SP8 and three-dimensional z-stack biofilm images were obtained from 30 randomly chosen frames using a z-step size of 0.7 μm . Images were analyzed with Volocity image analysis software (version 6.3; Perkin Elmer, Waltham, MA, USA) to determine the ratio of green to red fluorescence (GR), representing *Pg* and *Sg*, respectively. Control samples were used to subtract background levels of auto-fluorescence. Briefly, triplicate samples of *Sg* alone were immobilized without *Pg* or BAR in 12-well culture plates and the same procedures for dual-species biofilm were followed. *Sg*-only coverslips were visualized and images were analyzed as described above. The GR background was subtracted using the following formula: GR sample or control - GR *Sg*-only. Each treatment group (BAR-EFs or free BAR) was analyzed in triplicate and three independent frames were measured for each well. GraphPad InStat (La Jolla, CA) was used for data analysis and differences were considered to be statistically significant when $P \leq 0.05$. The percent inhibition of *Pg* adherence was calculated with the following formula: GR sample/GR control.

Biofilm Disruption Assay

The same procedures utilized in the inhibition assay were followed, except *Pg* was allowed to adhere to *streptococci* in the absence of BAR peptide or BAR-EFs to demonstrate the ability of BAR-incorporated EFs to disrupt or “treat” pre-

established biofilms. The resulting *Pg/Sg* biofilms were then treated for the maximum duration observed for free BAR to disrupt existing biofilms (3 hr)⁹⁵. Established biofilms were administered BAR-EFs, free BAR or blank EFs at various concentrations in 1mL PBS, and processed and analyzed as described above. The mean and standard deviation (SD) between samples were determined and the percent disruption of *Pg* adherence was calculated with the following formula: GR sample/GR control.

Tissue Culture

Telomerase immortalized gingival keratinocytes (TIGKs) were grown on 12-well collagen-coated plates (Becton Dickinson, Bedford, MA) and cultured using DermaLife K Calcium Free Medium (LifeFactors®) supplemented with penicillin/streptomycin (100 U/mL final concentration; St. Louis, MO), insulin (5 µg/mL), recombinant human (rh), L-glutamine (6 mM), apo-transferrin (5 µg/mL), epinephrine (1 µM), rh TGF-α (0.5 ng/mL), extract PTM, calcium chloride (0.06 mM) and hydrocortisone hemisuccinate (100 ng/mL). The cells were incubated at 37°C in the presence of 5% CO₂ for 6 days until they reached 95% confluence.

Determination of BAR and BAR-EFs *In Vitro* Toxicity

Hemolytic Assay: A sample of 250 µL of 1% sheep erythrocytes (Rockland Inc, Pennsylvania, USA) was suspended in sterile PBS. 1.3 and 3.4 µM (the maximum concentrations used in *in vitro* and *in vivo* studies) of BAR peptide or 10:90 PLGA:PEO BAR-EFs were added to sheep erythrocytes. Water replaced PBS as a positive control for cell hemolysis. The suspension was incubated at

37°C for 3 hr then centrifuged at 3,500 x g, Hemoglobin released due to cell lysis was analyzed by measuring the absorbance at 541 nm.

MTT Assay: TIGK cells were seeded in 12-well plates at a density of 6×10^4 cells in 1 mL media per well and incubated for 24 hr to allow for 60–70% confluency and sufficient adhesion. Cells were treated with 1.3 or 3.4 μM of BAR or BAR-EFs. After 24 hr, 100 μL of MTT solution was added to the media of all samples. After 4 hr incubation at 37°C, 550 μL of lysis buffer was added to the media of each well and plates were incubated for overnight. The absorbance of each well was read at 570 nm, and the sample absorbance was normalized to the absorbance of medium-only treated cells. Cells were treated with 10% DMSO media (100 μL DMSO in 900 μL media) as a positive control for cell death.

ATP Assay: The metabolic activity of cells was assessed by measuring total ATP levels using the CellTiter-Glo reagent (Promega, Madison WI), as described by the manufacturer. TIGK cells were seeded at a density of 6×10^4 cells in 1 mL media per well and incubated at 37°C, 5% CO_2 for 24 hr in a 12-well flat bottom plate. Cells were then incubated with BAR or BAR-EFs (1.3 or 3.4 μM) for 24 hr at 37°C in 5% CO_2 . Cells were then lysed with 500 μL of 0.1% Triton X-100 for 30 min at 37°C. The lysates were collected and centrifuged at 1,000 x g for 10 min at 4°C, and 50 μL of supernatant was mixed with 50 μL of CellTiter-Glo reagent. Samples were incubated at ambient temperature for 10 min in a black 96-well plate in the dark. Total luminescence was measured with a Victor 3 luminometer (Perkin-

Elmer, Inc). Cells incubated with 1 ng of staurosporine or with medium-only served as positive and negative controls for cell death, respectively.

LDH Assay: Cell membrane leakage was measured by assessing the release of lactate dehydrogenase (LDH). Extracellular LDH was quantified using a CytoTox96[®] non-radioactive cytotoxicity assay (Promega, Madison WI) as described by the manufacturer. TIGK cells were plated at density of 6×10^4 cells in 1 mL media per well in a 12-well flat bottom plate, and incubated at 37°C, 5% CO₂ for 24 hr. BAR or BAR-EFs (1.3 or 3.4 μ M) were added to cells in triplicate for 24 hr at 37°C in 5% CO₂. Fifty microliters of supernatant from free BAR and BAR-EFs-treated (1.3 and 3.4 μ M) cells were added to the LDH substrate and incubated at room temperature for 30 min. Then the reactions were terminated by adding 50 μ L of stop solution. LDH activity was determined by measuring the optical density of the solution at 490 nm. Positive control cells were treated by Staurosporine, while negative control cells treated with medium only.

Oxidative DNA Damage: Free radicals and other reactive species are generated from cells under stress and cause oxidative damage to biomolecules. DNA is the most targeted site of oxidative attack. Apurinic/apyrimidine (AP or abasic) site is a prevalent oxidative DNA damage lesion. OxiSelect[™] Oxidative DNA Damage Quantitation Kit (Cell Biolabs, INC., San Diego, CA, USA) was used to quantify AP sites in cells treated with free BAR or BAR-EFs (1.3 or 3.4 μ M) as described by the manufacturer. TIGK cells were plated at density of 6×10^4 cells in 1 mL media per well in a 12-well flat bottom plate, and incubated at 37°C, 5%

CO₂ for 24 hr. BAR or BAR- EFs (1.3 or 3.4 μM) were added to cells in triplicate for 24 hr at 37°C in 5% CO₂. Cells treated with medium-only and 2mM H₂O₂ served as negative and positive controls, respectively. Genomic DNA was isolated from TIGK cells by QIAamp DNA Mini kit (Qiagen). AP sites were determined in genomic DNA by using biotinylated aldehyde reactive probe (ARP) that reacts specifically with an aldehyde group of AP sites, then were colorimetric detected by a streptavidin–enzyme conjugate at 450 nm. The quantity of AP sites in DNA samples was determined by comparing the absorbance with standard curve of known amount of AP sites.

Statistical Analysis

Data from each of toxicity tests were analyzed using ANOVA after passing Bartlett's and Brown-Forsythe tests for homogeneity of variances using GraphPad InStat (La Jolla, CA). A pair-wise, parametric analysis of variance using a Bonferroni multiple comparison post hoc test was used to determine the statistical difference among the individual groups. A *P*-value of ≤ 0.05 was considered to be statistically significant.

Results

EF Characterization: EF Morphology, Diameter, BAR Loading, and Release

Fibers morphologies and diameters are shown in **Figures 4.2** and **4.3**. The average diameters of EFs ranged from 0.7 to 1.3 μm with no statistically significant

differences observed within or across different formulations, as a function of polymer type or blend ratio.

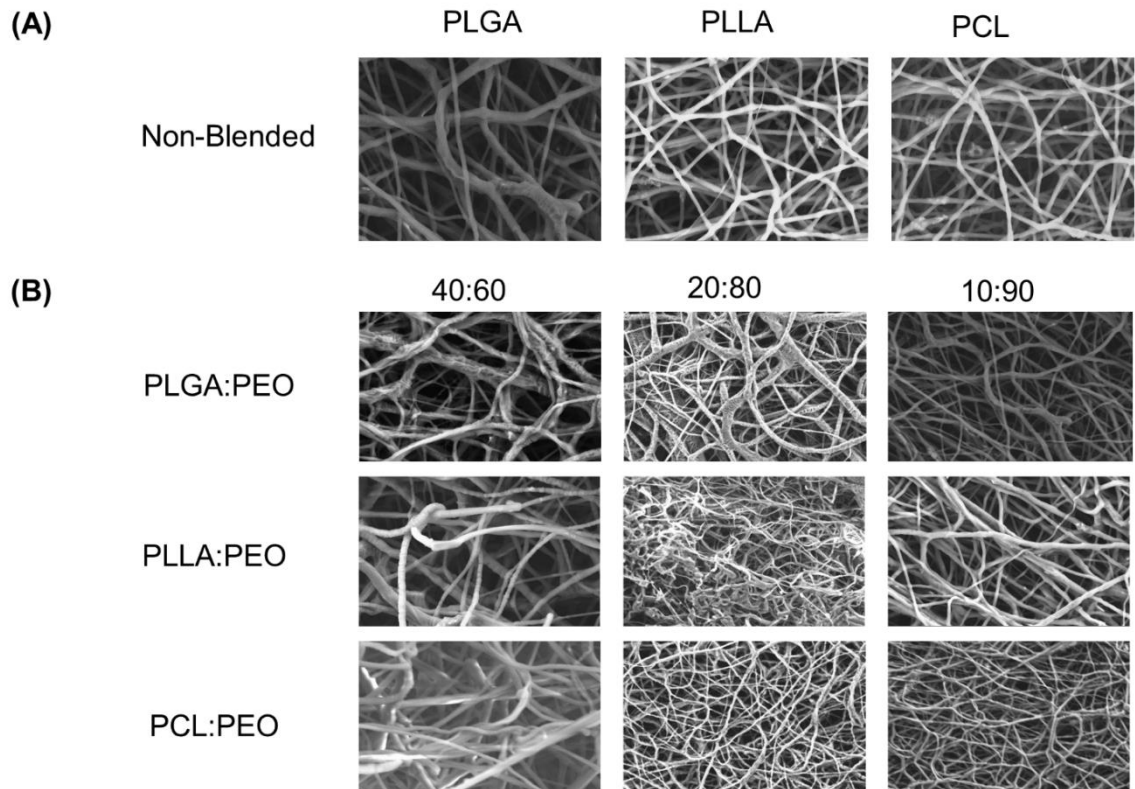


Figure 4.2 (A) SEM images of 1% w/w BAR PLGA, PLLA, and PCL non-blended fibers. (B) SEM images of 40:60, 20:80, and 10:90 1% w/w BAR blended PLGA:PEO, PLLA:PEO and PCL:PEO fibers.

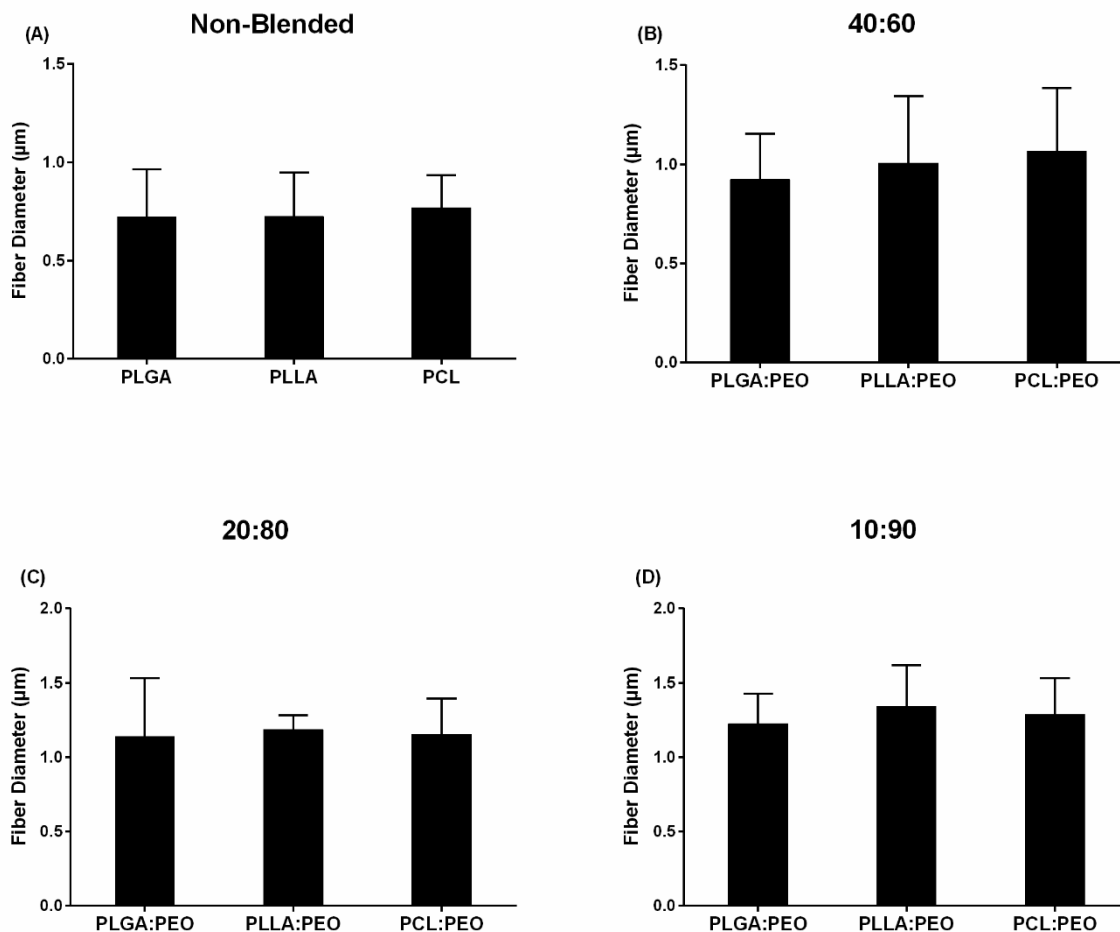


Figure 4.3 Average diameters of electrospun fibers measured from SEM images, using ImageJ. (A) Non-blended and blended (B) 40:60, (C) 20:80, and (D) 10:90 PLGA:PEO, PLLA:PEO and PCL:PEO 1% w/w BAR fibers. Error bars represent the mean \pm the standard deviation (n=3) of three independent runs.

BAR Loading and Release

The overall polymer yield after electrospinning ranged from 40-60% for the non-blended fiber formulations, while the blended fibers achieved higher yields spanning 80-90%. The total F-BAR loading for non-blended and blended EFs ranged between 4.6 – 6.9 μg BAR/mg polymer and 6.0 – 9.2 μg BAR/mg polymer,

respectively, indicating that high loading of F-BAR was achieved in all fiber formulations (**Table 4.1**). To determine the amount of F-BAR release from the different fiber formulations, F-BAR EFs were incubated in PBS at 37°C. The fluorescence of the collected supernatant was measured at 1, 2, 4, 8, 12 and 24 hr. **Figure 4.4** shows the cumulative release of F-BAR from non-blended EFs at each time point over a 24 hr duration. PLGA EFs demonstrated minimal release of F-BAR (9.5% of total loading) after 24 hr, while PLLA and PCL fibers showed even less release during the same duration. Overall, EFs consisting of only hydrophobic polymers (i.e., non-blended formulations) demonstrated minimal release relative to the PEO-blended EFs.

Figure 4.5 shows the release of F-BAR from blended PLGA:PEO, PLLA:PEO and PCL:PEO fibers with different blend ratios (40:60, 80:20, 90:10), as a function of hydrophobic polymer type. The importance of the PEO ratio in each hydrophobic fiber type, is shown in **Figure 4.5**, with the 10:90 formulation providing maximum release of F-BAR for each hydrophobic blend. Fibers comprised of 10:90 PLGA:PEO released 8.25 µg/mg, corresponding to 93% of the incorporated F-BAR within the first 2 hr, relative to PLLA:PEO and PCL:PEO 10:90 fibers with 65% and 45% of F-BAR release, respectively (**Figure 4.6**). A significant reduction in the release of F-BAR was observed after 2 hr for all 10:90 formulations. For the 20:80 blended formulations, the PLGA:PEO fibers showed maximum release of 88%, compared to PLLA:PEO and PCL:PEO at 58% and 25%, respectively, after 2 hr. Similar trends in F-BAR release were observed for the 40:60 formulations with PLGA:PEO exhibiting the maximum release of 78%,

and PLLA:PEO and PCL:PEO releasing 45% and 17% after 2 hr. Of the tested formulations 40:60 PLGA:PEO, PLLA:PEO and PCL:PEO released the least F-BAR within the first 2 hr, and a significant reduction in release was observed after ~4 hr for both the 20:80 and 40:60 formulations. Overall, the release trends for the different ratios of polymer blends were similar, with PLGA blends achieving the highest F-BAR release, followed by PLLA and PCL formulations.

Table 4.1 The amount of BAR loaded in non-blended and blended polymeric EF formulations ($\mu\text{g}/\text{mg}$) and percent of total BAR loaded in blended and blended EFs. High loading capacity and encapsulation efficiency was achieved with all fiber formulations. However, non-blended EFs showed comparatively lower polymer yield and encapsulation efficiency, relative to the blended EFs. Data represent the mean \pm standard deviation ($n=3$) of three independent samples.

| Fiber Formulation | Blend Ratio | Overall Polymer Yield (%) | Loading BAR/Fiber ($\mu\text{g}/\text{mg}$) | Encapsulation Efficiency (%) |
|--------------------------|--------------------|----------------------------------|---|-------------------------------------|
| PLGA | 100:0 | 59.0 | 6.9 ± 0.1 | 69 ± 2.5 |
| PCL | | 51.0 | 6.0 ± 0.4 | 60 ± 4.0 |
| PLLA | | 42.3 | 4.6 ± 0.6 | 46 ± 5.2 |
| PLGA:PEO | 40:60 | 82.9 | 7.4 ± 0.5 | 74 ± 5.5 |
| PCL:PEO | | 91.5 | 8.6 ± 0.2 | 86 ± 2.4 |
| PLLA:PEO | | 82.0 | 9.1 ± 0.3 | 92 ± 3.1 |
| PLGA:PEO | 20:80 | 80.9 | 8.8 ± 0.2 | 88 ± 2.6 |
| PCL:PEO | | 89.3 | 8.9 ± 0.4 | 89 ± 4.0 |
| PLLA:PEO | | 85.2 | 8.3 ± 0.4 | 83 ± 4.2 |
| PLGA:PEO | 10:90 | 82.8 | 8.8 ± 0.5 | 88 ± 5.6 |
| PCL:PEO | | 80.0 | 6.0 ± 0.4 | 60 ± 4.0 |
| PLLA:PEO | | 80.9 | 8.5 ± 0.3 | 85 ± 3.5 |

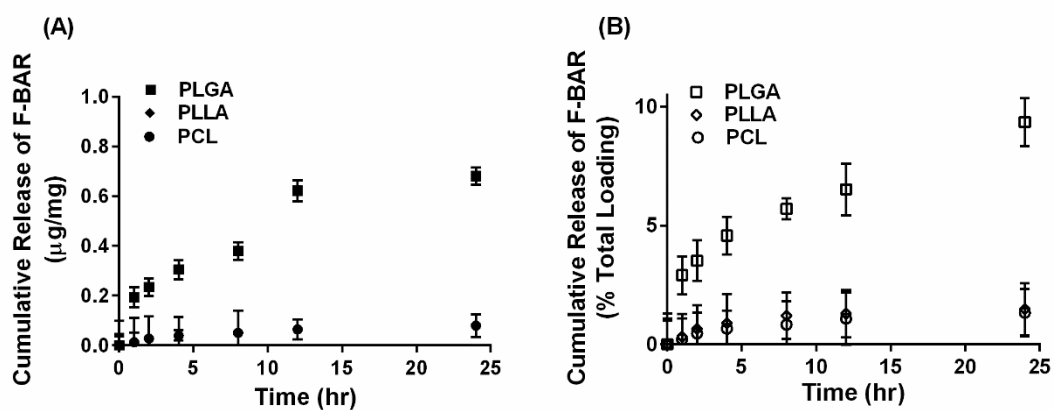


Figure 4.4 The cumulative release of F-BAR from 1% w/w F-BAR non-blended (100:0) PLGA, PLLA and PCL fibers. The cumulative release is reported as (A) µg F-BAR per mg of fiber, and (B) percent of total loaded F-BAR. PLGA showed the greatest release of incorporated BAR among the non-blended formulations at 24 hr. Error bars represent the mean ± the standard deviation (n=3) of three independent runs.

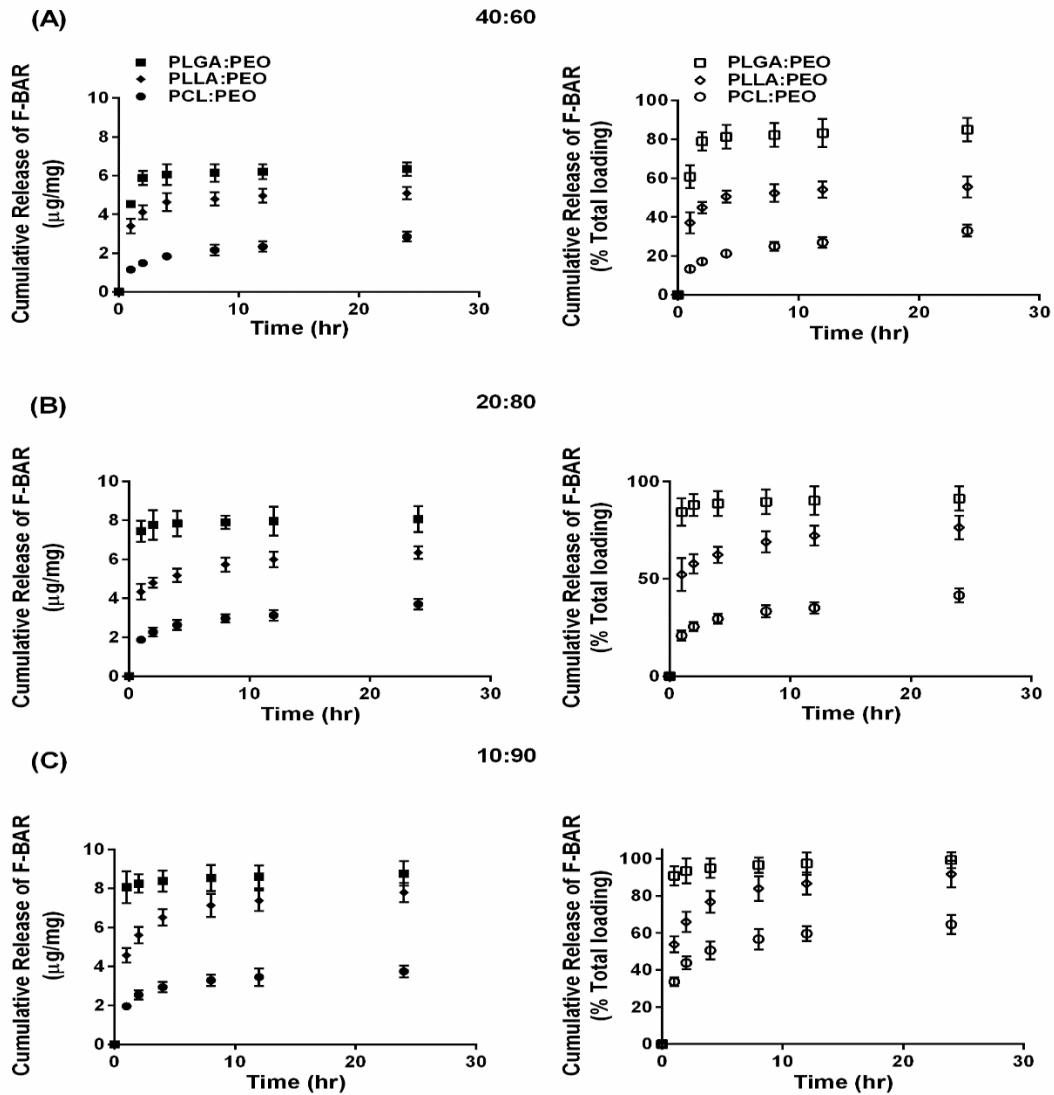


Figure 4.5 The cumulative release of F-BAR from 1% w/w F-BAR blended PLGA:PEO, PLLA:PEO and PCL:PEO fibers (A) 40:60, (B) 20:80, and (C) 10:90. The cumulative release is reported as the total quantity of F-BAR released on the left (μg F-BAR per mg of fiber), and as the percent of total loaded F-BAR on the right. Error bars represent the mean \pm the standard deviation ($n=3$) of three independent runs.

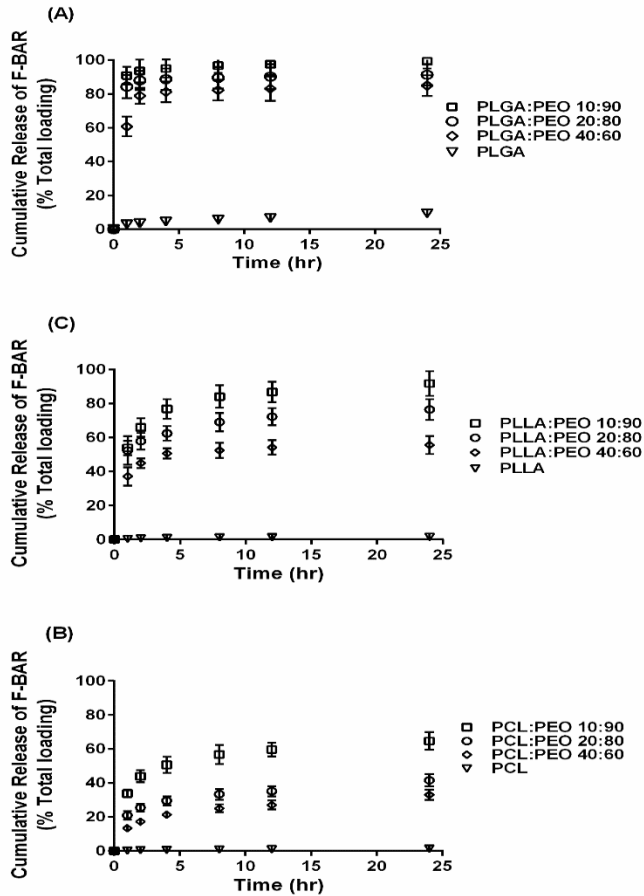


Figure 4.6 The cumulative release of F-BAR from the non-blended and PEO-blended formulations as a function of hydrophobic polymer type (A) PLGA, (B) PLLA, or (C) PCL and PEO ratio in each blend. The release of encapsulated BAR increases with an increase in PEO fraction. PLGA and PEO blends exhibit the most significant and rapid F-BAR release, relative to PLLA and PCL blends. For all polymer types, the 10:90 blends show the greatest release of BAR as compared to the 20:80 and 40:60 formulations at any given time point. PLGA:PEO (10:90) fibers provide the highest amount of BAR release across formulations. Data represent the mean \pm standard deviation ($n=3$) of three independent runs.

***Pg/Sg* Biofilm Inhibition**

Given that the PLGA blends achieved the highest release of F-BAR, the ability of the 10:90 PLGA:PEO BAR-EFs to inhibit or “prevent” *Pg* biofilm formation was assessed, relative to the administration of free BAR. To assess inhibition, 10:90 PLGA:PEO BAR-EFs or free BAR were administered to *Pg* for 24 hr. Subsequently, BAR-EF or free BAR-treated *Pg* was incubated with immobilized *Sg*. As shown in **Figures 4.7 and 4.9A**, *Pg* adherence was significantly reduced in the presence of 10:90 PLGA:PEO BAR-EFs. Biofilm formation was inhibited by 31, 42, or 82% by 0.3, 0.7, and 3.0 μM BAR-EFs. The maximum inhibition observed was similar to the 81% inhibition observed with free BAR (3 μM). BAR-incorporated EFs potently inhibited biofilm formation in a dose-dependent manner ($\text{IC}_{50} = 1.3 \mu\text{M}$); however, no statistically significant differences ($P > 0.05$) in inhibition between BAR-incorporated EFs and free BAR were observed.

***Pg/Sg* Biofilm Disruption**

The ability of the 10:90 PLGA:PEO BAR-incorporated EFs to disrupt or “treat” pre-existing *Pg/Sg* biofilms was assessed (**Figures 4.8 and 4.9B**). Dual-species biofilms were formed for 24 hr, and were subsequently incubated for 3 hr with BAR-incorporated EFs or free BAR. Biofilm formation was disrupted by 29, 34, or 66% by 0.3, 0.7, and 3.0 μM BAR-EFs. The maximum inhibition observed was similar to the 66% inhibition observed with free BAR (3 μM). Taken together, BAR-EFs exhibited efficient biofilm disruption ($\text{IC}_{50} = 2 \mu\text{M}$) that was similar to free BAR ($P > 0.05$).

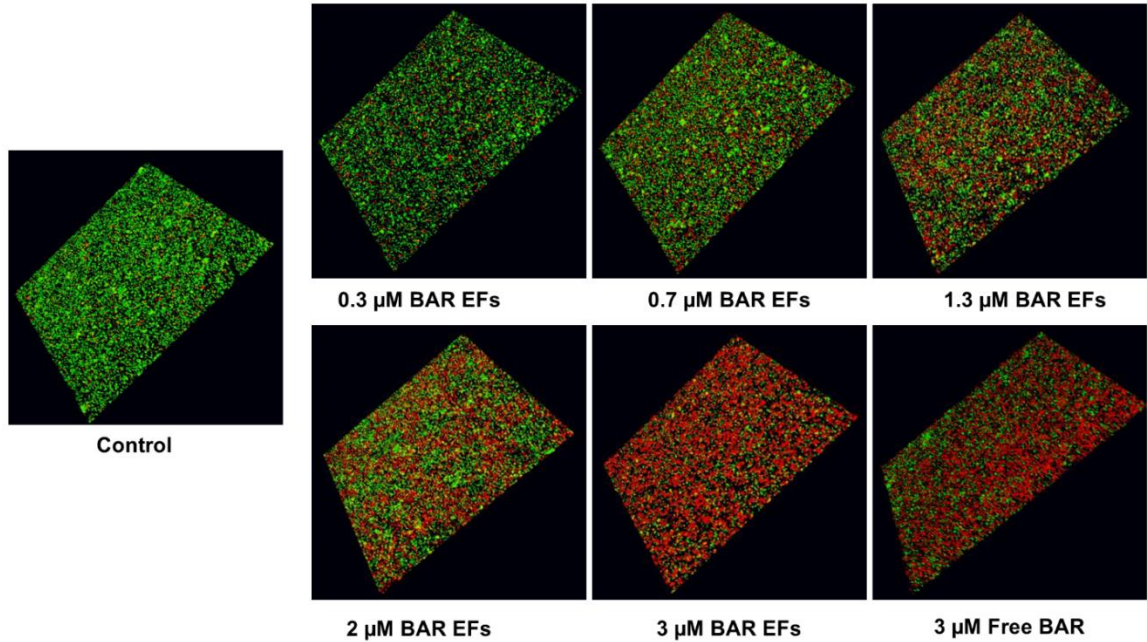


Figure 4.7 BAR-incorporated PLGA:PEO (10:90) EFs prevent *Pg* adherence to *Sg*. Biofilms were visualized with confocal microscopy and the ratio of green (*Pg*) to red (*Sg*) fluorescence in z-stack images was determined using Volocity image analysis software. Each grid represents 21 μm.

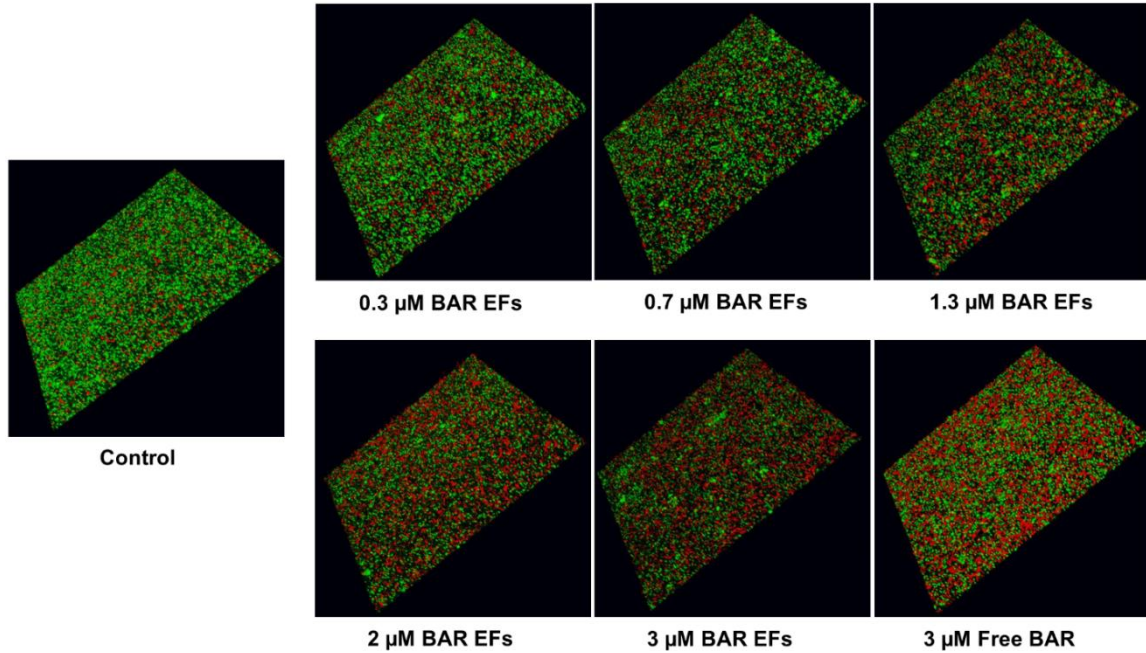


Figure 4.8 BAR-incorporated PLGA:PEO (10:90) EFs disrupt pre-established *Pg*-*Sg* biofilms. Biofilms were visualized with confocal microscopy and the ratio of green (*Pg*) to red (*Sg*) fluorescence in z-stack images was determined using Volocity image analysis software. Each grid represents 21 μm.

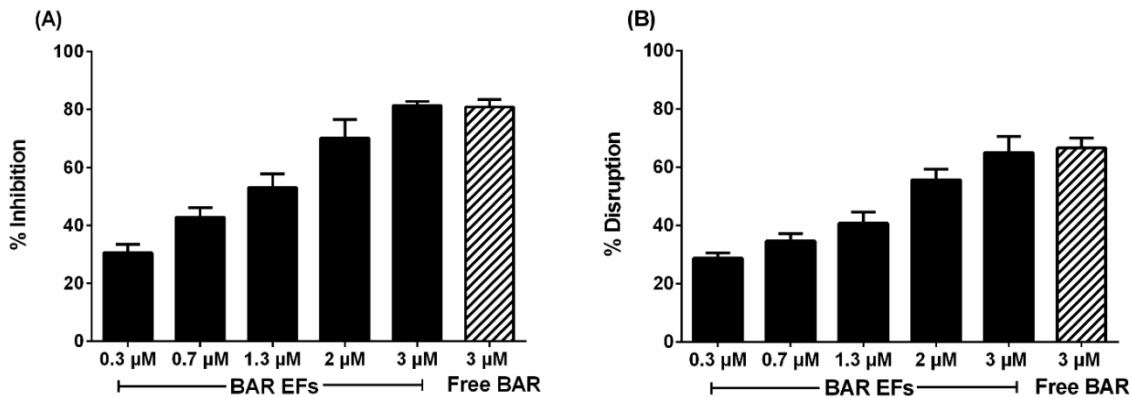


Figure 4.9 (A) Biofilm inhibition and (B) biofilm disruption, as a function of different concentrations of BAR-incorporated PLGA:PEO (10:90) EFs and free BAR (3 μM). Data represent the mean ± standard deviation (n=6).

Assessment of BAR and BAR-EFs *In Vitro* Cytotoxicity

Hemolytic Assay: The cytotoxicity of free BAR and 10:90 PLGA:PEO BAR-EFs was initially assessed by measuring the hemolytic activity against sheep red blood cells (RBCs). As shown in **Figure 4.10A**, neither free BAR nor BAR-EFs (1.3 or 3.4 μM) induced hemolysis of RBCs.

MTT Assay: To determine the effect of free BAR or BAR-EFs on TIGK cell viability, cells were treated with free BAR or BAR-EFs (1.3 or 3.4 μM) and viability was assessed using the MTT assay. As shown in **Figure 4.10B**, free BAR (1.3 or 3.4 μM) treated cells exhibited little non-significant loss in viability while BAR-EF (1.3 or 3.4 μM) treated cells showed higher viability, relative to medium-only treated cells.

ATP Assay: The metabolic activity of TIGK cells was assessed by measuring ATP levels. As shown in **Figure 4.10C**, cells treated with free BAR (1.3 or 3.4 μM) and BAR-EFs (1.3 μM) showed negligible decreases in ATP relative to medium-only treated cells, while, cells treated with BAR-EFs (3.4 μM) exhibited slightly lower levels of ATP relative to medium-only treated cells ($P \leq 0.01$). Staurosporine-treated cells demonstrated significantly lower levels of ATP ($P \leq 0.0001$) than were observed for medium-only, free BAR, and BAR-EF treated cells.

LDH Assay: Since some peptides are known to damage the cell membrane, LDH released in the cell media was evaluated as a marker for cell membrane integrity after free BAR or BAR-EF treatment. **Figure 4.10D** shows that free BAR or BAR-EFs (1.3 or 3.4 μM) induced a little non-significant increase in release of LDH from cells, relative to LDH levels released from medium-only treated cells. However, staurosporine induced a significantly higher level of LDH released from TIGK cells relative to LDH released from cells treated with medium-only, free BAR, and BAR-EFs ($P \leq 0.0001$).

Oxidative DNA Damage: AP sites were determined as oxidative stress marker for cells treated with free BAR or BAR-EFs (1.3 or 3.4 μM). As shown in **Figure 4.11**, free BAR or BAR-EF treated (1.3 or 3.4 μM) cells demonstrated negligible changes in AP sites relative to medium-only treated cells. While cells treated with 2 mM H_2O_2 exhibited a significant increase of AP sites relative to free BAR, BAR-EFs (1.3 or 3.4 μM) and medium-only treated cells (***, $P \leq 0.001$).

Results suggested that neither free BAR nor BAR-EFs (1.3 or 3.4 μM) induced oxidative stress in TIGK cells.

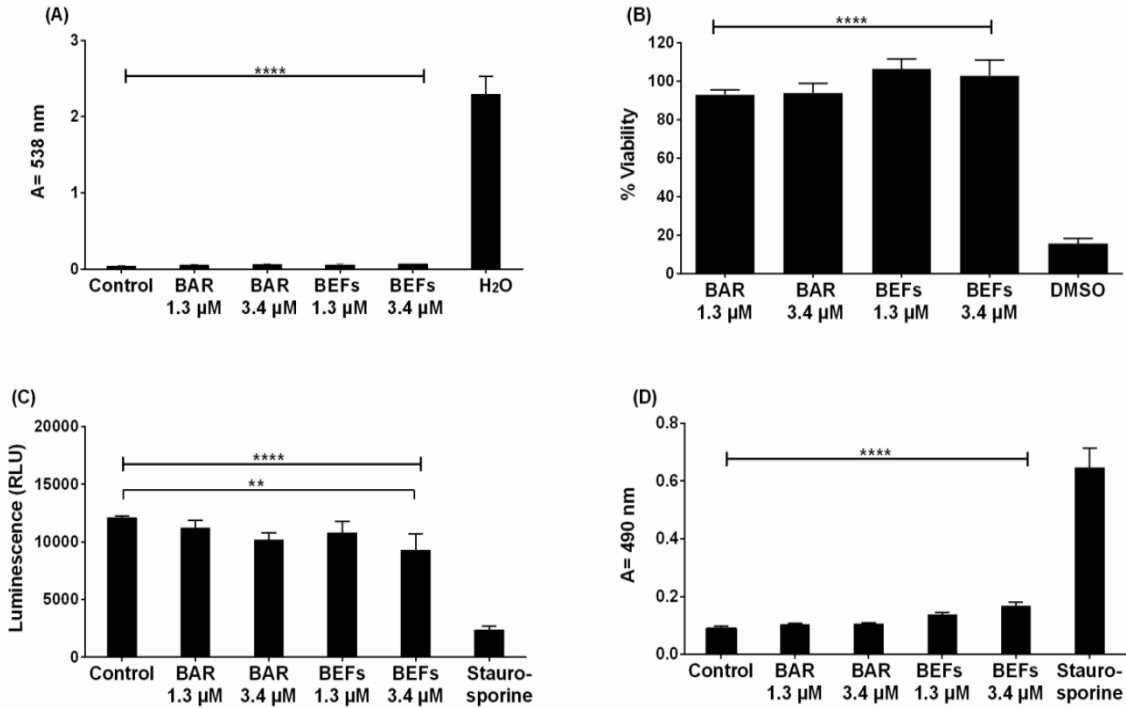


Figure 4.10 (A) The hemolytic activity of free BAR or 10:90 PLGA:PEO BAR-EFs (1.3, 3.4 μM) was assessed after administration to sheep erythrocytes for 3 hr. Free BAR and BAR-EFs showed negligible hemolysis for sheep erythrocyte relative to release from H₂O-treated cells (****, $P \leq 0.0001$). (B) Free BAR and BAR-EFs were non-toxic, relative to cells treated with DMSO (****, $P \leq 0.0001$). (C) BAR-EFs (3.4 μM) treated cells showed decreases in ATP levels relative to medium-only treated cells, while TIGK cells treated with staurosporine demonstrated lower ATP levels than the cells treated with medium-only, free BAR, and BAR-EFs (****, $P \leq 0.0001$). (D) None of free BAR or BAR-EF (1.3, 3.4 μM) treated cells released a significant level of LDH relative to medium-only treated cells. Staurosporine-treated cells demonstrated significantly elevated LDH levels (****, $P \leq 0.0001$). Data represent the mean \pm standard deviation ($n=5$) of five independent experiments.

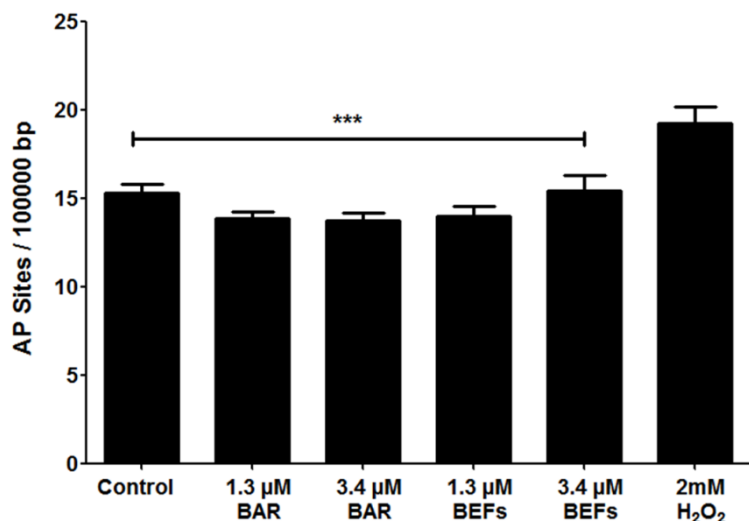


Figure 4.11 Amount of AP sites per 100000 bp of genomic DNA obtained from TIGK cells treated with free BAR or BAR-EFs (1.3, 3.4 μ M). Level of AP sites of cells treated with free BAR or BAR-EFs (1.3, 3.4 μ M) demonstrated negligible changes relative to medium only treated cells. However, TIGK cells treated with 2 mM H₂O₂ demonstrated significantly (***, $P \leq 0.001$) higher level of AP sites relative to control, free BAR and BAR-EFs (1.3, 3.4 μ M). Data represent the mean \pm standard deviation ($n=3$) of three independent runs.

Discussion

Periodontal disease is one of the most widespread oral diseases among the adult population worldwide, resulting in degradation of the supporting tissues of the teeth, and contributing to dental and systemic diseases^{41,161}. *Porphyromonas gingivalis*, both a prominent component of the oral microbiome and a successful colonizer of the oral epithelium¹⁶², has been suggested to function as a keystone pathogen, as it facilitates a change in both the amount and composition of the

normal oral microbiota and creates dysbiosis between the host and dental plaque⁴². The initial species-specific supragingival interaction between *Pg* and *Sg* is considered to initiate the biofilm formation process¹⁶³ and is mediated by interaction of the Mfa1 protein of *Pg* and the SspB polypeptide of *Sg*¹⁶⁴. Since this interaction is an initial event that promotes *Pg* colonization of the oral cavity, it represents an ideal point for therapeutic intervention.

A discrete motif of the SspB polypeptide designated, SspB Adhering Region (BAR), was identified¹⁶⁴, and a synthetic peptide encompassing this motif potentially limited *Pg* colonization both *in vitro* and *in vivo*. Despite this, BAR was shown to be less effective against well-established and complex biofilms, requiring prolonged exposure to be effective. The objective of this work was to synthesize and characterize EFs as a new dosage form to deliver the bioactive molecule, BAR, against biofilm formation for durations relevant to oral administration. We hypothesized that BAR-incorporated EFs, would provide a new platform to enable the short-term release of therapeutically relevant concentrations of BAR to be applied twice daily. Moreover, we hypothesized that BAR release from EFs may be modulated by changing the hydrophobic polymer type and PEO blend ratios.

Local drug delivery vehicles in the form of films¹⁶⁵, strips^{166,167}, and wafers¹⁶⁸ have been applied to periodontal disease, where the subgingival pockets act as a natural reservoir for these drug-loaded carriers. However, the methods used to fabricate these dosage forms include solvent casting, melt spinning and direct milling methods, which often prove to be labor intensive, time consuming, and

expensive. In contrast, electrospinning may provide a simple-to-use, time and cost-efficient process. In addition, EFs offer several advantages relative to other dosage forms including the large surface-to-volume ratio, which can provide increased contact between the encapsulated bioactive molecule and the surrounding medium and tissue environment; small diameter fibers for efficient drug release; the ability to tailor different drug release profiles; and mechanical stability¹⁶⁹. Here we envisioned that designing EFs targeted to the oral cavity may provide a new dosage form in which to administer BAR, relative to the administration of free BAR, and may provide a mechanism to improve therapeutic outcomes by increasing the localized concentration of BAR. Long-term, we envision BAR-EFs may be administered as dental strips or in gel form to degrade and avoid surgical removal after application.

To date, polymeric EFs have been used as delivery vehicles in several biomedical applications including wound dressing materials¹⁵⁸, tissue regeneration^{159,160}, and as drug delivery vehicles for bioactive molecules, antimicrobial agents⁹⁷, anti-inflammatory drugs¹⁷⁰, and anesthetics¹⁷¹. Moreover PLGA fibers have provided cell scaffolds¹⁶⁰, and have been combined with other polymers including PCL and PLA to deliver traditional antibiotics such as doxycycline⁹⁷ and metronidazole for the localized treatment of periodontitis^{98,172}. However, hydrophobic-only fibers have exhibited delivery limitations such as poor wettability, combined with inadequate flexibility and stiffness properties. Despite this, these and other more biodegradable fiber types such as polydioxanone and PLA:PCL/Gelatin fibers incorporating ciproflaxin and tetracycline respectively,

have significantly inhibited periodontal pathogens without affecting the growth of beneficial commensal oral bacteria^{173,174}.

Given this favorable potential, our goal was to fabricate and compare non-blended (hydrophobic-only polymer fibers) with blended BAR-incorporated EFs using a uniaxial electrospinning approach. We initially formulated 1% w/w fibers (BAR/polymer), resulting in a theoretical loading of 10 μg BAR per mg of polymer, a concentration shown in our previous work to inhibit biofilm formation. All resulting EFs demonstrated high F-BAR loading and encapsulation efficiency, ranging from 4.7 to 9.4 $\mu\text{g}/\text{mg}$ and 47-90%, respectively. However, the release kinetics of the non-blended PLGA, PLLA, and PCL fibers revealed minimal release of the total incorporated F-BAR over 24 hr. We attributed the high hydrophobicity of the non-blended PLGA, PLLA, and PCL fibers to minimal eluate penetration past the outermost fiber layer. Moreover, hydrophobic sequences in the BAR peptide may promote hydrophobic F-BAR interactions with the purely hydrophobic non-blended fibers, resulting in lower release.

While hydrophobic polymers have been used in numerous applications outside of the oral cavity, to obtain time frames of release relevant to oral delivery (once or twice daily), we sought to modulate fiber hydrophobicity with the addition of hydrophilic PEO in ratios (PLGA/PLA/PCL:PEO 40:60, 20:80 and 10:90). Previous work has shown that blending hydrophobic polymers with more hydrophilic polymers increases the release of biological molecules such as lysozyme, while maintaining protein activity¹⁷⁵. In addition, many studies have

shown that the addition of PEO to protein solutions can improve protein stability¹⁷⁵⁻¹⁷⁷. Moreover, recent studies demonstrated that incorporation of PEO with hydrophobic fibers increased the pore formation and fiber weight loss with rapid degradation rate relative to non-blended fibers^{178,179}.

By increasing the fiber hydrophilicity with the addition of PEO (PLGA:PEO 40:60, 20:80 and 10:90), BAR release was significantly improved in the blended fibers. This is in agreement with studies that have shown that by introducing hydrophilic PEO into fiber formulations, the physical and mechanical properties of the fiber change, while providing the ability to tune encapsulant (e.g., BAR) release¹⁷⁸. While hydrophobic polymers provide structural integrity to the scaffold, the PEO makes it more porous, enabling the release of the hydrophilic BAR peptide. Moreover, by incorporating PEO in EFs our initial goal was to formulate EFs that would rapidly degrade and release BAR, to avoid removal of EFs after administration. In addition, hydrophilic molecules have been shown to have more affinity and compatibility with PEO, explaining the initial burst release presented by the blended fibers. Last, we postulate that in addition to materials properties, the electrospinning process itself can affect encapsulant location within hydrophobic:hydrophilic blended fibers, prompting variable release kinetics. During electrospinning, the electric field may promote F-BAR aggregation close to the fiber surface, due to charge repulsion¹⁸⁰. This localization, potentially resulting in the release of F-BAR only near the fiber surface, may contribute to the burst release observed in all blended fiber formulations.

Among the hydrophobic polymers utilized, PLGA formulations demonstrated the highest release at early time points, followed by PLLA and PCL formulations. We propose that PLGA fibers demonstrate the highest release due to its amorphous and less hydrophobic properties, relative to the more hydrophobic PLLA and PCL polymers. Relative to PLGA:PEO and PLLA:PEO blends, we propose that PCL:PEO fibers demonstrated the least release due to its crystalline and slightly more hydrophobic features.

The PLGA:PEO (10:90) fibers exhibited 88% encapsulation efficiency and 90% release of F-BAR, the highest among all the blended and non-blended formulations within the first 2 hr, with PLLA:PEO (10:90) exhibiting 65% release, and PCL:PEO (10:90) releasing 45% in the same time frame. Negligible quantities of F-BAR were released after 24 hr. Taking both encapsulation efficiency and release properties into consideration, PLGA:PEO (10:90) was selected to evaluate biofilm efficacy. BAR-incorporated PGLA:PEO 90:10 EFs were evaluated to inhibit two-species biofilm formation and disrupt pre-existing biofilms, against an equimolar concentration of free BAR. BAR-EFs potently inhibited biofilm formation ($IC_{50} = 1.3 \mu M$) in a dose-dependent manner (**Figure 4.7**). In addition, BAR-EFs efficiently disrupted pre-existing dual-species biofilms ($IC_{50} = 2 \mu M$) (**Figures 4.8 and 4.9B**).

The fibers fabricated in this study were formulated with 1% w/w BAR:polymer. As such, they demonstrated high encapsulation efficiency spanning 60-90%, with burst release in the first 2 hr and minimal release thereafter. To

achieve the IC₅₀ of BAR (4 µg/mL) at every time point over the duration of 24 hr, loading capacity must be increased. However, previous work has shown that using a theoretical loading higher than 1 % w/w¹⁰⁰ via uniaxial blended spinning process may still result in significant initial burst release. To overcome burst release, optimize the release kinetics, and maintain peptide stability, techniques like co-axial or emulsion electrospinning may be adopted in future work^{181,182}. Several studies have used co-axial electrospinning to sustain the release of bioactive molecules. Moreover, the bioactivity of biological agents may also be maintained since it is not incorporated into the polymer/solvent solution prior to electrospinning¹⁸³. Alternatively, emulsion electrospinning may help to encapsulate the aqueous agents within the core, to provide sustained and incremental release of the encapsulant¹⁸². These advancements may be helpful in formulating prolonged-release fiber therapeutics for periodontitis as an intra-pocket delivery system, where the fibers can be immobilized in the subgingival pocket for a longer duration of time.

Targeted drug delivery is required to achieve effective therapy against periodontal diseases. Thus, different drug delivery vehicles like gels, nanoparticles, films and fibers have been developed to combat oral diseases²⁸. However, antibiotic side effects, desired release profiles, and non-specific targeting are still limitations facing antibiotic¹⁸⁴, anti-inflammatory¹⁸⁵ and antiseptic¹⁸⁶ loaded polymeric gels currently available to prevent and treat chronic periodontitis. Moreover, even with these formulations, high loading efficiency, sterility, and high cost are challenges that need to be addressed. In comparison,

delivery vehicles that enable the specific targeting of periodontal keystone pathogens may provide a path to develop a novel formulation that exerts potent prophylactic or therapeutic effect via specific interactions, in addition to providing adhesive properties and localized release with minimal side effects.

Our results demonstrated the feasibility, versatility and straightforward approach of electrospinning EFs that release therapeutically-relevant concentrations of BAR, to specifically target periodontal pathogens. Fibers with increasing PEO content significantly enhanced F-BAR release within 4 hr, while the most promising 10:90 PLGA:PEO formulation provided 95% F-BAR release after 4 hr, inhibited biofilms in a dose-dependent manner ($IC_{50} = 1.3 \mu M$), and efficiently disrupted dual-species biofilms ($IC_{50} = 2 \mu M$). Our results suggest that BAR-incorporated EFs may provide an alternative and specifically-targeted rapid-release platform to inhibit and disrupt dual-species biofilms, that we envision may be applied once or twice daily to exert prophylactic effect in the oral cavity without the need to remove the fibers after application. We acknowledge that *in vivo* delivery of BAR-EFs has challenge such as complex biofilm not be reflected the more ideal environment *in vitro* study. Thus, future studies will be focused on developing targeted BAR-EFs to overcome *in vivo* applications challenges and optimizing the release kinetics of BAR from blended EFs for more sustained durations of 12-24 hr, by utilizing altered fabrication procedures like emulsion and co-axial electrospinning^{181,182}.

CHAPTER 5

ASSESSMENT OF TARGETED BAR-ENCAPSULATED NPS AGAINST ORAL BIOFILMS

Introduction

Polymer NPs have been applied to a variety of applications in dentistry and have demonstrated success in reducing the number of intracellular bacteria relative to the administration of free antibiotic, and in penetrating alveolar bone trabeculae, underlying connective tissue, and even the periodontal pocket areas below the gum, due to the small NP size. Other NPs have targeted gingival cells in order to deliver higher local concentrations of antibiotic for a prolonged period^{85,86,127,152}. Polymer NPs have a variety of attributes including the ability to encapsulate both hydrophilic and hydrophobic cargos and to provide sustained-release of these encapsulated active agents. Moreover, surface-modification of NPs can increase efficaciousness by targeting active agent directly to impacted sites. Through surface-modification, polymer NPs may also enhance tissue adherence, resulting in the delivery of higher localized concentrations of drug, due to their inherent mucoadhesive properties, via hydrogen bonding, polymer entanglement with mucins and hydrophobic interactions, or through coating with mucoadhesive compounds like chitosan^{55,56,61,66,141,142}.

Despite the variety of mucoadhesive polymer NPs used to treat oral biofilms, there is currently a scarcity of drug delivery vehicles that enable specific and prolonged delivery of specifically-targeted biologic active agents to the oral cavity.

Previous work from our groups has demonstrated that BAR-encapsulated NPs may improve efficacy and longevity in the oral cavity, relative to free BAR¹⁴³. In addition, BAR-modified NPs delivered a high localized concentration of BAR peptide and improved BAR effectiveness through multivalent interactions with *Pg*, relative to administration of free BAR in *in vitro* and murine periodontitis models^{95,96}. While BAR-encapsulated and BAR-modified NPs demonstrated significant promise to prevent and treat oral biofilms, retention in the oral cavity is known to be a challenge for mobile NP delivery vehicles. Free NPs may be removed by salivary flow, resulting in lower retention in the oral cavity, necessitating higher concentrations of delivery to maintain efficacy.

Previous studies have sought to address this challenge by integrating carboxymethyl cellulose (CMC)¹²³, poly acrylic acid (Carbopol)¹⁸⁷, polyethylene glycol (PEG)^{92,188}, polyvinyl alcohol (PVA)¹⁸⁹ or polyvinyl pyrrolidone (PVP)^{189,190} into NPs to localize and maintain active agent for longer durations in the oral cavity. Another study developed chitosan-coated PLGA NPs to promote mucoadhesion to the buccal surface to localize lovastatin and tetracycline within the oral cavity. PLGA-lovastatin-chitosan-tetracycline nanoparticles demonstrated higher localized concentration of tetracycline with sustained-release for a prolonged period due to the mucoadhesive properties of the NPs and the slow degradation

rate of chitosan⁹⁰. In addition, recently, minocycline-loaded poly(ethylene glycol)-poly(lactic acid) (PEG-PLA) NPs were surface-modified with RGD peptides to target gingival epithelial cells. Targeted minocycline NPs demonstrated potent anti-periodontitis activity relative to non-targeted NPs and free minocycline in dogs. Moreover, RGD-modified minocycline NPs delivered a higher localized concentration of minocycline to the gingiva and retained the effective concentration for a longer time, relative to minocycline-loaded NPs⁹⁴.

While a variety of broadly active mucoadhesive molecules have been used to increase adhesion and retention in the oral cavity, an alternative approach is to exploit known protein-protein interactions that drive interspecies coaggregations between oral organisms to promote adhesion to, and target specific niches in the oral microbiome. For example, recent studies have demonstrated that coaggregation factor A (CafA) is a cell surface protein of *Actinomyces oris* that promotes *Actinomyces/Streptococcus* coaggregation¹⁹¹. Thus CafA represents an ideal targeting molecule to promote NP adherence to *Sg* and specifically deliver active agent to this niche. We propose that NP modification with CafA will enhance targeting to streptococcal cells, an initial niche of *Pg* in the oral cavity⁵⁴. By targeting NPs to this niche, we hypothesize that CafA-modified BAR-encapsulated NPs will deliver higher localized concentrations of BAR and will be retained for a longer duration, due to specific adhesion to *Sg*.

Materials and Methods

Peptide Synthesis

BAR peptide is comprised of residues 1167 to 1193 of the SspB (Antigen I/II) protein of *Sg* with the sequence NH₂-LEAAPKKVQDLLKKANITVKGAFQLFS-COOH¹¹². To facilitate conjugation of BAR to the NP surface, the peptide was synthesized with an N-terminal biotin. Biotinylated BAR was subsequently attached to NPs that had been modified with palmitylated avidin, as previously described⁹⁵. To enable peptide quantification and detection, some preparations of BAR were modified such that the epsilon amine of the underlined lysine residue of BAR was covalently reacted with 6-carboxyfluorescein to produce fluorescent BAR (F-BAR). All preparations of peptides were synthesized by BioSynthesis, Inc. (Lewisville, TX) and were guaranteed to have greater than 90% purity via RP-HPLC analysis.

CafA Synthesis

CafA synthesis was done in the laboratory of Dr. Donald Demuth by Jinlian Tan. Genomic DNA of *Actinomyces oris* (ATCC 43146) was isolated from 10 mL of an overnight culture using the Wizard Genomic DNA purification kit (Promega, Madison WI) as specified by manufacturer. The *cafA* gene was amplified by PCR using 200 ng of genomic DNA as the template and 30 pmol each of the following primers: Forward: 5'- AAG GAT CCC TGA GGC CGT TCA -3'; Reverse: 5'- CCG GAA TTC TAC GAC TTG CGG TTG GAG-3'. PCR amplification was conducted by denaturation at 94°C for 2 min, annealing of primers and template at 63°C for

30 s, strand extension at 72°C for 2 min 45 s, for 30 cycles followed by a final extension cycle at 72°C for 5 min.

The PCR product was subsequently electrophoresed in 1% agarose at 90 V for 40 min and the *cafA* band was excised and purified using the gel purification kit (Qiagen). The purified *cafA* DNA (1 µg) and a sample of the pGEX-6p-1 expression vector (0.5 µg) were digested with *Bam*HI and *Eco*RI overnight at 37°C. Prior to ligation, 50 µL of the digested vector were dephosphorylated with 4 µL calf intestinal alkaline phosphatase (NEB) at 37°C for 30 min. Subsequently, 3 µL of protease K were added and incubated for 30 min at 50°C to terminate the reaction. The vector and *cafA* fragments were purified using the DNA clean and concentrator kit (Zymoresearch) and ligated with T4 ligase. Ligation reactions comprised three µL vector, 5 µL *cafA* fragment, 1 µL 10x ligase buffer and 1 µL T4 ligase.

The ligation mixture was initially transformed into *E. coli* Top 10. Fifty µL of competent *E. coli* Top 10 were incubated with 5 µL of ligation mixture on ice for 30 min., then the sample was heat shocked at 42°C for 45 s and placed on ice for 2 min. Two hundred µL of SOC media were added, the sample was incubated at 37°C for 1 hr and plated on LB agar. After overnight incubation at 37°C, single colonies were selected and cultured in 5 ml LB broth supplemented with 100 µg ampicillin. Plasmid purification was carried out using the mini prep kit (Qiagen) and the *cafA* insert was excised and confirmed by sequencing.

For CafA expression, the purified *cafA* plasmid was transformed into *E. coli* BL21 using the transformation protocol described above. After selecting and confirming the appropriate transformant, 400 mL of LB broth was inoculated with 10 mL of an overnight culture and incubated to OD_{600nm} of 0.5. Protein expression was induced by the addition of 0.5mM IPTG and the culture was then incubated at 18°C for 17h. After centrifugation at 6000 rpm, the cell pellet was suspended in 40 mL 50mM Tris, 100mM NaCl, 1mg/ml lysozyme, 10ug/ml Dnase I, protease inhibitor cocktail, 10mM CHAPS, incubated overnight at 4°C, then for an additional 2 hr at 25°C. The cell suspension was then sonicated for 2 min on ice.

CafA purification was carried out with the Pierce GST Spin Purification Kit (Thermo Fisher). Seventeen mL of crude cell lysate were bound to the GST column for 2 hr at room temperature and the column was then centrifuged to remove unbound protein according to the specifications of the manufacturer. After washing the column with loading buffer, the GST tag was cleaved by the addition of 50 µL precision protease (GE Health) and overnight incubation at 4°C. Released CafA was then collected by centrifugation. The sample was then sequentially dialyzed against 30 mM, 20 mM, and 10 mM Tris for 2 hr each. CafA purity was determined by PAGE gels and protein concentration was determined using the BCA assay (Pierce).

Synthesis of CafA-Palmitate

NPs were conjugated with CafA-palmitate as previously described^{96,122,146}. Briefly, 8 mg of CafA were dissolved in 1.2 mL of 2% (w/v) sodium deoxycholate

(NaDC) in PBS and warmed to 37°C. CafA was then reacted with 14-fold molar excess of the palmitic acid-N-hydroxysuccinimide ester (PA-NHS; Sigma-Aldrich, St Louis, MO, USA). Palmitic acid-N-hydroxysuccinimide ester was dissolved in 2% (w/v) NaDC at 0.5 mg/mL, and sonicated until well-mixed. Eight hundred microliters of the PA-NHS solution were added in drops to the reaction vial containing CafA and allowed to react overnight at 37°C. The reaction solution was then dialyzed in 1.2 L of 0.15% (w/v) NaDC in PBS at 37°C using a 3,500 molecular weight cut-off dialysis tube to remove free PA-NHS. After overnight dialysis at 37°C, CafA-palmitate was transferred to a storage vial and stored at 4°C until use.

CafA Surface-Modified Nanoparticle Synthesis

CafA surface-modified NPs were synthesized using a previously described single-emulsion technique^{88,121}. PLGA with a 50:50 monomer ratio and 0.55–0.75 dL/g inherent viscosity, was purchased from LACTEL®. Briefly, 100 mg PLGA was dissolved in 2 mL dichloromethane (DCM) overnight. The following day, 2 mL of a 5% (w/v) polyvinyl alcohol (PVA) solution was mixed with 2 mL of 4 mg/mL CafA-palmitate. The 2 mL PLGA/DCM solution was added dropwise to 4 mL PVA/CafA-palmitate solution while vortexing. The NP solution was added to 50 mL of 0.3% PVA for 3 hr to evaporate residual DCM. After evaporation, the NP solution was centrifuged at 13,000 rpm (20,442 x g) at 4°C. Supernatant was discarded, and the NPs were washed two times with deionized water (diH₂O) by centrifugation at 13,000 rpm (20,442 x g) at 4°C to obtain NPs with sizes less than

~200 nm. After washing, CafA surface-modified NPs were suspended in 5 mL of diH₂O, frozen at -80°C, and lyophilized.

Surface-modified NPs encapsulating the fluorescent dye Coumarin 6 (C6) or F-BAR were synthesized for binding, loading and controlled release studies. C6-containing NPs were synthesized using an oil-in-water (o/w) single-emulsion technique^{122,192}. Briefly, C6 was dissolved in 200 µL dichloromethane (DCM) overnight at a concentration of 15 µg/mg PLGA. In parallel, 100 mg of PLGA crystals was dissolved in 2 mL of DCM overnight. The following day, the PLGA/DCM solution was vortexed while adding C6 DCM solution and was subsequently sonicated. Next, 2 mL of the PLGA/DCM/BAR solution was added dropwise to mixture of 2 mL of 5% (w/v) polyvinyl alcohol (PVA) and either 2 mL of 5 mg/mL avidin-palmitate or 2 mL of 4 mg/mL CafA-palmitate while vortexing and was subsequently sonicated. Residual DCM was evaporated by adding the NPs solution to 50 mL of 0.3% PVA for 3 hr while mixing. The same procedures as described above were conducted to synthesize blank surface-modified NPs.

F-BAR-encapsulated CafA-modified NPs were synthesized similarly using a double-emulsion technique. F-BAR was dissolved in 200 µL Tris EDTA buffer at a concentration of 43 µg BAR/mg PLGA and protected from light during synthesis¹⁴³. All other conditions were as stated above.

NP Characterization: NP Morphology, Size, CafA Conjugation, Controlled Release

Unhydrated NP morphology, diameter, and size distribution were determined using scanning electron microscopy (SEM, XL-30 ESEM-FEG SEM, FEI Company, USA). Lyophilized NPs were mounted on carbon tape and sputter coated with a thin layer of gold/palladium. Average diameters of 500 particles were determined from SEM images (n=3) using image analysis software (ImageJ, National Institutes of Health, version 1.5a, ImageJ.nih.gov). Dynamic light scattering and zeta potential analyses were performed to determine the hydrodynamic diameter and surface charge of hydrated NPs. The unhydrated and hydrated diameters of NPs are typically assessed to establish the size characteristics within different conditions of dry storage and more physiologically relevant aqueous environments. Briefly, a 1 mg/mL sample of CafA-modified PLGA NPs in diH₂O was prepared. After vortexing and sonication, samples were diluted at a 1:50 ratio in diH₂O. One mL was aliquoted to the cuvette for analysis (Malvern, Malvern, UK (Zetasizer Nano ZS90), courtesy of Dr. Martin O'Toole, Univ. of Louisville) to measure dynamic light scattering and zeta potential with Zetasizer Nano software. Samples were run in triplicate, using a refractive index of 1.57 for PLGA, absorption coefficient of 1, and water refractive index of 1.33.

To measure the amount of CafA that was conjugated to the NP surface the microBCA assay was conducted and compared to a CafA standard^{95,146}. After conjugation, NPs were centrifuged and washed twice with diH₂O to remove

unbound CafA from the formulated NPs. NPs were then suspended in PBS:DMSO (1:99) to create a 1 mg/mL NP solution and the resulting samples were transferred to a microtiter plate in triplicate. Total NP-associated absorbance was determined using Victor3 Multilabel spectrophotometer (562 nm), and the concentration of CafA was determined from a standard curve of known CafA⁹⁵.

For CafA-modified F-BAR-encapsulated NPs and unmodified F-BAR-encapsulated NPs, *in vitro* release was measured by gentle agitation of NPs in PBS (pH 7.4) at 37°C. At fixed time points (1, 2, 4, 8, 24 hr), samples were collected and the amount of F-BAR released from the NPs was quantified by measuring fluorescence (488/518 nm excitation/emission).

Stability of the CafA-NP Interaction

The stability of the CafA palmitate interaction with the NP surface was tested by assessing the release of the CafA ligand from the NP surface with respect to time. Similar to loading experiments, the CafA concentration was determined using microBCA assay by measuring absorbance at 562 nm^{95,96} and comparing to a standard curve of CafA.

Growth of Bacterial Strains

Pg (ATCC 33277) was grown in Trypticase soy broth (Difco Laboratories Inc., Livonia, MI, USA) supplemented with 0.5% (w/v) yeast extract, 1 µg/mL menadione, and 5 µg/mL hemin. The medium was reduced for 24 hr under anaerobic conditions (10% CO₂, 10% H₂, and 80% N₂) and *Pg* was subsequently

inoculated and grown anaerobically for 48 hr at 37°C. *Sg* DL-1 was cultured aerobically without shaking in brain-heart infusion broth (Difco Laboratories Inc.) supplemented with 1% yeast extract for 16 hr at 37°C¹¹¹⁻¹¹³.

Time-Dependent Binding of CafA-Modified NPs to *Sg*

The binding of CafA-modified NPs was compared to NPs that were modified with the same density of a non-specific positively-charged protein, avidin, through similar palmitic acid chemistry. *Sg* was harvested from culture and the bacterial concentration was determined by measuring the O.D. at 600 nm from twenty-fold diluted cultures of *Sg*. *Sg* cells were plated and then incubated with CafA-modified and avidin-modified NPs. One hundred microliters of 0.2 OD *Sg* were added to the 96-well culture plate and incubated at 4°C overnight. The next day, wells were blocked for non-specific binding with 300 µL of 0.3% bovine serum albumin (BSA) for 1 hr. After washing three times with 1x phosphate buffer saline with 0.05% Tween (PBST), 100 µL of CafA-modified C6 NPs (0.25 mg/mL), avidin-modified C6 NPs (0.25 mg/mL) and PBST were added to wells in triplicate, and then incubated on a rocker platform for 1 hr. After washing, the quantity of CafA-modified and avidin-modified C6 NPs binding to *Sg* was determined by measuring the fluorescence (485/520 nm excitation/emission) after subtraction of the control, in which *Sg* was incubated with PBST only, and this reading was considered as time zero with 100% binding. One hundred µL of PBST were added to each well and incubated with gentle agitation. After 1, 2, 4, 8, 12 and 24 hr the quantity of

CafA-modified and avidin-modified C6 NPs bound to Sg was determined by measuring fluorescence.

Results

Quantification of the Total CafA Payload of CafA-Modified NPs

The amount of CafA bound to the NP surface directly correlated with the input concentration of CafA, and the maximum surface density of CafA was achieved by increasing the input concentration of CafA as shown in **Figure 5.1**. A maximum density of 36 μg CafA/mg NP was incorporated on the PLGA NP surface using an input concentration of 80 μg CafA per mg NP, yielding 45% conjugation efficiency.

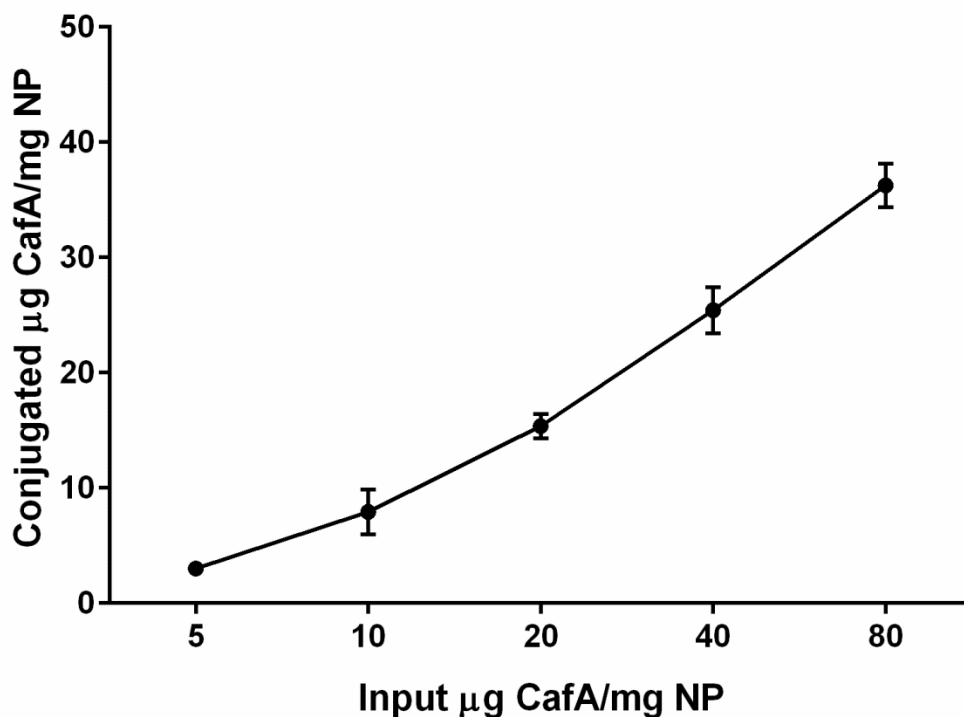


Figure 5.1 The total amount of CafA bound to the surface of PLGA NPs was determined using the microBCA assay. The amount of incorporated CafA on NP surface is directly correlated to the input amount of CafA during fabrication.

CafA-modified Adhesion and Retention to *Sg*

To determine how long CafA-modified NPs remain bound to *Sg*, streptococcal cells were immobilized and CafA-modified NPs or avidin-modified NPs were incubated with *Sg* for 1 hr. The quantity of CafA-modified and avidin-modified C6 NPs initially bound to *Sg* after this hour was considered “time zero” and was set to the maximum (100%) binding achievable. The quantity of CafA-modified NPs and avidin-modified NPs retained (remaining bound) after 1, 2, 4, and 8 hr were determined, and compared to the amount bound during the initial 1

hr period. As shown in **Figure 5.2**, after 1 hr, 5.7 μg of CafA-modified NPs were bound to Sg, relative to 2.5 μg of the control, avidin-modified NP group, resulting in a 2.3-fold increase in binding, due to CafA surface modification. After 8 hr, 3.7 μg of CafA-modified NPs and 1.4 μg of avidin-modified NPs were bound to Sg, resulting in a 2.5-fold increase in binding (**Figure 5.2A**). This corresponded to 65% of CafA-modified NPs and 56% of non-specific avidin-modified NPs bound, suggesting that surface modification with CafA strongly impacts NP adhesion and retention (**Figure 5.3B**). In addition, CafA-modified NPs demonstrated stronger initial binding and a similar but less pronounced decrease in binding with respect to time, relative to avidin-modified NPs.

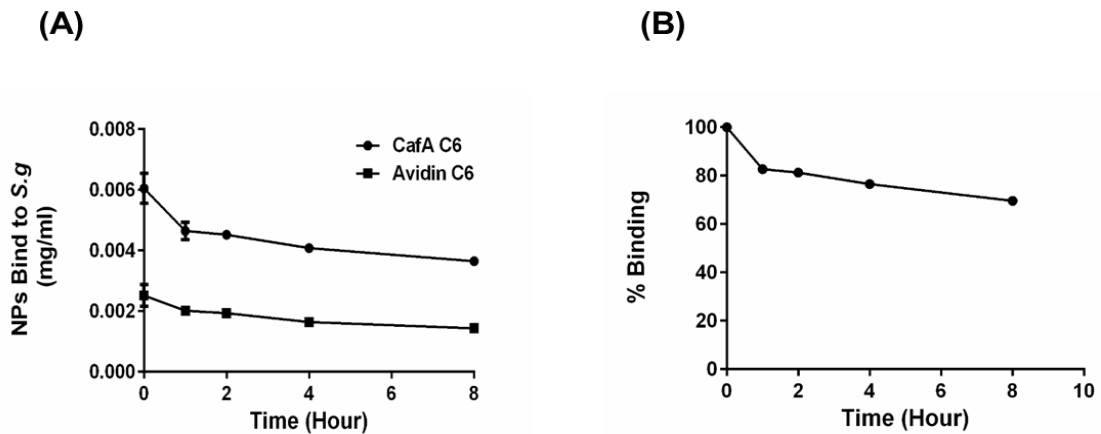


Figure 5.4 (A) CafA-modified C6 NPs initially ($t = 0$) bind to Sg with 2.3-fold greater concentration (5.7 $\mu\text{g}/\text{mL}$), relative to avidin-modified C6 NPs (2.5 $\mu\text{g}/\text{mL}$) and maintain a 2.5-fold increase in binding (3.7 $\mu\text{g}/\text{mL}$) after 8 hr, relative to avidin-modified C6 NPs (1.4 μg). (B) 65% of CafA-modified C6 NPs retain binding to Sg after 8 hr.

Quantification of BAR Release

To assess BAR release from the NPs, the fluorescence of supernatant from 1, 2, 4, 8, 24 hr release time points was measured and compared to a known standard of F-BAR in PBS. Loading experiments demonstrated that both unmodified and CafA-modified PLGA NPs highly encapsulated BAR with 16.95 ± 0.8 and 15.73 ± 1.9 μg of BAR per mg of NP, respectively, corresponding to encapsulation efficiencies of 39.4 and 36.5% (**Table 5.1**). Release experiments demonstrated that 10.3 $\mu\text{g}/\text{ml}$ of encapsulated BAR was released from CafA-modified BAR-encapsulated NPs, while 15.5 $\mu\text{g}/\text{mg}$ of encapsulated BAR was released from unmodified BAR-encapsulated NPs within 24 hr (**Figure 5.3**).

Table 5.1 The amount of BAR (μg) loaded in unmodified and CafA-modified NPs (mg).

| NP Type | BAR input ($\mu\text{g}/\text{mg}$) | BAR output ($\mu\text{g}/\text{mg}$) | Encapsulation Efficiency (%) |
|-------------------|---------------------------------------|--|------------------------------|
| Unmodified NPs | 43 | 16.95 ± 0.8 | 39.4 |
| CafA-modified NPs | 43 | 15.73 ± 1.9 | 36.5 |

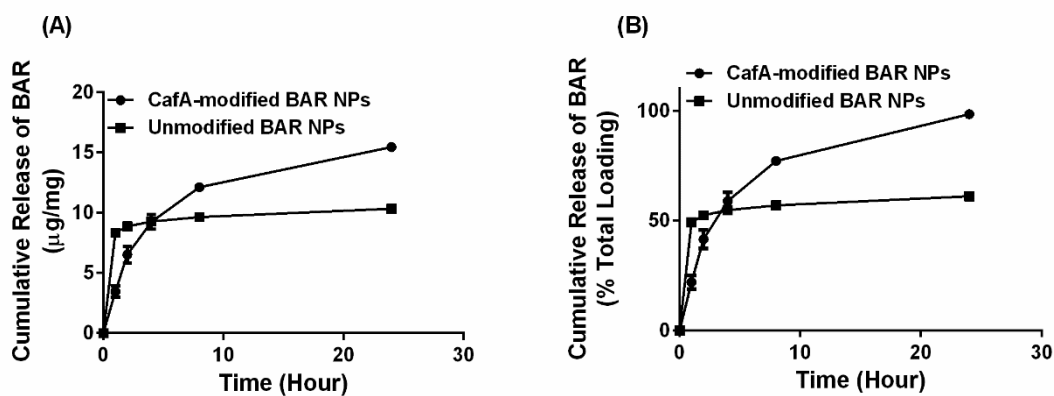


Figure 5.5 (A) Cumulative release of BAR as a function of mass (μg BAR per mg NP) and (B) percent of total BAR loaded over 24 hr.

Stability of the CafA-NP Interaction

The stability of CafA binding to the NP surface was assessed by incubating CafA-modified NPs with agitation in 1x PBS at 37°C for 24 hr. Quantification of CafA release into the supernatant after 1, 2, 4, 8, and 24 hr was evaluated using the microBCA assay, and the percent of CafA retained on the NP surface relative to the amount loaded was determined. Over $82 \pm 3\%$ of the initial CafA remained conjugated to PLGA NPs after 24 hr indicating a stable interaction with the NP surface (**Figure 5.4**).

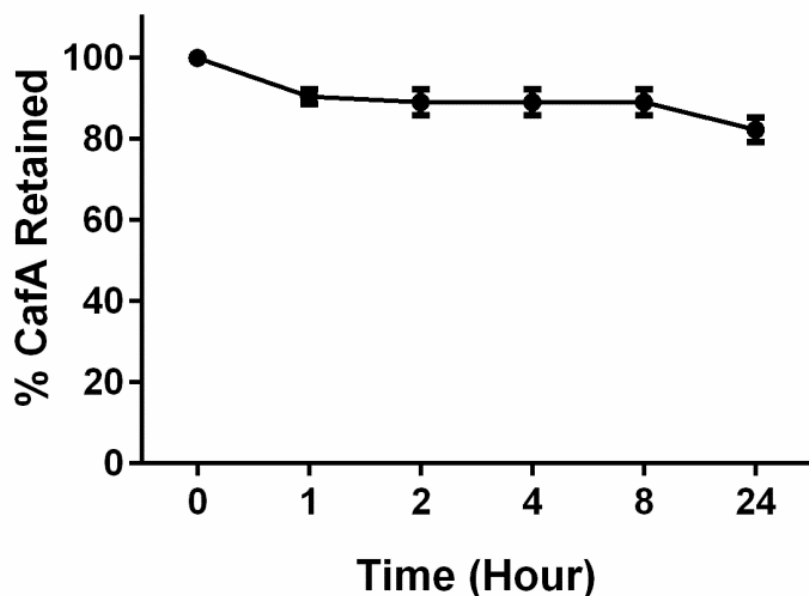


Figure 5.6 Percent of CafA retained on the PLGA NP surface after 24 hr.

Thus far we have established this approach to fabricate CafA-modified BAR-encapsulated NPs with a high and stable surface density of CafA. CafA-modified NPs highly encapsulated BAR peptide with more gradual and increased release, relative to unmodified BAR NPs. These results suggest that CafA-modified NPs may be a promising platform to maintain BAR concentration in the oral cavity for 12 to 24 hr for once or twice daily application. In addition, studies demonstrate the utility of modifying BAR-encapsulated NPs with CafA to achieve efficient binding and retention to *Sg* for at least 8 hr, relative to avidin-modified NPs.

The next steps we envision are to assess the functional activity of CafA-modified BAR-encapsulated NPs against novel 3D dental mimetic tissue with dual-species biofilm *in vitro* and in murine model of periodontitis.

CHAPTER 6

OVERALL DISCUSSION AND CONCLUSION

Periodontal disease is a group of chronic inflammatory diseases that is globally prevalent, affecting ~46% of U.S adults and 30-50% of people globally. *Porphyromonas gingivalis* has been identified as a “keystone” pathogen involved in the initiation and progression of periodontal inflammatory disease, by disrupting host-microbe homeostasis and inducing population changes in the subgingival biofilm¹⁰⁸. This disruption and colonization is initially prompted by association of *Pg* with oral streptococci in the supragingival niche, and is thus an ideal target for therapeutic intervention⁹.

Previous work in our groups has shown that a region of the streptococcal antigen denoted BAR inhibits *Pg/Sg* interaction and biofilm formation both *in vitro* and in a murine model of periodontitis¹¹¹⁻¹¹³. Moreover, recent studies demonstrated the potential of BAR surface-modified PLGA nanoparticles to deliver a high localized concentration of peptide to subgingival niches⁹⁵. While surface-modified NPs were shown to potently inhibit biofilm formation via multivalency, the development of a formulation that can release BAR peptide, within a time frame relevant to oral delivery, had not been investigated.

Moreover, the potential of a new dosage form that might increase the convenience and flexibility of administering a specific peptide into the oral cavity had not been explored by our groups. With this in mind, the aims of this dissertation were to translate our previous *in vitro* BAR-modified NP work to a murine model of periodontitis⁹⁵, investigate the potential of novel BAR-encapsulated NPs to inhibit and disrupt biofilm formation for prolonged durations relevant to oral delivery, and develop rapid-release BAR-EFs that may, in future work, be applied twice daily to release therapeutically relevant concentrations of BAR in the oral cavity.

To date, a variety of groups have developed polymeric delivery vehicles to improve traditional prevention and treatment approaches to periodontal diseases⁸⁶. However, polymeric delivery vehicles have been primarily developed to deliver antibiotics^{85,86,90,152,153} for prolonged durations, and to decrease antibiotic dose, administration frequency, and associated adverse effects. However, antibacterial resistance and non-specificity still remain challenges to effectively eradicate initial and recurrent biofilms, pathogen resistance, and associated diseases^{35,37,107}.

While recent studies have demonstrated some success using various polymeric NPs in dental pathogen murine models^{85,86}, these studies have focused on targeting antibiotic NP formulations to epithelial cells with gingival targeting RGD peptides. Results from these studies indicated that NP surface-modification improved NP attachment to epithelial cells, maintaining antibacterial (i.e., minocycline) concentrations in gingival fluid for prolonged durations and improved

therapeutic activity relative to unmodified NPs⁹⁴. Other studies have similarly sought to use RGD⁹⁴, or more general bioadhesive molecules such as chitosan^{124,126} or dimethyl-octyl ammonium¹³⁴, to obtain improved localization and adhesion to the dental surface. Strong mucoadhesive properties and adhesion to the tooth surface¹²⁴ were demonstrated for antibacterial NPs modified with these agents.

Polymeric electrospun fibers have been used as delivery vehicles in several biomedical applications including wound dressing materials¹⁵⁸, tissue regeneration^{159,160}, and as drug delivery vehicles for bioactive molecules, antimicrobial agents¹⁹³, anti-inflammatory drugs¹⁷⁰, and anesthetics¹⁷¹. Moreover fibers have provided cell scaffolds with PLGA EFs¹⁶⁰, in combination with PCL and PLA to deliver doxycycline¹⁹³ and metronidazole⁹⁸.

Specific to oral delivery, electrospun fibers have been investigated for antibiotic, anti-inflammatory and analgesic delivery, periodontal tissue regeneration, and to act as implantable drugs and growth factor-releasing scaffolds that help repair surgical sites^{97,160,170,171}. Previous studies demonstrated that metronidazole-loaded PLA or PCL fibers showed sustained-release of metronidazole with potent antibacterial activity, however poor wettability and stiffness limited the use of PLA and PCL alone without hydrophilic fiber blend for local periodontitis treatment^{98,172}. In addition, PLA:PCL/Gelatin fibers containing tetracycline demonstrated significant inhibition of oral biofilms *in vitro*, suggesting that tetracycline-loaded fibers may act as potent antibacterial implant for dental

application; however, non-specific activity of tetracycline may affect the growth of commensal beneficial oral bacteria¹⁷⁴.

In comparison with limited and mostly non-specific approaches to prevent or treat periodontal diseases, the goal of this work was to incorporate a pathogen-specific biological active agent within a NP surface modification or encapsulation, to exploit the specific and adhesive interactions between two bacteria known to initiate the process of periodontal infections. We showed that not only can this specific peptide target biofilm interactions, but that by conjugating BAR to a NP surface or encapsulating BAR within PLGA NPs or EFs, we can achieve safe and enhanced potency, attributed to multivalency and prolonged activity, in a murine model of infection and *in vitro*. Moreover, the use of biodegradable FDA-approved polymers as a core platform, offers the potential for the incorporation of other complementary active agents, and more seamless integration in pre-clinical and clinical studies.

Lastly, while BAR-encapsulated and BAR-modified NPs demonstrate significant promise, their retention in the oral cavity is considered to be a challenge regardless of active agent and delivery vehicle. To address this challenge, our ongoing studies are focused on first developing NP formulations that can localize and retain BAR for longer durations in the oral cavity by using CafA-modified NPs to target Sg in oral niches.

Certainly, the drug delivery system plays a vital role in controlling the therapeutic effect of the active agent through optimizing the rate of drug release.

Many dosage forms are designed to release the active agent immediately (rapid-release) or provide delayed (prolonged) and extended-release products. Extended-release dosage forms can consist of sustained-release formulations that release agents over a specific time period, or controlled-release formulations that maintain the release of active agent at a constant rate for a specific duration¹⁹⁴.

In the long-term, we seek to formulate BAR-modified NPs or CafA-modified BAR-encapsulated NPs to more conveniently administer to the oral cavity in a mouthwash, oral varnish or gel formulation, with the goal of retaining BAR in oral niches for durations spanning 12-24 hr. In addition, our results utilizing BAR-incorporated EFs to inhibit oral biofilm formation raise the possibility that this formulation can be developed in the form of strips or gum to release peptide over a time window of hours. We envision that formulating this extended-release platform may be applied once or twice daily to exert prophylactic effect in the oral cavity without the need to remove the fibers after application.

Conclusion and Future Work

Incorporation of BAR peptide in NPs provides gradual release of BAR peptide, while offering a platform to improve efficacy and potentially longevity in the oral cavity, compared to the transient activity of free BAR. In addition, BAR-incorporated EFs may provide an alternative and specifically-targeted rapid-release platform to inhibit and disrupt dual-species biofilms, that we envision may be applied once or twice daily to exert prophylactic effect in the oral cavity without the need to remove the fibers after application. BAR-modified NPs offered a

platform that provided higher localized concentration of BAR in the oral cavity via multivalent interactions.

In future studies, we intend to examine different temporal administration regimens to optimize prevention and treatment approaches with these platforms. In addition, we plan to extend our studies to assess the kinetics of BAR-delivery vehicles in the oral cavity after gingival application.

In the longer term, we seek to formulate these NPs into a mouthwash or gel for more convenient application to the oral cavity. In addition, we envision BAR-EFs may be administered as dental strips or in gel form to degrade and avoid surgical removal after application. While existing products designed for localized periodontal prevention and treatment contain antibiotics, analgesic, or anesthetic cargos, we envision that this technology may offer a new way to deliver specifically-acting biologics to the oral cavity.

REFERENCES

1. Genco RJ, Van Dyke TE. Prevention: Reducing the risk of CVD in patients with periodontitis. *Nature reviews Cardiology*. 2010;7(9):479-480.
2. Lundberg K, Wegner N, Yucel-Lindberg T, Venables PJ. Periodontitis in RA-the citrullinated enolase connection. *Nature reviews Rheumatology*. 2010;6(12):727-730.
3. Eke PI, Dye BA, Wei L, Thornton-Evans GO, Genco RJ, Cdc Periodontal Disease Surveillance workgroup: James Beck GDRP. Prevalence of periodontitis in adults in the United States: 2009 and 2010. *J Dent Res*. 2012;91(10):914-920.
4. Kassebaum NJ, Bernabe E, Dahiya M, Bhandari B, Murray CJ, Marcenes W. Global burden of severe periodontitis in 1990-2010: a systematic review and meta-regression. *J Dent Res*. 2014;93(11):1045-1053.
5. Listl S, Galloway J, Mossey PA, Marcenes W. Global Economic Impact of Dental Diseases. *J Dent Res*. 2015;94(10):1355-1361.
6. Tonetti MS, Jepsen S, Jin L, Otomo-Corgel J. Impact of the global burden of periodontal diseases on health, nutrition and wellbeing of mankind: A call for global action. *J Clin Periodontol*. 2017;44(5):456-462.
7. Pihlstrom BL, Michalowicz BS, Johnson NW. Periodontal diseases. *Lancet*. 2005;366(9499):1809-1820.
8. Baumgartner A, Thurnheer T, Luthi-Schaller H, Gmur R, Belibasakis GN. The phylum Synergistetes in gingivitis and necrotizing ulcerative gingivitis. *Journal of medical microbiology*. 2012;61(Pt 11):1600-1609.
9. Chapple ILC, Mealey BL, Van Dyke TE, et al. Periodontal health and gingival diseases and conditions on an intact and a reduced periodontium: Consensus report of workgroup 1 of the 2017 World Workshop on the Classification of Periodontal and Peri-Implant Diseases and Conditions. *Journal of periodontology*. 2018;89 Suppl 1:S74-S84.
10. Teughels W, Dhondt R, Dekeyser C, Quirynen M. Treatment of aggressive periodontitis. *Periodontology 2000*. 2014;65(1):107-133.
11. Lang N BP, Cullinan M, Jeffcoat M, Mombelli A, Murakami S, Page R, Papapanou P, Tonetti M, Dyke T V. Consensus Report: Aggressive Periodontitis. . *Annals of periodontology*. 1999;4:1.
12. Gibbs RS. The relationship between infections and adverse pregnancy outcomes: an overview. *Annals of periodontology*. 2001;6(1):153-163.
13. Han YW, Redline RW, Li M, Yin L, Hill GB, McCormick TS. *Fusobacterium nucleatum* induces premature and term stillbirths in pregnant mice: implication of oral bacteria in preterm birth. *Infection and immunity*. 2004;72(4):2272-2279.
14. Bearfield C, Davenport ES, Sivapathasundaram V, Allaker RP. Possible association between amniotic fluid micro-organism infection and microflora in the mouth. *BJOG : an international journal of obstetrics and gynaecology*. 2002;109(5):527-533.

15. Paoletti R, Gotto AM, Jr., Hajjar DP. Inflammation in atherosclerosis and implications for therapy. *Circulation*. 2004;109(23 Suppl 1):III20-26.
16. D'Aiuto F, Nibali L, Parkar M, Suvan J, Tonetti MS. Short-term effects of intensive periodontal therapy on serum inflammatory markers and cholesterol. *J Dent Res*. 2005;84(3):269-273.
17. Curtis MA, Macey M, Slaney JM, Howells GL. Platelet activation by Protease I of *Porphyromonas gingivalis* W83. *FEMS microbiology letters*. 1993;110(2):167-173.
18. Beck JD, Eke P, Heiss G, et al. Periodontal disease and coronary heart disease: a reappraisal of the exposure. *Circulation*. 2005;112(1):19-24.
19. Pussinen PJ, Alfthan G, Tuomilehto J, Asikainen S, Jousilahti P. High serum antibody levels to *Porphyromonas gingivalis* predict myocardial infarction. *European journal of cardiovascular prevention and rehabilitation : official journal of the European Society of Cardiology, Working Groups on Epidemiology & Prevention and Cardiac Rehabilitation and Exercise Physiology*. 2004;11(5):408-411.
20. Pussinen PJ, Jousilahti P, Alfthan G, Palosuo T, Asikainen S, Salomaa V. Antibodies to periodontal pathogens are associated with coronary heart disease. *Arteriosclerosis, thrombosis, and vascular biology*. 2003;23(7):1250-1254.
21. Coburn BW, Sayles HR, Payne JB, et al. Performance of self-reported measures for periodontitis in rheumatoid arthritis and osteoarthritis. *Journal of periodontology*. 2015;86(1):16-26.
22. Koziel J, Mydel P, Potempa J. The link between periodontal disease and rheumatoid arthritis: an updated review. *Current rheumatology reports*. 2014;16(3):408.
23. Taylor GW. Bidirectional interrelationships between diabetes and periodontal diseases: an epidemiologic perspective. *Annals of periodontology*. 2001;6(1):99-112.
24. Saremi A, Nelson RG, Tulloch-Reid M, et al. Periodontal disease and mortality in type 2 diabetes. *Diabetes care*. 2005;28(1):27-32.
25. Garcia RI, Nunn ME, Vokonas PS. Epidemiologic associations between periodontal disease and chronic obstructive pulmonary disease. *Annals of periodontology*. 2001;6(1):71-77.
26. Fourrier F, Duvivier B, Boutigny H, Roussel-Delvallez M, Chopin C. Colonization of dental plaque: a source of nosocomial infections in intensive care unit patients. *Critical care medicine*. 1998;26(2):301-308.
27. Fourrier F, Cau-Pottier E, Boutigny H, Roussel-Delvallez M, Jourdain M, Chopin C. Effects of dental plaque antiseptic decontamination on bacterial colonization and nosocomial infections in critically ill patients. *Intensive care medicine*. 2000;26(9):1239-1247.
28. Garg T, Singh O, Arora S, Murthy R. Scaffold: a novel carrier for cell and drug delivery. *Critical reviews in therapeutic drug carrier systems*. 2012;29(1):1-63.
29. Herrera D, Matesanz P, Bascones-Martinez A, Sanz M. Local and systemic antimicrobial therapy in periodontics. *The journal of evidence-based dental practice*. 2012;12(3 Suppl):50-60.
30. Drisko CH. Nonsurgical periodontal therapy. *Periodontology 2000*. 2001;25:77-88.
31. Walker CB, Gordon JM, Magnussen I, Clark WB. A Role for Antibiotics in the Treatment of Refractory Periodontitis. *Journal of periodontology*. 1993;64 Suppl 8S:772-781.
32. Badersten A, Nilveus R, Egelberg J. Effect of nonsurgical periodontal therapy. I. Moderately advanced periodontitis. *J Clin Periodontol*. 1981;8(1):57-72.

33. Haffajee AD, Cugini MA, Dibart S, Smith C, Kent RL, Jr., Socransky SS. The effect of SRP on the clinical and microbiological parameters of periodontal diseases. *J Clin Periodontol.* 1997;24(5):324-334.
34. Quirynen M, Teughels W, De Soete M, van Steenberghe D. Topical antiseptics and antibiotics in the initial therapy of chronic adult periodontitis: microbiological aspects. *Periodontology 2000.* 2002;28:72-90.
35. Drisko CH. Non-surgical pocket therapy: pharmacotherapeutics. *Annals of periodontology.* 1996;1(1):491-566.
36. Hussain M, Stover CM, Dupont A. P. gingivalis in Periodontal Disease and Atherosclerosis - Scenes of Action for Antimicrobial Peptides and Complement. *Frontiers in immunology.* 2015;6:45.
37. Walker CB. The acquisition of antibiotic resistance in the periodontal microflora. *Periodontology 2000.* 1996;10:79-88.
38. Rosier BT, De Jager M, Zaura E, Krom BP. Historical and contemporary hypotheses on the development of oral diseases: are we there yet? *Frontiers in cellular and infection microbiology.* 2014;4:92.
39. Loesche WJ. The specific plaque hypothesis and the antimicrobial treatment of periodontal disease. *Dental update.* 1992;19(2):68, 70-62, 74.
40. Socransky SS. Microbiology of periodontal disease -- present status and future considerations. *Journal of periodontology.* 1977;48(9):497-504.
41. Socransky SS, Haffajee AD, Cugini MA, Smith C, Kent RL, Jr. Microbial complexes in subgingival plaque. *J Clin Periodontol.* 1998;25(2):134-144.
42. Darveau RP, Hajishengallis G, Curtis MA. Porphyromonas gingivalis as a potential community activist for disease. *J Dent Res.* 2012;91(9):816-820.
43. Siqueira JF, Jr., Rocas IN. As-yet-uncultivated oral bacteria: breadth and association with oral and extra-oral diseases. *Journal of oral microbiology.* 2013;5.
44. Handelsman J. Metagenomics: application of genomics to uncultured microorganisms. *Microbiology and molecular biology reviews : MMBR.* 2004;68(4):669-685.
45. Datta HK, Ng WF, Walker JA, Tuck SP, Varanasi SS. The cell biology of bone metabolism. *Journal of clinical pathology.* 2008;61(5):577-587.
46. Hajishengallis G, Darveau RP, Curtis MA. The keystone-pathogen hypothesis. *Nature reviews Microbiology.* 2012;10(10):717-725.
47. Hajishengallis G, Lamont RJ. Beyond the red complex and into more complexity: the polymicrobial synergy and dysbiosis (PSD) model of periodontal disease etiology. *Molecular oral microbiology.* 2012;27(6):409-419.
48. Hajishengallis G, Liang S, Payne MA, et al. Low-abundance biofilm species orchestrates inflammatory periodontal disease through the commensal microbiota and complement. *Cell host & microbe.* 2011;10(5):497-506.
49. Hasturk H, Kantarci A, Goguet-Surmenian E, et al. Resolvin E1 regulates inflammation at the cellular and tissue level and restores tissue homeostasis in vivo. *Journal of immunology.* 2007;179(10):7021-7029.
50. Page RC, Lantz MS, Darveau R, et al. Immunization of Macaca fascicularis against experimental periodontitis using a vaccine containing cysteine proteases purified from Porphyromonas gingivalis. *Oral microbiology and immunology.* 2007;22(3):162-168.
51. Darveau RP, Belton CM, Reife RA, Lamont RJ. Local chemokine paralysis, a novel pathogenic mechanism for Porphyromonas gingivalis. *Infection and immunity.* 1998;66(4):1660-1665.

52. Marsh PD. Microbial ecology of dental plaque and its significance in health and disease. *Advances in dental research*. 1994;8(2):263-271.
53. Demuth DR, Irvine DC, Costerton JW, Cook GS, Lamont RJ. Discrete protein determinant directs the species-specific adherence of Porphyromonas gingivalis to oral streptococci. *Infection and immunity*. 2001;69(9):5736-5741.
54. Brooks W, Demuth DR, Gil S, Lamont RJ. Identification of a Streptococcus gordonii SspB domain that mediates adhesion to Porphyromonas gingivalis. *Infection and immunity*. 1997;65(9):3753-3758.
55. Abou Neel EA, Bozec L, Perez RA, Kim HW, Knowles JC. Nanotechnology in dentistry: prevention, diagnosis, and therapy. *International journal of nanomedicine*. 2015;10:6371-6394.
56. De Jong WH, Borm PJ. Drug delivery and nanoparticles: applications and hazards. *International journal of nanomedicine*. 2008;3(2):133-149.
57. Hainfeld JF, Slatkin DN, Smilowitz HM. The use of gold nanoparticles to enhance radiotherapy in mice. *Phys Med Biol*. 2004;49(18):N309-315.
58. Paciotti GF, Myer L, Weinreich D, et al. Colloidal gold: a novel nanoparticle vector for tumor directed drug delivery. *Drug Deliv*. 2004;11(3):169-183.
59. Malarkodi C, Rajeshkumar S, Paulkumar K, Vanaja M, Gnanajobitha G, Annadurai G. Biosynthesis and Antimicrobial Activity of Semiconductor Nanoparticles against Oral Pathogens. *Bioinorg Chem Appl*. 2014;2014:347167.
60. Chen MH. Update on dental nanocomposites. *J Dent Res*. 2010;89(6):549-560.
61. Mitra SB, Wu D, Holmes BN. An application of nanotechnology in advanced dental materials. *J Am Dent Assoc*. 2003;134(10):1382-1390.
62. Xu HH, Moreau JL, Sun L, Chow LC. Strength and fluoride release characteristics of a calcium fluoride based dental nanocomposite. *Biomaterials*. 2008;29(32):4261-4267.
63. Xu HH, Weir MD, Sun L. Nanocomposites with Ca and PO₄ release: effects of reinforcement, dicalcium phosphate particle size and silanization. *Dent Mater*. 2007;23(12):1482-1491.
64. Muller RH, Mader K, Gohla S. Solid lipid nanoparticles (SLN) for controlled drug delivery - a review of the state of the art. *Eur J Pharm Biopharm*. 2000;50(1):161-177.
65. Wissing SA, Kayser O, Muller RH. Solid lipid nanoparticles for parenteral drug delivery. *Adv Drug Deliv Rev*. 2004;56(9):1257-1272.
66. Galindo-Rodriguez SA, Allemann E, Fessi H, Doelker E. Polymeric nanoparticles for oral delivery of drugs and vaccines: a critical evaluation of in vivo studies. *Critical reviews in therapeutic drug carrier systems*. 2005;22(5):419-464.
67. Kumari A, Yadav SK, Yadav SC. Biodegradable polymeric nanoparticles based drug delivery systems. *Colloids Surf B Biointerfaces*. 2010;75(1):1-18.
68. Correa JM, Mori M, Sanches HL, da Cruz AD, Poiate E, Jr., Poiate IA. Silver nanoparticles in dental biomaterials. *International journal of biomaterials*. 2015;2015:485275.
69. Garcia-Contreras R, Argueta-Figueroa L, Mejia-Rubalcava C, et al. Perspectives for the use of silver nanoparticles in dental practice. *International dental journal*. 2011;61(6):297-301.
70. Morones JR, Elechiguerra JL, Camacho A, et al. The bactericidal effect of silver nanoparticles. *Nanotechnology*. 2005;16(10):2346-2353.
71. Suhani MF, Baciut G, Baciut M, Suhani R, Bran S. Current perspectives regarding the application and incorporation of silver nanoparticles into dental biomaterials. *Clujul medical*. 2018;91(3):274-279.

72. Lin CC, Yeh YC, Yang CY, et al. Selective binding of mannose-encapsulated gold nanoparticles to type 1 pili in Escherichia coli. *Journal of the American Chemical Society*. 2002;124(14):3508-3509.
73. Williams DN, Ehrman SH, Pulliam Holoman TR. Evaluation of the microbial growth response to inorganic nanoparticles. *Journal of nanobiotechnology*. 2006;4:3.
74. Ahmad Z, Vargas-Reus MA, Bakhshi R, et al. Antimicrobial properties of electrically formed elastomeric polyurethane-copper oxide nanocomposites for medical and dental applications. *Methods in enzymology*. 2012;509:87-99.
75. Ren G, Hu D, Cheng EW, Vargas-Reus MA, Reip P, Allaker RP. Characterisation of copper oxide nanoparticles for antimicrobial applications. *International journal of antimicrobial agents*. 2009;33(6):587-590.
76. Yoon KY, Hoon Byeon J, Park JH, Hwang J. Susceptibility constants of Escherichia coli and Bacillus subtilis to silver and copper nanoparticles. *The Science of the total environment*. 2007;373(2-3):572-575.
77. Jones N, Ray B, Ranjit KT, Manna AC. Antibacterial activity of ZnO nanoparticle suspensions on a broad spectrum of microorganisms. *FEMS microbiology letters*. 2008;279(1):71-76.
78. Vargas-Reus MA, Memarzadeh K, Huang J, Ren GG, Allaker RP. Antimicrobial activity of nanoparticulate metal oxides against peri-implantitis pathogens. *International journal of antimicrobial agents*. 2012;40(2):135-139.
79. Feng QL, Wu J, Chen GQ, Cui FZ, Kim TN, Kim JO. A mechanistic study of the antibacterial effect of silver ions on Escherichia coli and Staphylococcus aureus. *Journal of biomedical materials research*. 2000;52(4):662-668.
80. Kim JS, Kuk E, Yu KN, et al. Antimicrobial effects of silver nanoparticles. *Nanomedicine : nanotechnology, biology, and medicine*. 2007;3(1):95-101.
81. Yamanaka M, Hara K, Kudo J. Bactericidal actions of a silver ion solution on Escherichia coli, studied by energy-filtering transmission electron microscopy and proteomic analysis. *Applied and environmental microbiology*. 2005;71(11):7589-7593.
82. Karlsson HL, Cronholm P, Gustafsson J, Moller L. Copper oxide nanoparticles are highly toxic: a comparison between metal oxide nanoparticles and carbon nanotubes. *Chemical research in toxicology*. 2008;21(9):1726-1732.
83. Nair S, Sasidharan A, Divya Rani VV, et al. Role of size scale of ZnO nanoparticles and microparticles on toxicity toward bacteria and osteoblast cancer cells. *Journal of materials science Materials in medicine*. 2009;20 Suppl 1:S235-241.
84. Nel AE, Madler L, Velegol D, et al. Understanding biophysicochemical interactions at the nano-bio interface. *Nature materials*. 2009;8(7):543-557.
85. Horev B, Klein MI, Hwang G, et al. pH-activated nanoparticles for controlled topical delivery of farnesol to disrupt oral biofilm virulence. *ACS nano*. 2015;9(3):2390-2404.
86. Yao W, Xu P, Pang Z, et al. Local delivery of minocycline-loaded PEG-PLA nanoparticles for the enhanced treatment of periodontitis in dogs. *International journal of nanomedicine*. 2014;9:3963-3970.
87. Danhier F, Ansorena E, Silva JM, Coco R, Le Breton A, Preat V. PLGA-based nanoparticles: an overview of biomedical applications. *Journal of controlled release : official journal of the Controlled Release Society*. 2012;161(2):505-522.
88. Martin DT, Steinbach JM, Liu J, et al. Surface-modified nanoparticles enhance transurothelial penetration and delivery of survivin siRNA in treating bladder cancer. *Molecular cancer therapeutics*. 2014;13(1):71-81.

89. Steinbach JM. Protein and oligonucleotide delivery systems for vaginal microbicides against viral STIs. *Cellular and molecular life sciences : CMLS*. 2015;72(3):469-503.
90. Lee BS, Lee CC, Wang YP, et al. Controlled-release of tetracycline and lovastatin by poly(D,L-lactide-co-glycolide acid)-chitosan nanoparticles enhances periodontal regeneration in dogs. *International journal of nanomedicine*. 2016;11:285-297.
91. Madhumathi K, Sampath Kumar TS. Regenerative potential and anti-bacterial activity of tetracycline loaded apatitic nanocarriers for the treatment of periodontitis. *Biomedical materials*. 2014;9(3):035002.
92. Kashi TS, Eskandarion S, Esfandyari-Manesh M, et al. Improved drug loading and antibacterial activity of minocycline-loaded PLGA nanoparticles prepared by solid/oil/water ion pairing method. *International journal of nanomedicine*. 2012;7:221-234.
93. Albuquerque MT, Evans JD, Gregory RL, Valera MC, Bottino MC. Antibacterial TAP-mimic electrospun polymer scaffold: effects on *P. gingivalis*-infected dentin biofilm. *Clin Oral Investig*. 2016;20(2):387-393.
94. Yao W, Xu P, Zhao J, et al. RGD functionalized polymeric nanoparticles targeting periodontitis epithelial cells for the enhanced treatment of periodontitis in dogs. *Journal of colloid and interface science*. 2015;458:14-21.
95. Kalia P, Jain A, Radha Krishnan R, Demuth DR, Steinbach-Rankins JM. Peptide-modified nanoparticles inhibit formation of *Porphyromonas gingivalis* biofilms with *Streptococcus gordonii*. *International journal of nanomedicine*. 2017;12:4553-4562.
96. Mahmoud MY, Steinbach-Rankins JM, Demuth DR. Functional assessment of peptide-modified PLGA nanoparticles against oral biofilms in a murine model of periodontitis. *Journal of controlled release : official journal of the Controlled Release Society*. 2019;297:3-13.
97. Chaturvedi TP, Srivastava R, Srivastava AK, Gupta V, Verma PK. Doxycycline Poly E-Caprolactone Nanofibers in Patients with Chronic Periodontitis – A Clinical Evaluation. *Journal of Clinical and Diagnostic Research*. 2013;7(10):2339-2342.
98. Reise M, Wyrwa R, Muller U, et al. Release of metronidazole from electrospun poly(L-lactide-co-D/L-lactide) fibers for local periodontitis treatment. *Dent Mater*. 2012;28(2):179-188.
99. Chou S-F, Woodrow KA. Relationships between mechanical properties and drug release from electrospun fibers of PCL and PLGA blends. *Journal of the Mechanical Behavior of Biomedical Materials*. 2017;65:724-733.
100. Kim K, Luu YK, Chang C, et al. Incorporation and controlled release of a hydrophilic antibiotic using poly(lactide-co-glycolide)-based electrospun nanofibrous scaffolds. *Journal of controlled release : official journal of the Controlled Release Society*. 2004;98(1):47-56.
101. Sundararaj SC, Thomas MV, Peyyala R, Dziubla TD, Puleo DA. Design of a multiple drug delivery system directed at periodontitis. *Biomaterials*. 2013;34(34):8835-8842.
102. Li WJ, Laurencin CT, Caterson EJ, Tuan RS, Ko FK. Electrospun nanofibrous structure: a novel scaffold for tissue engineering. *Journal of biomedical materials research*. 2002;60(4):613-621.
103. Jun Z, Hou HQ, Schaper A, H. Wendorff J, Greiner A. *Poly-L-Lactide Nanofibers by Electrospinning—Influence of Solution Viscosity and Electrical Conductivity on Fiber Diameter and Fiber Morphology*. Vol 32003.

104. Son WK, Youk JH, Lee TS, Park WH. The effects of solution properties and polyelectrolyte on electrospinning of ultrafine poly(ethylene oxide) fibers. *Polymer*. 2004;45(9):2959-2966.
105. Ellen RP. Periodontal care for community-dwelling older adults. *The Journal of prosthetic dentistry*. 1994;72(5):500-506.
106. Kaldahl WB, Kalkwarf KL, Patil KD, Molvar MP, Dyer JK. Long-term evaluation of periodontal therapy: I. Response to 4 therapeutic modalities. *Journal of periodontology*. 1996;67(2):93-102.
107. Allaker RP, Ian Douglas CW. Non-conventional therapeutics for oral infections. *Virulence*. 2015;6(3):196-207.
108. Honda K. Porphyromonas gingivalis sinks teeth into the oral microbiota and periodontal disease. *Cell host & microbe*. 2011;10(5):423-425.
109. Lamont RJ, El-Sabaeny A, Park Y, Cook GS, Costerton JW, Demuth DR. Role of the Streptococcus gordonii SspB protein in the development of Porphyromonas gingivalis biofilms on streptococcal substrates. *Microbiology*. 2002;148(Pt 6):1627-1636.
110. Park Y, Simionato MR, Sekiya K, et al. Short fimbriae of Porphyromonas gingivalis and their role in coadhesion with Streptococcus gordonii. *Infection and immunity*. 2005;73(7):3983-3989.
111. Daep CA, James DM, Lamont RJ, Demuth DR. Structural characterization of peptide-mediated inhibition of Porphyromonas gingivalis biofilm formation. *Infection and immunity*. 2006;74(10):5756-5762.
112. Daep CA, Lamont RJ, Demuth DR. Interaction of Porphyromonas gingivalis with oral streptococci requires a motif that resembles the eukaryotic nuclear receptor box protein-protein interaction domain. *Infection and immunity*. 2008;76(7):3273-3280.
113. Daep CA, Novak EA, Lamont RJ, Demuth DR. Structural dissection and in vivo effectiveness of a peptide inhibitor of Porphyromonas gingivalis adherence to Streptococcus gordonii. *Infection and immunity*. 2011;79(1):67-74.
114. de Freitas LM, Calixto GM, Chorilli M, et al. Polymeric Nanoparticle-Based Photodynamic Therapy for Chronic Periodontitis in Vivo. *International journal of molecular sciences*. 2016;17(5).
115. Makadia HK, Siegel SJ. Poly Lactic-co-Glycolic Acid (PLGA) as Biodegradable Controlled Drug Delivery Carrier. *Polymers*. 2011;3(3):1377-1397.
116. Patel A, Patel M, Yang X, Mitra AK. Recent advances in protein and Peptide drug delivery: a special emphasis on polymeric nanoparticles. *Protein and peptide letters*. 2014;21(11):1102-1120.
117. Singh R, Lillard JW, Jr. Nanoparticle-based targeted drug delivery. *Experimental and molecular pathology*. 2009;86(3):215-223.
118. de Sousa FF, Ferraz C, Rodrigues LK, Nojosa Jde S, Yamauti M. Nanotechnology in dentistry: drug delivery systems for the control of biofilm-dependent oral diseases. *Current drug delivery*. 2014;11(6):719-728.
119. Elsabahy M, Wooley KL. Design of polymeric nanoparticles for biomedical delivery applications. *Chemical Society reviews*. 2012;41(7):2545-2561.
120. Steinbach JM, Weller CE, Booth CJ, Saltzman WM. Polymer nanoparticles encapsulating siRNA for treatment of HSV-2 genital infection. *Journal of controlled release : official journal of the Controlled Release Society*. 2012;162(1):102-110.
121. Sims LB, Curtis LT, Frieboes HB, Steinbach-Rankins JM. Enhanced uptake and transport of PLGA-modified nanoparticles in cervical cancer. *Journal of nanobiotechnology*. 2016;14:33.

122. Steinbach JM, Seo YE, Saltzman WM. Cell penetrating peptide-modified poly(lactic-co-glycolic acid) nanoparticles with enhanced cell internalization. *Acta biomaterialia*. 2016;30:49-61.
123. Cai X, Han B, Liu Y, Tian F, Liang F, Wang X. Chlorhexidine-Loaded Amorphous Calcium Phosphate Nanoparticles for Inhibiting Degradation and Inducing Mineralization of Type I Collagen. *ACS applied materials & interfaces*. 2017;9(15):12949-12958.
124. Chronopoulou L, Nocca G, Castagnola M, et al. Chitosan based nanoparticles functionalized with peptidomimetic derivatives for oral drug delivery. *New biotechnology*. 2016;33(1):23-31.
125. Benoit DS, Koo H. Targeted, triggered drug delivery to tumor and biofilm microenvironments. *Nanomedicine (Lond)*. 2016;11(8):873-879.
126. Takahashi C, Akachi Y, Ogawa N, et al. Morphological study of efficacy of clarithromycin-loaded nanocarriers for treatment of biofilm infection disease. *Medical molecular morphology*. 2017;50(1):9-16.
127. Wayakanon K, Thornhill MH, Douglas CW, et al. Polymersome-mediated intracellular delivery of antibiotics to treat Porphyromonas gingivalis-infected oral epithelial cells. *FASEB journal : official publication of the Federation of American Societies for Experimental Biology*. 2013;27(11):4455-4465.
128. Sindhura Reddy N, Sowmya S, Bumgardner JD, Chennazhi KP, Biswas R, Jayakumar R. Tetracycline nanoparticles loaded calcium sulfate composite beads for periodontal management. *Biochimica et biophysica acta*. 2014;1840(6):2080-2090.
129. Lee SF, Hulbah M, Halperin SA. Development of a gene delivery system in Streptococcus gordonii using thymidylate synthase as a selection marker. *Journal of microbiological methods*. 2016;125:43-48.
130. Tiyafoonchai W, Rodleang I, Ounaroon A. Mucoadhesive polyethylenimine-dextran sulfate nanoparticles containing Punica granatum peel extract as a novel sustained-release antimicrobial. *Pharmaceutical development and technology*. 2015;20(4):426-432.
131. Moulari B, Lboutounne H, Chaumont JP, Guillaume Y, Millet J, Pellequer Y. Potentiation of the bactericidal activity of Harungana madagascariensis Lam. ex Poir. (Hypericaceae) leaf extract against oral bacteria using poly (D, L-lactide-co-glycolide) nanoparticles: in vitro study. *Acta odontologica Scandinavica*. 2006;64(3):153-158.
132. Liu L, Shu S, Cheung GS, Wei X. Effect of miR-146a/bFGF/PEG-PEI Nanoparticles on Inflammation Response and Tissue Regeneration of Human Dental Pulp Cells. *BioMed research international*. 2016;2016:3892685.
133. Napimoga MH, da Silva CA, Carregaro V, et al. Exogenous administration of 15d-PGJ2-loaded nanocapsules inhibits bone resorption in a mouse periodontitis model. *Journal of immunology*. 2012;189(2):1043-1052.
134. Zaltsman N, Ionescu AC, Weiss EI, Brambilla E, Beyth S, Beyth N. Surface-modified nanoparticles as anti-biofilm filler for dental polymers. *PloS one*. 2017;12(12):e0189397.
135. Ahuja A AJ, Shareef A, Khar R. Formulation and development of targeted retentive device for the treatment of periodontal infections with amoxicillin trihydrate. *Indian J Pharm Sci* 2006;68:6.
136. Somayaji BV, Jariwala U, Jayachandran P, Vidyalakshmi K, Dudhani RV. Evaluation of antimicrobial efficacy and release pattern of tetracycline and

- metronidazole using a local delivery system. *Journal of periodontology*. 1998;69(4):409-413.
137. Wade WG, Moran J, Morgan JR, Newcombe R, Addy M. The effects of antimicrobial acrylic strips on the subgingival microflora in chronic periodontitis. *J Clin Periodontol*. 1992;19(2):127-134.
 138. Tonetti MS, Pini-Prato G, Cortellini P. Principles and clinical applications of periodontal controlled drug delivery with tetracycline fibers. *The International journal of periodontics & restorative dentistry*. 1994;14(5):421-435.
 139. Lu Z, Rong K, Li J, Yang H, Chen R. Size-dependent antibacterial activities of silver nanoparticles against oral anaerobic pathogenic bacteria. *Journal of materials science Materials in medicine*. 2013;24(6):1465-1471.
 140. Martinez-Gutierrez F, Thi EP, Silverman JM, et al. Antibacterial activity, inflammatory response, coagulation and cytotoxicity effects of silver nanoparticles. *Nanomedicine : nanotechnology, biology, and medicine*. 2012;8(3):328-336.
 141. Ensign LM, Cone R, Hanes J. Oral drug delivery with polymeric nanoparticles: the gastrointestinal mucus barriers. *Adv Drug Deliv Rev*. 2012;64(6):557-570.
 142. Lai SK, Wang YY, Hanes J. Mucus-penetrating nanoparticles for drug and gene delivery to mucosal tissues. *Adv Drug Deliv Rev*. 2009;61(2):158-171.
 143. Mahmoud MY, Demuth DR, Steinbach-Rankins JM. BAR-encapsulated nanoparticles for the inhibition and disruption of Porphyromonas gingivalis-Streptococcus gordonii biofilms. *Journal of nanobiotechnology*. 2018;16(1):69.
 144. Fasting C, Schalley CA, Weber M, et al. Multivalency as a chemical organization and action principle. *Angewandte Chemie*. 2012;51(42):10472-10498.
 145. Mammen M, Choi SK, Whitesides GM. Polyvalent Interactions in Biological Systems: Implications for Design and Use of Multivalent Ligands and Inhibitors. *Angewandte Chemie*. 1998;37(20):2754-2794.
 146. Fahmy TM, Samstein RM, Harness CC, Mark Saltzman W. Surface modification of biodegradable polyesters with fatty acid conjugates for improved drug targeting. *Biomaterials*. 2005;26(28):5727-5736.
 147. Park J, Mattessich T, Jay SM, Agawu A, Saltzman WM, Fahmy TM. Enhancement of surface ligand display on PLGA nanoparticles with amphiphilic ligand conjugates. *Journal of controlled release : official journal of the Controlled Release Society*. 2011;156(1):109-115.
 148. Garlet GP, Avila-Campos MJ, Milanezi CM, Ferreira BR, Silva JS. Actinobacillus actinomycetemcomitans-induced periodontal disease in mice: patterns of cytokine, chemokine, and chemokine receptor expression and leukocyte migration. *Microbes and infection*. 2005;7(4):738-747.
 149. Rojo-Botello NR, Garcia-Hernandez AL, Moreno-Fierros L. Expression of toll-like receptors 2, 4 and 9 is increased in gingival tissue from patients with type 2 diabetes and chronic periodontitis. *Journal of periodontal research*. 2012;47(1):62-73.
 150. Howarth M, Chinnapen DJ, Gerrow K, et al. A monovalent streptavidin with a single femtomolar biotin binding site. *Nature methods*. 2006;3(4):267-273.
 151. Hotze EM, Phenrat T, Lowry GV. Nanoparticle aggregation: challenges to understanding transport and reactivity in the environment. *Journal of environmental quality*. 2010;39(6):1909-1924.
 152. Pinon-Segundo E, Ganem-Quintanar A, Alonso-Perez V, Quintanar-Guerrero D. Preparation and characterization of triclosan nanoparticles for periodontal treatment. *International journal of pharmaceutics*. 2005;294(1-2):217-232.

153. Qin Y, Yuan M, Li L, Li W, Xue J. Formulation and evaluation of in situ forming PLA implant containing tinidazole for the treatment of periodontitis. *Journal of biomedical materials research Part B, Applied biomaterials*. 2012;100(8):2197-2202.
154. Ma M, Kazemzadeh-Narbat M, Hui Y, et al. Local delivery of antimicrobial peptides using self-organized TiO₂ nanotube arrays for peri-implant infections. *Journal of biomedical materials research Part A*. 2012;100(2):278-285.
155. Yazici H, O'Neill MB, Kacar T, et al. Engineered Chimeric Peptides as Antimicrobial Surface Coating Agents toward Infection-Free Implants. *ACS applied materials & interfaces*. 2016;8(8):5070-5081.
156. Yoshinari M, Kato T, Matsuzaka K, Hayakawa T, Shiba K. Prevention of biofilm formation on titanium surfaces modified with conjugated molecules comprised of antimicrobial and titanium-binding peptides. *Biofouling*. 2010;26(1):103-110.
157. Li MH, Zong H, Leroueil PR, Choi SK, Baker JR, Jr. Ligand Characteristics Important to Avidity Interactions of Multivalent Nanoparticles. *Bioconjugate chemistry*. 2017;28(6):1649-1657.
158. Liu M, Duan XP, Li YM, Yang DP, Long YZ. Electrospun nanofibers for wound healing. *Materials science & engineering C, Materials for biological applications*. 2017;76:1413-1423.
159. Yang F, Both SK, Yang X, Walboomers XF, Jansen JA. Development of an electrospun nano-apatite/PCL composite membrane for GTR/GBR application. *Acta biomaterialia*. 2009;5(9):3295-3304.
160. Inanc B, Arslan YE, Seker S, Elcin AE, Elcin YM. Periodontal ligament cellular structures engineered with electrospun poly(DL-lactide-co-glycolide) nanofibrous membrane scaffolds. *Journal of biomedical materials research Part A*. 2009;90(1):186-195.
161. Griffen AL, Beall CJ, Campbell JH, et al. Distinct and complex bacterial profiles in human periodontitis and health revealed by 16S pyrosequencing. *The ISME journal*. 2012;6(6):1176-1185.
162. Yilmaz O. The chronicles of Porphyromonas gingivalis: the microbium, the human oral epithelium and their interplay. *Microbiology*. 2008;154(Pt 10):2897-2903.
163. Kolenbrander PE, London J. Adhere today, here tomorrow: oral bacterial adherence. *Journal of Bacteriology*. 1993;175(11):3247-3252.
164. Daep CA, James DM, Lamont RJ, Demuth DR. Structural Characterization of Peptide-Mediated Inhibition of Porphyromonas gingivalis Biofilm Formation. *Infection and Immunity*. 2006;74(10):5756-5762.
165. Shifrovitch Y, Binderman I, Bahar H, Berdicevsky I, Zilberman M. Metronidazole-loaded bioabsorbable films as local antibacterial treatment of infected periodontal pockets. *Journal of periodontology*. 2009;80(2):330-337.
166. Friesen LR, Williams KB, Krause LS, Killoy WJ. Controlled local delivery of tetracycline with polymer strips in the treatment of periodontitis. *Journal of periodontology*. 2002;73(1):13-19.
167. Leung WK, Jin L, Yau JY, Sun Q, Corbet EF. Microflora cultivable from minocycline strips placed in persisting periodontal pockets. *Archives of oral biology*. 2005;50(1):39-48.
168. Bromberg LE, Braman VM, Rothstein DM, et al. Sustained release of silver from periodontal wafers for treatment of periodontitis. *Journal of controlled release : official journal of the Controlled Release Society*. 2000;68(1):63-72.
169. Su Y, Li X, Tan L, Chen H, Xiumei M. *Poly(l-lactide-co-ε-caprolactone) electrospun nanofibers for encapsulating and sustained releasing proteins*. Vol 502009.

170. Batool F, Morand DN, Thomas L, et al. Synthesis of a Novel Electrospun Polycaprolactone Scaffold Functionalized with Ibuprofen for Periodontal Regeneration: An In Vitro and In Vivo Study. *Materials*. 2018;11(4).
171. Zafar M, Najeeb S, Khurshid Z, et al. Potential of Electrospun Nanofibers for Biomedical and Dental Applications. *Materials*. 2016;9(2).
172. Zamani M, Morshed M, Varshosaz J, Jannesari M. Controlled release of metronidazole benzoate from poly epsilon-caprolactone electrospun nanofibers for periodontal diseases. *Eur J Pharm Biopharm*. 2010;75(2):179-185.
173. Bottino MC, Arthur RA, Waeiss RA, Kamocki K, Gregson KS, Gregory RL. Biodegradable nanofibrous drug delivery systems: effects of metronidazole and ciprofloxacin on periodontopathogens and commensal oral bacteria. *Clin Oral Investig*. 2014;18(9):2151-2158.
174. Shahi RG, Albuquerque MTP, Munchow EA, Blanchard SB, Gregory RL, Bottino MC. Novel bioactive tetracycline-containing electrospun polymer fibers as a potential antibacterial dental implant coating. *Odontology*. 2017;105(3):354-363.
175. Li Y, Jiang H, Zhu K. Encapsulation and controlled release of lysozyme from electrospun poly(epsilon-caprolactone)/poly(ethylene glycol) non-woven membranes by formation of lysozyme-oleate complexes. *Journal of materials science Materials in medicine*. 2008;19(2):827-832.
176. Casper CL, Yamaguchi N, Kiick KL, Rabolt JF. Functionalizing Electrospun Fibers with Biologically Relevant Macromolecules. *Biomacromolecules*. 2005;6(4):1998-2007.
177. Li C, Vepari C, Jin HJ, Kim HJ, Kaplan DL. Electrospun silk-BMP-2 scaffolds for bone tissue engineering. *Biomaterials*. 2006;27(16):3115-3124.
178. Evrova O, Hosseini V, Milleret V, et al. Hybrid Randomly Electrospun Poly(lactic-co-glycolic acid):Poly(ethylene oxide) (PLGA:PEO) Fibrous Scaffolds Enhancing Myoblast Differentiation and Alignment. *ACS applied materials & interfaces*. 2016;8(46):31574-31586.
179. Kim TG, Lee DS, Park TG. Controlled protein release from electrospun biodegradable fiber mesh composed of poly(epsilon-caprolactone) and poly(ethylene oxide). *International journal of pharmaceutics*. 2007;338(1-2):276-283.
180. Szentivanyi A, Chakradeo T, Zernetsch H, Glasmacher B. Electrospun cellular microenvironments: Understanding controlled release and scaffold structure. *Adv Drug Deliv Rev*. 2011;63(4-5):209-220.
181. Sebe I, Szabo P, Kallai-Szabo B, Zelko R. Incorporating small molecules or biologics into nanofibers for optimized drug release: A review. *International journal of pharmaceutics*. 2015;494(1):516-530.
182. Li X, Su Y, Liu S, Tan L, Mo X, Ramakrishna S. Encapsulation of proteins in poly(L-lactide-co-caprolactone) fibers by emulsion electrospinning. *Colloids Surf B Biointerfaces*. 2010;75(2):418-424.
183. Ji W, Yang F, van den Beucken JJ, et al. Fibrous scaffolds loaded with protein prepared by blend or coaxial electrospinning. *Acta biomaterialia*. 2010;6(11):4199-4207.
184. Maze GI, Reinhardt RA, Payne JB, et al. Gingival fluid tetracycline release from bioerodible gels. *J Clin Periodontol*. 1996;23(12):1133-1136.
185. Srinivas M, Medaiah S, Girish S, Anil M, Pai J, Walvekar A. The effect of ketoprofen in chronic periodontitis: A clinical double-blind study. *Journal of Indian Society of Periodontology*. 2011;15(3):255-259.

186. Ma ZW, Zhang YJ, Wang R, Wang QT, Dong GY, Wu ZF. [An animal experiment for the regeneration of periodontal defect by application of the dual-release chitosan thermosensitive hydrogel system]. *Zhonghua kou qiang yi xue za zhi = Zhonghua kouqiang yixue zazhi = Chinese journal of stomatology*. 2008;43(5):273-277.
187. Kilicarslan M, Koerber M, Bodmeier R. In situ forming implants for the delivery of metronidazole to periodontal pockets: formulation and drug release studies. *Drug Dev Ind Pharm*. 2014;40(5):619-624.
188. Endo K, Ueno T, Kondo S, et al. Tumor-targeted chemotherapy with the nanopolymer-based drug NC-6004 for oral squamous cell carcinoma. *Cancer Sci*. 2013;104(3):369-374.
189. Nafee NA, Ismail FA, Boraie NA, Mortada LM. Mucoadhesive buccal patches of miconazole nitrate: in vitro/in vivo performance and effect of ageing. *International journal of pharmaceutics*. 2003;264(1-2):1-14.
190. Diaz del Consuelo I, Falson F, Guy RH, Jacques Y. Ex vivo evaluation of bioadhesive films for buccal delivery of fentanyl. *Journal of controlled release : official journal of the Controlled Release Society*. 2007;122(2):135-140.
191. Reardon-Robinson ME, Wu C, Mishra A, et al. Pilus hijacking by a bacterial coaggregation factor critical for oral biofilm development. *Proceedings of the National Academy of Sciences of the United States of America*. 2014;111(10):3835-3840.
192. Cu Y, Saltzman WM. Controlled surface modification with poly(ethylene)glycol enhances diffusion of PLGA nanoparticles in human cervical mucus. *Mol Pharm*. 2009;6(1):173-181.
193. Chaturvedi TP, Srivastava R, Srivastava AK, Gupta V, Verma PK. Doxycycline Poly E-Caprolactone Nanofibers in Patients with Chronic Periodontitis – A Clinical Evaluation. *Journal of Clinical and Diagnostic Research : JCDR*. 2013;7(10):2339-2342.
194. Rades YPaT. *Pharmaceutics - Drug Delivery and Targeting*. Pharmaceutical Press; 2009.

CURRICULUM VITAE

Mohamed Y. Mahmoud, BVSc, MVSc.
University of Louisville
Ph.D. Candidate
Pharmacology & Toxicology Department
Phone: 502-221-5110
Emails:
myabde01@louisville.edu
m.yehia.abdaleem@cu.edu.eg

Education:

Ph.D. Candidate (2016-present)

Pharmacology and Toxicology Department,
School of Medicine, University of Louisville, USA

Master's Degree of Toxicology (2013-2015)

Toxicology and Forensic Medicine Department
College of Veterinary Medicine, Cairo University, Egypt

Bachelor's of Veterinary Medical Sciences (2006-2011)

College of Veterinary Medicine, Cairo University, Egypt

Professional Experience:

Assistant Lecturer of Toxicology and Forensic Medicine, Faculty of Veterinary Medicine, Cairo University, Giza, Egypt (2015-2016)

Teaching Assistant of Toxicology and Forensic medicine, Faculty of Veterinary Medicine, Cairo University, Giza, Egypt (2012-2014)

Knowledge and Expertise:

I have been involved in teaching and training undergraduate and graduate students on different toxicology techniques in laboratories, farms and field cure trips. I have contributed to laboratory analysis (biochemistry, cytology and molecular biology).

Award/Honors:

2018: University of Louisville Graduate Student Council Travel Award

2013: Certificate of Excellence from the Development and Training Unit, College of Veterinary Medicine, Cairo University.

2013: Certificate of Appreciation from the College of Veterinary Medicine, Cairo University.

2011: Ranked 5th / class of 600, College of Veterinary Medicine, Cairo University.

Submitted Peer-Reviewed Journal Publications:

- **Mohamed Y. Mahmoud**, Sonali Sapare, Keegan C. Curry, Donald R. Demuth, Jill M. Steinbach-Rankins. "Rapid-Release Polymeric Fibers for Inhibition of *Porphyromonas gingivalis* and *Streptococcus gordonii* Biofilms", March 2019.

Published Peer-Reviewed Journal Publications:

- **Mahmoud MY**, Steinbach-Rankins JM, Demuth DR. Functional assessment of peptide-modified PLGA nanoparticles against oral biofilms in a murine model of periodontitis. *Journal of controlled release: official journal of the Controlled Release Society*. Jan 25 2019;297:3-13.
- Lee Sims, Kevin Tyo, Sanaya Stocke, **Mohamed Y. Mahmoud**, Aparna Ramasubramanian, and Jill M. Steinbach-Rankins. "Surface-Modified Melphalan Nanoparticles for Intravitreal Chemotherapy of Retinoblastoma", accepted March 2019.
- **Mahmoud MY**, Demuth DR, Steinbach-Rankins JM. BAR-encapsulated nanoparticles for the inhibition and disruption of *Porphyromonas gingivalis*-*Streptococcus gordonii* biofilms. *Journal of nanobiotechnology*. Sep 15 2018;16(1):69.
- **Mohamed. Y. Abdelaleem**, Mohamed. S. Mowad, Eiman. A. Mohamed and Osama .S. El-tawil "Cytotoxicity of Silver Nanoparticles (AgNps) in Freshly Prepared Isolated Rat Hepatocytes" *Life Sci J* 2015;12(1):94-103.

In Preparation Peer-Reviewed Journal Publications:

- **Mohamed Y. Mahmoud**, Donald R. Demuth, Jill M. Steinbach-Rankins. "Existing Non-Specific and Future Approaches to Prevent and Treat Oral Infections".

Conference Presentations / Abstracts

Oral Presentations:

- **Mohamed Y. Mahmoud**, Sonali Sapare, Donald R. Demuth, Jill M. Steinbach-Rankins. "*Functional Assessment of BAR-Encapsulated Nanoparticles and Electrospun Fibers against Oral Biofilms*", BMES Conference; October 2018.
- **Mohamed Y. Mahmoud**, Donald R. Demuth, Jill M. Steinbach-Rankins. "*BAR-Encapsulated Nanoparticles against P. gingivalis Biofilm Formation*", KY Nano/AM symposium; August 2018.
- **Mohamed Y. Mahmoud**, Donald R. Demuth, Jill M. Steinbach-Rankins. "*BAR-Encapsulated and BAR-Modified Nanoparticles for Oral Biofilm Applications*", CRS Conference; July 2018.
- **Mohamed. Y. Abdelaleem**, Mohamed. S. Mowad, Eiman. A. Mohamed and Osama .S. El-tawil. "*In vitro comparison of cytotoxicity and genotoxicity between silver nanoparticles and microparticles*", EGY-TOX Conference; May 2015.

Poster Presentations:

- **Mohamed Y. Mahmoud**, Donald Demuth, Jill Steinbach-Rankins. "*BAR-Modified Nanoparticles against P. gingivalis Virulence in Murine Model of Periodontitis*", Research Louisville; September 2018.
- **Mohamed Y. Mahmoud**, Donald Demuth, Jill Steinbach-Rankins. "*Assessing BAR-Peptide Nanoparticle Effectiveness against P. gingivalis Biofilm Formation*", Research Louisville; September 2017.
- **Mohamed. Y. Abdelaleem**, Mohamed. S. Mowad, Eiman. A. Mohamed and Osama .S. El-tawil. "*Cytotoxicity and genotoxicity of silver nanoparticles on isolated rat hepatocytes*", EUROTOX Congress; September 2014.

Community Service:

College of Veterinary Medicine, Cairo University: Field Cure Trips in Cairo and Giza (2013 - Present).

Research Interests:

My research interests have included the following: development of nanoparticles as a delivery vehicle; cytotoxicity and genotoxicity of nanomaterials in animal and cellular models (*in vivo/in vitro*); cancer technologies; development of novel dosage forms; oral and topical drug delivery; and gene delivery.

Key Skills:

- Broad experience in the design and synthesis of different nanoparticle and electrospun fiber formulations and their characterization using scanning electron microscopy, DLS/ Zetasizer, surface-modification quantification, loading, and controlled release through working as a Ph.D. student in the laboratory of Dr. Steinbach-Rankins, University of Louisville.
- Expertise in the growth and assessment of bacterial biofilms, and assessment of biofilm inhibition and disruption using confocal microscopy and quantification by Volocity software.
- *In vivo* assessment of oral biofilm development and inhibition, and toxicity studies including: LDH, ATP, MTT, hemolysis, apoptosis, and flow cytometry.
- Wide experience in veterinary toxicology techniques (*in vitro, in vivo*, genotoxicity, mycotoxins analysis, pesticides evaluation, oxidative stress detection in blood and tissue, DNA damage, and mutation parameters).
- Broad experience in biological applications of silver nanomaterials.
- Practical experience in laboratory animal management.
- High interest in Biostatistics, Statistical packages (SPSS).
- Well-developed communication skills honed through frequent production of reports, scientific writing, and the written and oral presentations of work-related material.